12-2010

Tantalum Carbene and Imide Complexes. Synthesis, Characterization, and Pathways of Formation

Julia Kathryn Covington Abbott
University of Tennessee - Knoxville, jcoving7@utk.edu

To the Graduate Council:

I am submitting herewith a dissertation written by Julia Kathryn Covington Abbott entitled "Tantalum Carbene and Imide Complexes. Synthesis, Characterization, and Pathways of Formation." I have examined the final electronic copy of this dissertation for form and content and recommend that it be accepted in partial fulfillment of the requirements for the degree of Doctor of Philosophy, with a major in Chemistry.

Ziling Xue, Major Professor

We have read this dissertation and recommend its acceptance:

Craig Barnes, Robert Hinde, Claudia Rawn

Accepted for the Council:

Carolyn R. Hodges

Vice Provost and Dean of the Graduate School

(Original signatures are on file with official student records.)

To the Graduate Council:

I am submitting herewith a dissertation written by Julia Kathryn Covington Abbott entitled “Tantalum Carbene and Imide Complexes. Synthesis, Characterization, and Pathways of Formation.” I have examined the final electronic copy of this dissertation for form and content and recommend that it be accepted in partial fulfillment of the requirements for the degree of Doctor of Philosophy, with a major in Chemistry.

Ziling (Ben) Xue, Major Professor

We have read this dissertation
and recommend its acceptance:

Craig E. Barnes

Robert J. Hinde

Claudia J. Rawn

Accepted for the Council:

Carolyn R. Hodges

Vice Provost and Dean of the Graduate School

(Original signatures are on file with official student records.)

TANTALUM CARBENE AND IMIDE COMPLEXES. SYNTHESIS, CHARACTERIZATION, AND PATHWAYS OF FORMATION

A Dissertation

Presented for the

Doctor of Philosophy Degree

The University of Tennessee, Knoxville

Julia Kathryn Covington Abbott

December 2010

DEDICATION

This dissertation is dedicated to my wonderful husband, Josh, for the patience he shows me every day, and to my parents, Dean and Merry, for the love and support they have given me throughout my life. I especially would like to dedicate this to my aunt, Connie Lapp, and in the memory of my uncle, J.C. Lapp. Without them, I would never be where I am today. I appreciate them more than they will ever know.

ACKNOWLEDGEMENTS

There are many people who I would like to thank who have helped me during my graduate studies. I would first like to thank my advisor, Dr. Ziling (Ben) Xue for his patience and guidance during my time at UTK. He has been an excellent mentor and teacher and I have enjoyed my time in his lab. I would also like to acknowledge my committee members: Dr. Craig Barnes, Dr. Robert Hinde, and Dr. Claudia Rawn for their time and consideration of my dissertation. I would like to extend a special thanks to Dr. Barnes for being so helpful and understanding with the X-ray diffractometer. I would also like to thanks Dr. Carlos Steren for all his help with the NMR, especially all the extra time he booked for me while I was working on kinetics.

There are so many people behind the scenes in the chemistry department that keep everything going day to day; I do not know where to begin. I would like to thank Bill Gurley. He helped me with everything from the X-ray and NMR to my personal computers. I also enjoyed the time I spent in the electronics shop talking politics and life with Bill and Gary Wynn. I would like to thank the rest of the electronics shop as well: Gary, Johnny Jones, and Jim Murphy. Thanks for all your help with the X-ray!

Next I would like to thank Art Pratt. I am a little clumsy sometimes, and I appreciate all the repairs he did for me on short notice. I am glad I was on the “right” list. I would also like to thank Gene French in the machine shop for his help with the X-ray and with other random things in our lab. I would really like to thank Pete Janutolo at Bruker AXS Inc. I would never have made it through my time as X-ray operator without him. Thanks for keeping me sane and being so patient with me.

I would like to thank all the wonderful people in the business office: Sharon Marshall for helping me get everything paid for with all the X-ray repairs, Darrell Lay for helping me place lots of orders, Gail Cox for always having a smile and being helpful whenever I needed it, and Tray Allen for helping me ship things at the last minute and filling all my liquid nitrogen tanks. I would also like to extend a special thanks to Tom Toney in the main office, for making reimbursments for travel so much easier.

I would like to thank my past and present group members for help in the lab, little chats here and there, and keeping me sane. I want to extend a special thanks to Nathan Carrington, Tara Williams, He (Steve) Qiu, Li Yong, Shujian (Jim) Chen, Jun Jin, Ruizhuo Ouyang, Caleb Dyer, Royce Dansby-Sparks and Josh Abbott, all members of our ever evolving, now defunct, lunch group. It was always the best hour of my day. I would also like to acknowledge other members in the group, Adam Lamb, Bhavna Sharma, Seth Hunter, Kristie Armstrong, Clarissa Tatum, Stefanie Bragg, and Jonathan Fong.

I would like to thank some other fellow grad students that have come and gone through the years. Kasey Hill, Jenny Oran, and Amber Wellman, thanks for laughing loud enough for me to be able to hear you down the hall. It always put a smile on my face, and the 4th floor is so much quieter now that you all have gone. Erin Losey (Moehlen), nothing in particular, just thanks! Royce, I do not know what I would have done without you in the last five years. You have been amazing, and I really miss our morning coffee sessions. No coworker will ever be so great!

Finally, I would like to thank my family. My parents, Dean and Merry, you guys are amazing. Who ever thought two librarians would pop out a scientist? I miss you all the time, but I know you raised me to go off and live my own life and I love you for it. My brother, Sam, we may have fought a lot growing up, but you are pretty cool now. To my aunt, Connie, you are great. I will always remember the summer you had me meet all the different people at Corning. I am glad that you and J.C. were so involved in my education and life. Lastly, I want to thank Josh. You are my rock, I do not know how you put up with me sometimes, but you do. I am so thankful to have you going through life beside me. Just remember I will be there for you 100% when you are writing your dissertation.

I would like to thank the National Science Foundation for supporting my graduate research.

ABSTRACT

This dissertation focuses on two different types of organometallic compounds, carbenes and imides. The first project deals with the archetypal Schrock carbene, and the second project studies complexes that contain metal-nitrogen bonds, both amides and imides.

A summary of the research in this dissertation is discussed in Chapter 1. Chapter 2 begins the studies of the archetypal Schrock carbene, $(Bu^tCH_2)_3Ta=CHBu^t$. The studies include the synthesis of deuterated compounds $(Bu^tCD_2)_3TaCl_2$ and Bu^tCD_2Li, observation and identification of the intermediate, $Ta(CD_2Bu^t)_5$, and kinetic studies of the conversion of $Ta(CD_2Bu^t)_5$ to $(Bu^tCD_2)_3Ta=CDBu^t$, giving the activation parameters and a kinetic isotope effect for the conversion. The work here confirms that the pentaneopentyltantalum is the precursor to the archetypal Schrock carbene.

Chapter 3 studies the effects of isotopic substitution on NMR chemical shifts of complexes in Chapter 2. Conformations of $(Bu^tCD_2)_3TaCl_2$ and $Ta(CD_2Bu^t)_5$ have also been investigated.

Chapter 4 begins the study of compounds containing metal-nitrogen bonds. Guanidinate imides $Ta(NMe_2)(=NSiMe_3)[RNC(NMe_2)NR]_2$ (R = Cy, Pr^i) have been prepared from the reactions of $Ta(NMe_2)_4[N(SiMe_3)_2]$ with two equivalents of carbodiimides, RN=C=NR. The two guanidinate imides have been characterized by NMR spectroscopy and elemental analysis. In addition, the structure of $Ta(NMe_2)(=NSiMe_3)[CyNC(NMe_2)NCy]_2$ has been studied by single crystal X-ray

diffraction. Under heating, $Ta(NMe_2)_4[N(SiMe_3)_2]$ undergoes an unprecedented elimination of $Me_3Si\text{-}NMe_2$, converting the amide ligand $–N(SiMe_3)_2$ to the imide ligand $=NSiMe_3$ to give an intermediate $Ta(NMe_2)_3(=NSiMe_3)$. In the presence of CyN=C=NCy, the carbodiimide captures the intermediate to give another intermediate, $Ta(NMe_2)_2(=NSiMe_3)[CyNC(NMe_2)NCy]$. Subsequent second carbodiimide insertion leads to the formation of the final product $Ta(NMe_2)(=NSiMe_3)[CyNC(NMe_2)NCy]_2$. The remaining amide ligand, $–NMe_2$, in $Ta(NMe_2)(=NSiMe_3)[CyNC(NMe_2)NCy]_2$ and $Ta(NMe_2)(=NSiMe_3)[Pr^iNC(NMe_2)NPr^i]_2$ gives two separate resonances in the proton NMR spectrum at room temperature indicating inequivalence of the two methyl groups. The interconversion of the methyl groups in the former has been studied with variable-temperature NMR.

Chapter 5 studies the synthesis and characterization of metal cage complexes $[(Me_2N)_3MO]_4$ (M = Nb, Ta). Single crystal X-ray diffraction studies show a cubane-like structure with M-O bridges. Variable-temperature NMR of the inequivalent amide methyl groups $–NMe_AMe_B$ has also been carried out to find the activation parameters for the exchange.

TABLE OF CONTENTS

LIST OF TABLES

LIST OF FIGURES

LIST OF SCHEMES

NUMBERING SCHEME FOR COMPOUNDS IN THE TEXT

1	$Ta(CH_2Bu^t)_5$
1-*d*$_{10}$	$Ta(CD_2Bu^t)_5$
2	$(Bu^tCH_2)_3Ta{=}CHBu^t$
2-*d*$_7$	$(Bu^tCD_2)_3Ta{=}CDBu^t$
3	$(Bu^tCH_2)_3TaCl_2$
3-*d*$_6$	$(Bu^tCD_2)_3TaCl_2$
4	$(Bu^tCH_2)_4TaCl$
4-*d*$_8$	$(Bu^tCD_2)_4TaCl$
5	$(Bu^tCH_2)_2Ta(=CHBu^t)Cl$
6	$Ta(CH_2SiMe_3)_5$
7	$(Me_3SiCH_2)_3Ta{=}CHSiMe_3$
8	$(Me_3SiCH_2)_2Ta(\mu\text{-}CSiMe_3)_2Ta(CH_2SiMe_3)_2$
9	$Ta(CH_2Ph)_5$
10	$Ta(CH_2CH_3)_5$
11	$Ta(NMe_2)(=NSiMe_3)[CyNC(NMe_2)NCy]_2$
12	$Ta(NMe_2)(=NSiMe_3)[Pr^iNC(NMe_2)NPr^i]_2$
13	$Ta(NMe_2)_4[N(SiMe_3)_2]$
14	$Me_3Si\text{-}NMe_2$
15	$Ta(NMe_2)_3(=NSiMe_3)$
16	$Ta(NMe_2)_2(=NSiMe_3)[CyNC(NMe_2)NCy]$
17	$Nb(NMe_2)_5$
18	$Ta(NMe_2)_5$

19 $[(Me_2N)_3NbO]_4$

20 $[(Me_2N)_3TaO]_4$

21 $Nb(NMe_2)_4[N(Me)CH_2NMe_2]$

22 $Ta(NMe_2)_4[N(Me)CH_2NMe_2]$

23 $TaCl(NMe_2)_4$

24 $[(Me_2N)_3TaCl]_2O$

Chapter 1

Introduction

1.1. Forward

The first metal-carbon double bond complex, or carbene, was discovered in 1964[1] and the first metal-carbon triple bond complex, or carbyne, in 1973[2] by E. O. Fischer and coworkers (Eqs. 1.1 and 1.2). Fischer carbene and carbyne complexes are usually formed with late transition metal centers in low oxidation states. The complexes typically contain π-acceptor ligands, except for the carbene ligand itself which can contain π-donor substituents such as $–OCH_3$.

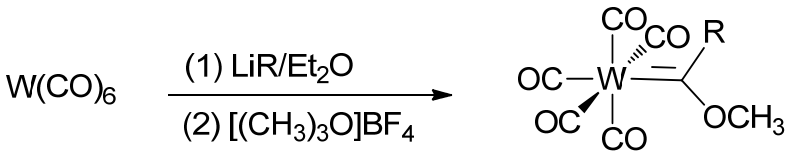

Eq. 1.1

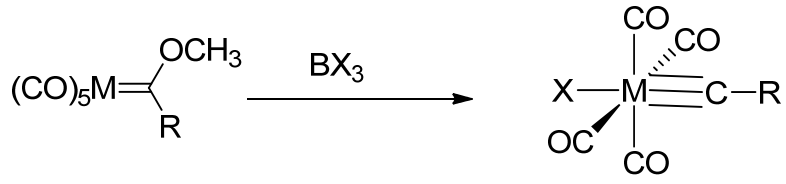

M = Cr, Mo, W
X = Cl, Br, I
R = Me, Et, Ph

Eq. 1.2

In contrast to the Fischer carbenes and carbynes, in 1973, an attempt to synthesize pentaneopentyltantalum, by R. R. Schrock, resulted instead in the

synthesis of the first high oxidation state, early transition metal carbene complex,[3] later named the Schrock carbene (Eq. 1.3). The first Schrock carbyne complex was published in 1978[4] (Eq. 1.4). Schrock-type carbenes and carbynes contain non π-acceptor ligands and a non π-donor R group on the carbene ligand.

$$(Bu^tCH_2)_3TaCl_2 \xrightarrow{2\ Bu^tCH_2Li} (Bu^tCH_2)_3Ta{=}CHBu^t \qquad \text{Eq. 1.3}$$

$$WCl_6 \xrightarrow{6\ Bu^tCH_2Li} (Bu^tCH_2)_3W{\equiv}CBu^t \qquad \text{Eq. 1.4}$$

Both Fischer and Schrock complexes proved to be useful in a number of applications. Since the time of their discovery, the chemistry of compounds containing metal-carbon multiple bonds has grown steadily.

Carbenes play a major role as catalysts for olefin metathesis. Olefin metathesis (also known as alkene metathesis, Scheme 1.1) is a process in which a C=C double bond is broken and the resulting RHC= group is exchanged between the alkenes.[5]

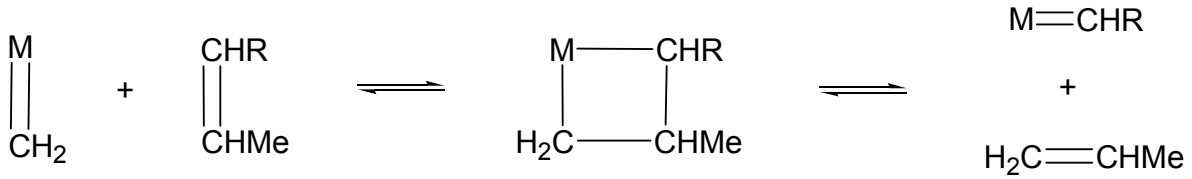

Scheme 1.1. Mechanism for olefin metathesis.

The mechanism of olefin metathesis was elucidated by Chauvin in the early 1970's.[6] With the advancements of catalysts to increase the efficiency of the reactions, olefin metathesis reactions have become a more prominent industrial process, and are used primarily for the functionalization of alkenes and for polymer syntheses. The process is "green" in that the only reagents are olefins and the metal carbene catalyst, and the only byproduct is a volatile olefin, such as ethylene.[7] The two most common carbene catalysts for olefin metathesis are known as the Grubbs and Schrock catalysts (Figure 1.1).

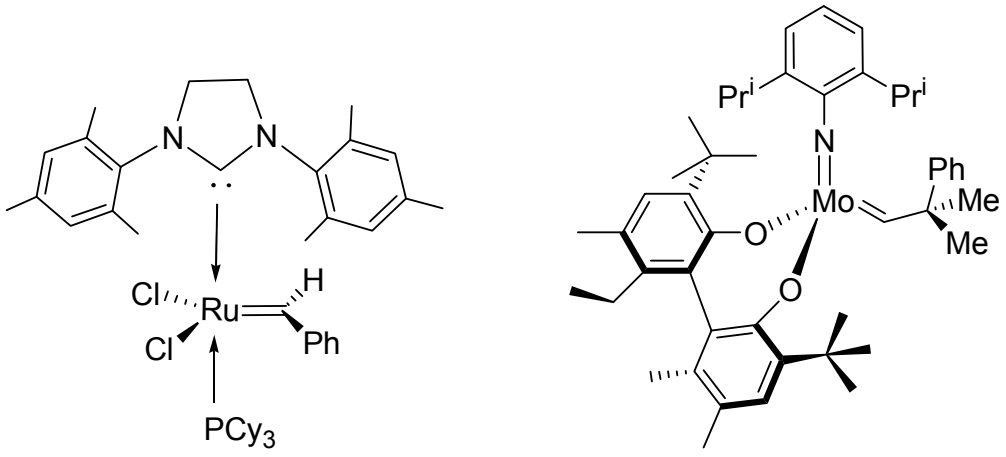

Figure 1.1. Typical Grubbs (left) and Schrock (right) catalysts.

The Grubbs catalyst is Ru based, and air stable. The original compound contained two PCy_3 ligands. The currently used second generation Grubbs catalyst had replaced one of the PCy_3 ligands with an N-heterocyclic carbene (NHC). It was found that by replacing a phosphine with an NHC, the reactivity of the catalyst was increased by a factor of 100-1000.[8]

The Mo based Schrock catalysts are air-sensitive, and Grubbs catalysts are usually air-stable. Thus Schrock catalysts are often handled under inert atmosphere, and are better catalysts for some reactions including asymmetric metathesis because Schrock catalysts can be made chiral.[9] The first part of this dissertation will focus on the original carbene compound, $(Bu^tCH_2)_3Ta{=}CHBu^t$, first synthesized by Schrock that led to his eventual discoveries of olefin metathesis catalysts.

Another focus in inorganic and organometallic chemistry is the synthesis of metal oxides for use as the insulating layer in microelectronic devices. Figure 1.2 shows a transistor in a Very-Large-Scale-Integration (VLSI) device. As electronic devices as a whole become smaller, the transistors must get smaller as well. However, a problem arises when the insulating oxide layer gets too thin.[10,11] The most common oxide in use is SiO_2 due to its easy preparation from silicon wafers. Unfortunately, SiO_2 has a low dielectric constant (k = 3.9). Because of the low k, as the layer thickness decreases (below 2 nm) the gate current leakage becomes unacceptably high making it inadequate as a gate material.[10] Metal oxides such as Ta_2O_5 (k = 26) are being studied because of their high dielectric constants and their potential to form films of less than two nanometers. These oxides are often made

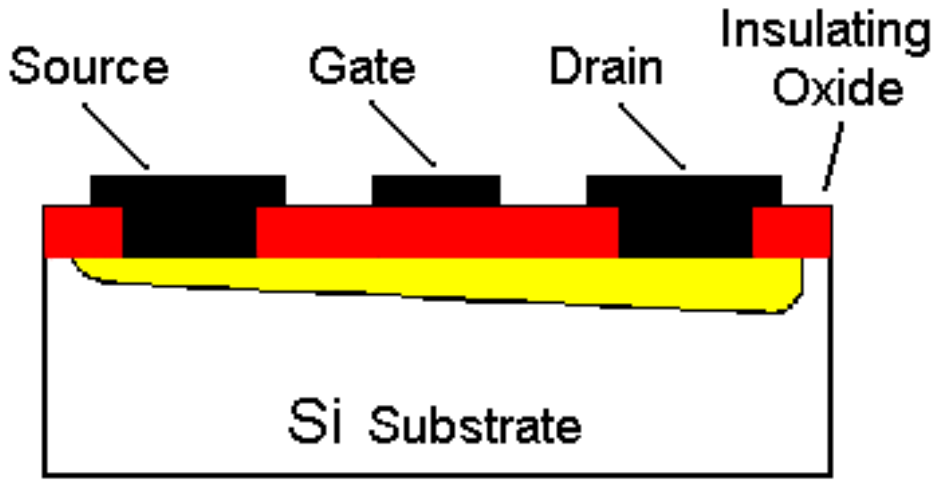

Figure 1.2. Transistor for a VLSI device.

through reactions of metal amides with oxygen or water. For example, $Ta(NR_2)_5$ has been used to prepare Ta_2O_5 thin films.[12] The second part of this dissertation focuses on different metal amide complexes that might serve as precursors for the insulating oxide layer of microelectronic devices.

1.2. Current Dissertation

This dissertation focuses on the study of the archetypal Schrock carbene, novel tantalum imide complexes, and tantalum and niobium amide complexes. More specifically, the mechanism and kinetics of the formation of the archetypal Schrock carbene, $(Bu^tCH_2)_3Ta{=}CHBu^t$ (**2**), as well as the characterization of its intermediate

was discussed. Also, the conformation of the intermediate, $Ta(CH_2Bu^t)_5$ (**1**), and the effects on chemical shift with isotopic substitution have been studied. Novel tantalum guanidinate imide complexes have been synthesized and characterized, and the pathway of their formation has been investigated. Finally, the reactions of water with known tantalum and niobium compounds have been studied, and the products have been characterized.

1.2.1. Chapter 2

The archetypal Schrock carbene, $(Bu^tCH_2)_3Ta{=}CHBu^t$ (**2**), was first prepared in 1974 from the reaction of $(Bu^tCH_2)_3TaCl_2$ (**3**) with 2 equivalents of Bu^tCH_2Li. The desired product, $Ta(CH_2Bu^t)_5$ (**1**), was not observed at that time. Two possible pathways were proposed for the formation of **2**. The first involves **1** as a possible intermediate in the reaction that proceeds through α-hydrogen abstraction to give the final product, **2**. The second path involves another intermediate, "$(Bu^tCH_2)_2Ta(=CHBu^t)Cl$" (**5**). Since that time, the discovery of **2** has led to major advancements in the field of organometallic chemistry. In this chapter, deuterium-labeled $Ta(CD_2Bu^t)_5$ (**1-*d*$_{10}$**) was found to be an intermediate in the reaction of $(Bu^tCD_2)_3TaCl_2$ (**3-*d*$_6$**) with 2 equivalents of Bu^tCD_2Li, thus confirming the pathway in the formation of **2**. Due to a kinetic isotope effect, $Ta(CD_2Bu^t)_5$ (**1-*d*$_{10}$**) has a much longer life than $Ta(CH_2Bu^t)_5$ (**1**), thus making it easier to study by NMR spectroscopy. ^1H, ^2H, and ^{13}C NMR were used to identify and characterize **1-*d*$_{10}$** in detail. Kinetic studies of the $Ta(CD_2Bu^t)_5$ (**1-*d*$_{10}$**) → $(Bu^tCD_2)_3Ta{=}CDBu^t$ (**2-*d*$_7$**) and $Ta(CH_2Bu^t)_5$ (**1**) → $(Bu^tCH_2)_3Ta{=}CHBu^t$ (**2**) conversions were also studied showing a kinetic isotope

effect (KIE) of 14.1(0.8) at 273 K. In addition, kinetic studies of the **1-d_{10}** → **2-d_7** conversion at 273-298 K gave activation parameters $\Delta H^{\neq}_{D}$ = 21.1(1.5) kcal/mol, $\Delta S^{\neq}_{D}$ = -4(6) eu, and $\Delta G^{\neq}_{D,273K}$ = 22(3) kcal/mol for the α-deuterium abstraction reaction. $\Delta G^{\neq}_{H,273K}$ for the α-hydrogen abstraction reaction of $Ta(CH_2Bu^t)_5$ (**1**) was also calculated using the KIE value and the Eyring equation to give a value of 21(3) kcal/mol.

1.2.2. Chapter 3

The effect isotopic substitution has on the chemical shift of other atoms in a compound is studied using $(Bu^tCD_2)_3TaCl_2$ (**3-d_6**), $Ta(CD_2Bu^t)_5$ (**1-d_{10}**), and $(Bu^tCD_2)_3Ta{=}CDBu^t$ (**2-d_7**) and their non-deuterated counterparts. Variable temperature NMR was used to study conformational changes in $(Bu^tCD_2)_3TaCl_2$ (**3-d_6**) and $Ta(CD_2Bu^t)_5$ (**1-d_{10}**). Computational studies were preformed for comparison to NMR data and to further probe the structure of $Ta(CD_2Bu^t)_5$ (**1-d_{10}**).

1.2.3. Chapter 4

The novel complex $Ta(NMe_2)(=NSiMe_3)[CyNC(NMe_2)NCy]_2$ (**11**) has been prepared from the reaction of $Ta(NMe_2)_4[N(SiMe_3)_2]$ (**13**) and two equivalents of CyN=C=NCy and characterized by single crystal X-ray diffraction and NMR. The remaining amide ligand in **11** was found to have two separate resonances in the ^1H NMR spectrum indicating inequivalence between the two methyl groups. The interconversion of these groups was studied with variable-temperature ^1H NMR. The coalescence temperature was found to be 393 K, and the rate of the interchange

between the two methyl groups at the coalescence temperature was 1181 s^{-1}. The high coalescence temperature indicates that the energy required to break the π bond between the tantalum and nitrogen is high. Mechanistic studies of the formation of **11** show that, when heated, **13** undergoes unpreprecedented α-$SiMe_3$ abstraction by a $–NMe_2$ ligand to give imide $Ta(NMe_2)_3(=NSiMe_3)$ (**15**) and $Me_3Si\text{-}NMe_2$ (**14**). Heating a mixture of **13** and one equivalent of CyN=C=NCy yields $Ta(NMe_2)(=NSiMe_3)[CyNC(NMe_2)NCy]$ (**16**) as an intermediate in the formation of **11**. The observation of **15** and **16** indicates that the formation of the imide through elimination of $Me_3Si\text{-}NMe_2$ occurs *before* the first carbodiimide insertion, and the carbodiimide captures imide $Ta(NMe_2)_3(=NSiMe_3)$ (**15**) to give **16**. Subsequent, second carbodiimide insertion yields **11**. An analog, $Ta(NMe_2)(=NSiMe_3)[Pr^iNC(NMe_2)NPr^i]_2$ (**12**), was also synthesized. NMR studies indicate that the compound is isostructural to **11**.

1.2.4. Chapter 5

It was found that the reactions between $M(NMe_2)_5$ (M = Nb, **17**; Ta, **18**) and water yield "$(Me_2N)_3M=O$" as tetramers **19** and **20**. Initial NMR studies show that there are temperature dependant inequivalencies in the methyl groups of the amide ligands. The X-ray crystal structure shows that there is a *cis*/*trans* relationship between the methyl groups of the amide ligands and the oxygen atoms bound to the metals. This relationship is the cause of the inequivalence. This was investigated further utilizing two dimensional and variable-temperature NMR. The VT NMR studies examined the rate of conversion between the two methyl groups and gave

the activation parameters $\Delta H^{\neq}$ = –0.3(0.3) kcal/mol, $\Delta S^{\neq}$ = –49(2) eu, $\Delta G^{\neq}_{308K}$ = 15.4(0.6) kcal/mol for **19** and $\Delta H^{\neq}$ = –0.2(0.3) kcal/mol, $\Delta S^{\neq}$ = –50(5) eu, $\Delta G^{\neq}_{308K}$ = 15.4(1.5) kcal/mol for **20**.

Chapter 2

Kinetic and Mechanistic Studies of the Conversion of Pentaneopentyltantalum to the Archetypical Alkylidene Complex

2.1. Introduction

Metal complexes containing a metal carbon double bond (carbenes) have been of recent interest.[7,13-46] Two types of carbene complexes are known: electron-rich, low oxidation state transition metal complexes (Fischer-type)[5,13-16] and electron-deficient, high oxidation state transition metal complexes (Schrock-type, also called alkylidene complexes).[5,17-19] Since Hérrison and Chauvin proposed the catalytic olefin metathesis mechanism involving M=CHR species,[6,47] studies of metal carbene chemistry have led to the development of Mo and W catalysts by the Schrock group[48] and Ru catalysts by the Grubbs group.[49] One particular complex that has played a crucial role in metal carbene chemistry is $(Bu^tCH_2)_3Ta{=}CHBu^t$ (**2**).[3,50-54] It was the first isolated, high oxidation state alkylidene complex,[3,50] and this discovery led to the development of a new field in organometallic chemistry.[3,5,17,18,50-54] Studies of this and other Ta alkylidene complexes have also helped the design and synthesis of the most active alkylidene catalysts for olefin metathesis.[48]

$(Bu^tCH_2)_3Ta{=}CHBu^t$ (**2**) was initially prepared from the reaction of $(Bu^tCH_2)_3TaCl_2$ (**3**) with 2 equivalents of Bu^tCH_2Li,[3] and additional studies suggested that the first step in the reaction was the substitution of a chloride ligand in **3** to yield

$(Bu^tCH_2)_4TaCl$ (**4**).[3,50] Two paths were postulated for the conversion of **4** to **2** (Scheme 2.1).[50] One route involves the initial formation of pentaneopentyltantalum $Ta(CH_2Bu^t)_5$ (**1**), followed by α-H abstraction between two alkyl ligands to give $(Bu^tCH_2)_3Ta{=}CHBu^t$ (**2**) (Route 1). The other route involves initial α-H abstraction in $(Bu^tCH_2)_4TaCl$ (**4**) to give "$(Bu^tCH_2)_2Ta(=CHBu^t)Cl$" (**5**), followed by substitution of the chloride ligand in **5** to yield **2**.

Previous study of the mechanistic pathways in the formation of $(Bu^tCH_2)_3Ta{=}CHBu^t$ (**2**) led to direct observation of $Ta(CH_2Bu^t)_5$ (**1**) in the NMR spectra of the reactions of $(Bu^tCH_2)_3TaCl_2$ (**3**) with 2 equivalent of Bu^tCH_2Li and $(Bu^tCH_2)_4TaCl$ (**4**) with 1 equivalent of Bu^tCH_2Li.[55,56] $Ta(CH_2Bu^t)_5$ (**1**) was, however, short-lived, and its ^1H NMR peaks at 233 K are in a small region (0.8-1.5 ppm) that is crowded with peaks of $(Bu^tCH_2)_3TaCl_2$ (**3**), axial and equatorial ligands in $(Bu^tCH_2)_4TaCl$ (**4**), Bu^tCH_2Li, $(Bu^tCH_2)_3Ta{=}CHBu^t$ (**2**), and CMe_4, leading to partial overlap of NMR peaks.[55,56] No kinetic study of the α-H abstraction reaction in $Ta(CH_2Bu^t)_5$ (**1**) yielding the archetypical alkylidene complex, $(Bu^tCH_2)_3Ta{=}CHBu^t$ (**2**), was performed. The observation of $Ta(CH_2Bu^t)_5$ (**1**), and the slow α-H abstraction reaction in $(Bu^tCH_2)_4TaCl$ (**4**) [to yield "$(Bu^tCH_2)_2Ta(=CHBu^t)Cl$" (**5**)][56] in comparison to the relatively quick formation of $(Bu^tCH_2)_3Ta{=}CHBu^t$ (**2**) from the reaction of $(Bu^tCH_2)_4TaCl$ (**4**) with 1 equivalent of Bu^tCH_2Li led us to suggest that Route 1 in Scheme 2.1 is the path to give **2**.[55,56]

Given the critical importance of $(Bu^tCH_2)_3Ta{=}CHBu^t$ (**2**) in the Schrock-type, high oxidation state transition metal carbene chemistry, and its role in the

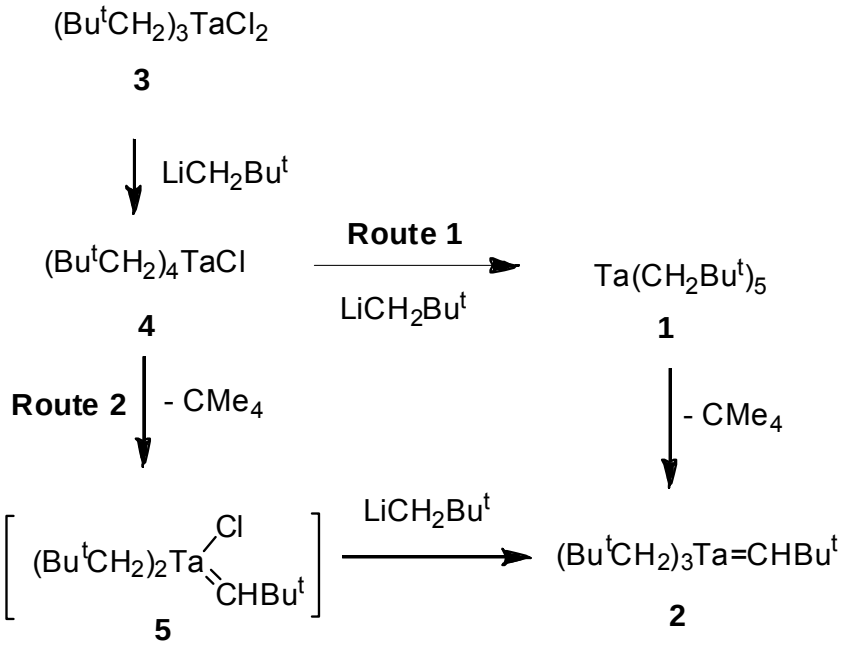

Scheme 2.1. Proposed mechanistic pathways in the formation of **2**.

development of olefin metathesis catalysts, we have sought to provide unambiguous evidence of the presence of $Ta(CH_2Bu^t)_5$ (**1**) as the precursor to the formation of $(Bu^tCH_2)_3Ta{=}CHBu^t$ (**2**), and to confirm the assignment of the NMR resonances of **1**. In addition, we were interested in the kinetics of the α-H abstraction reaction of $Ta(CH_2Bu^t)_5$ (**1**), leading to the formation of the first characterized M=C bond in high oxidation state metal complexes. We have reasoned that, if the α-hydrogen atoms in $Ta(CH_2Bu^t)_5$ (**1**) were replaced by deuterium atoms to give $Ta(CD_2Bu^t)_5$ (**1-*d*$_{10}$**), the lifetime of **1-*d*$_{10}$** would be much longer due to a kinetic isotope effect in the α-H/D abstraction, assuming the rate of formation of **2**/$(Bu^tCD_2)_3Ta{=}CDBu^t$ (**2-*d*$_7$**) depends in part on the α-H/D abstraction. The longer lifetime of $Ta(CD_2Bu^t)_5$ (**1-*d*$_{10}$**) would provide an opportunity to observe and characterize this important intermediate. In addition, only the methyl resonances in $(Bu^tCD_2)_3TaCl_2$ (**3-*d*$_6$**), $(Bu^tCD_2)_4TaCl$ (**4-*d*$_8$**), Bu^tCD_2Li, and $(Bu^tCD_2)_3Ta{=}CDBu^t$ (**2-*d*$_7$**) would be observed in the ^{1}H NMR spectrum of the reaction between $(Bu^tCD_2)_3TaCl_2$ (**3-*d*$_6$**) and Bu^tCD_2Li. In other words, there would be half the number of peaks in the ^{1}H NMR spectrum of the mixture containing $Ta(CD_2Bu^t)_5$ (**1-*d*$_{10}$**) as in the mixture containing $Ta(CH_2Bu^t)_5$ (**1**). Use of **1-*d*$_{10}$** would also allow its observation and characterization by deuterium NMR spectroscopy. The $-CD_2-$ peak of $Ta(CD_2Bu^t)_5$ (**1-*d*$_{10}$**) in the ^{2}H NMR spectrum would help confirm the assignment of the $-CH_2-$ resonances of **1**. In addition to measuring a kinetic isotope effect of the α-H/D abstraction in **1**/**1-*d*$_{10}$**, we also reasoned that $Ta(CD_2Bu^t)_5$ (**1-*d*$_{10}$**) would provide a unique opportunity to study in detail the kinetics of the formation of the archetypical alkylidene complex, and allow us to measure the activation enthalpy ($\Delta H^{\neq}_D$) and entropy ($\Delta S^{\neq}_D$) of this reaction. We

have prepared $Ta(CD_2Bu^t)_5$ (**1-*d*$_{10}$**) in situ, and characterized it by NMR spectroscopy. The kinetics of α-H abstraction in $Ta(CH_2Bu^t)_5$ (**1**) at 273 K and α-D abstraction in **1-*d*$_{10}$** at 273-298 K have also been studied. These studies are reported here.

2.2. Results and Discussion

2.2.1. Preparation of $Ta(CD_2Bu^t)_5$ (1-*d*$_{10}$) and Its Conversion to $(Bu^tCD_2)_3Ta{=}CDBu^t$ (2-*d*$_7$)

$Ta(CD_2Bu^t)_5$ (**1-*d*$_{10}$**) was prepared from either $(Bu^tCD_2)_3TaCl_2$ (**3-*d*$_6$**) and 2 equivalents of Bu^tCD_2Li or $(Bu^tCD_2)_4TaCl$ (**4-*d*$_8$**) and 1 equivalent of Bu^tCD_2Li in toluene-*d*$_8$ for ^1H NMR spectroscopy or in toluene (with a small amount of toluene-*d*$_8$) for ^2H NMR spectroscopy (Scheme 2.2). Chloride substitutions in both reactions were found to be faster than the α-deuterium abstraction in $Ta(CD_2Bu^t)_5$ (**1-*d*$_{10}$**). Since **4-*d*$_8$** is unstable, subsequent studies focused on the reaction of $(Bu^tCD_2)_3TaCl_2$ (**3-*d*$_6$**) with Bu^tCD_2Li.

^1H NMR spectra of the reaction between $(Bu^tCD_2)_3TaCl_2$ (**3-*d*$_6$**) and 2 equivalents of Bu^tCD_2Li to give $(Bu^tCD_2)_3Ta{=}CDBu^t$ (**2-*d*$_7$**) are given in Figure 2.1. Both $(Bu^tCD_2)_4TaCl$ (**4-*d*$_8$**) and $Ta(CD_2Bu^t)_5$ (**1-*d*$_{10}$**) were observed as intermediates. The peaks at 1.30 and 1.09 ppm were assigned to the equatorial and axial methyl groups, respectively, in $(Bu^tCD_2)_4TaCl$ (**4-*d*$_8$**). The intensities quickly reached a maximum about 30 min after the start of the reaction at 293 K, and then started to decrease as the monochloride **4-*d*$_8$** was converted to $Ta(CD_2Bu^t)_5$ (**1-*d*$_{10}$**).

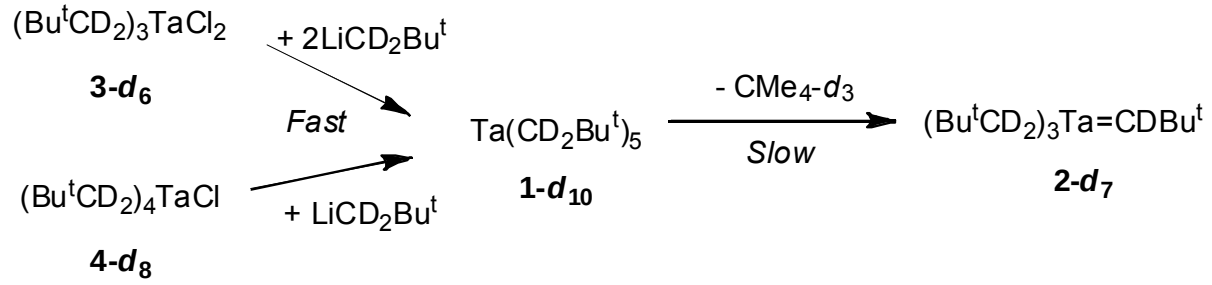

Scheme 2.2. Preparation of $Ta(CD_2Bu^t)_5$ (**1-*d*$_{10}$**) and its conversion to $(Bu^tCD_2)_3Ta{=}CDBu^t$ (**2-*d*$_7$**).

At 283 K, a single peak at 1.25 ppm was assigned to the methyl groups in **1-*d*$_{10}$**. This peak is close to that of the methyl groups in $Ta(CH_2Bu^t)_5$ (**1**) at 1.27 ppm at 258 K.[55,56] After the Bu^tCD_2Li peak at 1.12 ppm disappeared and the conversion of $(Bu^tCD_2)_3TaCl_2$ (**3-*d*$_6$**) and $(Bu^tCD_2)_4TaCl$ (**4-*d*$_8$**) to **1-*d*$_{10}$** was complete, the NMR probe was set to a desired temperature to observe the conversion of **1-*d*$_{10}$** to $(Bu^tCD_2)_3Ta{=}CDBu^t$ (**2-*d*$_7$**). Kinetic studies of the formation of **2-*d*$_7$** are discussed below.

The reaction of $(Bu^tCD_2)_3TaCl_2$ (**3-*d*$_6$**) with 2 equivalents of Bu^tCD_2Li to give $(Bu^tCD_2)_3Ta{=}CDBu^t$ (**2-*d*$_7$**) was also monitored by ^2H NMR spectroscopy. The reactants, **3-*d*$_6$** and Bu^tCD_2Li, intermediates $(Bu^tCD_2)_4TaCl$ (**4-*d*$_8$**) and $Ta(CD_2Bu^t)_5$ (**1-*d*$_{10}$**), and product **2-*d*$_7$** are expected to give resonances for their α-D atoms. ^2H NMR spectra of the reaction are given in Figure 2.2. At 283 K, the $–CD_2–$ groups of $Ta(CD_2Bu^t)_5$ (**1-*d*$_{10}$**) were observed at 1.39 ppm. This peak is close to the peak at 1.42 ppm in the ^1H NMR spectrum at 258 K for the $–CH_2–$ groups in

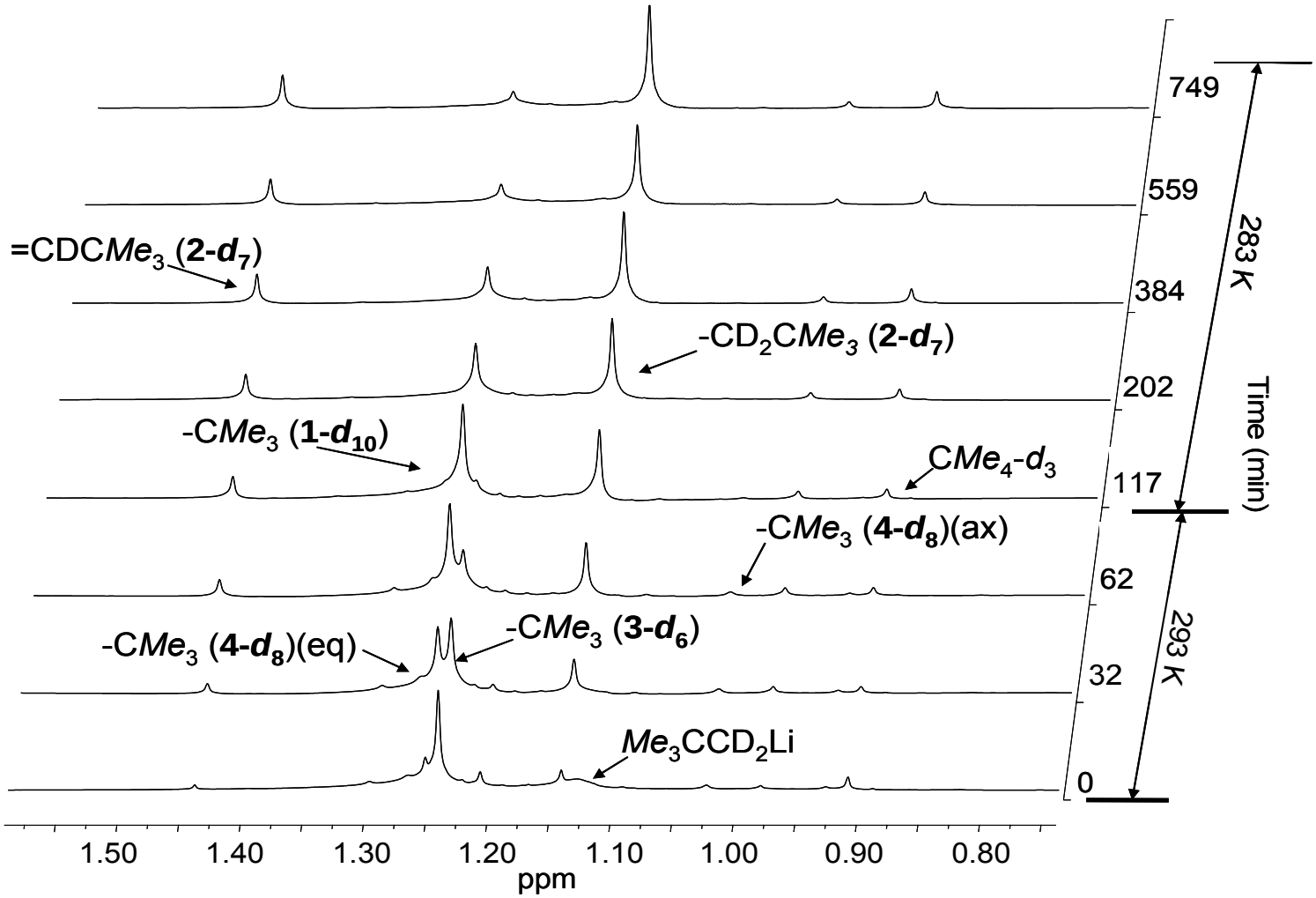

Figure 2.1. ^{1}H NMR spectra of the reaction between $(Bu^{t}CD_2)_3TaCl_2$ (**3-*d*$_6$**) and 2 equivalents of $Bu^{t}CD_2Li$ to give $(Bu^{t}CD_2)_3Ta{=}CDBu^{t}$ (**2-*d*$_7$**) in toluene-*d*$_8$.

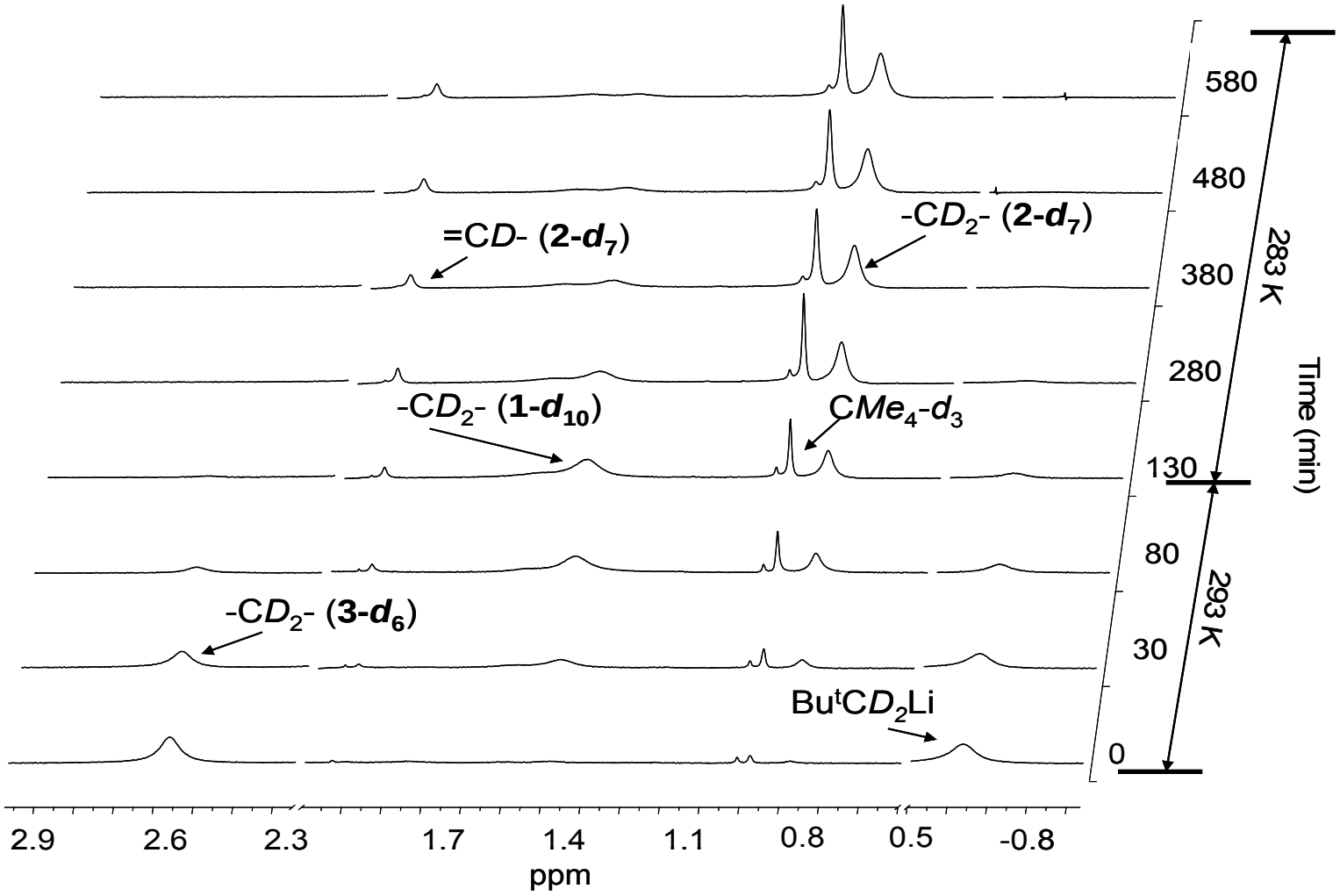

Figure 2.2. ^{2}H NMR spectra of the reaction between $(Bu^tCD_2)_3TaCl_2$ (**3-*d*$_6$**) and 2 equivalents of Bu^tCD_2Li to give $(Bu^tCD_2)_3Ta{=}CDBu^t$ (**2-*d*$_7$**) in toluene.

$Ta(CH_2Bu^t)_5$ (**1**),[55,56] supporting the assignment of this resonance in ^1H NMR spectra. The $–CD_2–$ peak of **1-*d*$_{10}$** reaches its maximum at approximately the same time as the methyl groups (1.25 ppm) in $Ta(CD_2Bu^t)_5$ (**1-*d*$_{10}$**) in the ^1H NMR spectra. These observations are consistent with the assignment of the $–CD_2–$ and $–CMe_3$ resonances in the NMR spectra to the same complex, **1-*d*$_{10}$**.

In the ^{13}C NMR spectra at 268 K, the $–CD_2–$ peak of $Ta(CD_2Bu^t)_5$ (**1-*d*$_{10}$**) was observed as a quintet at 114.8 ppm with a coupling constant $J_{C\text{-}D}$ of 15.9 Hz. In comparison, the $–CH_2–$ peak of $Ta(CH_2Bu^t)_5$ (**1**) was observed at 115.9 ppm with $J_{C\text{-}H}$ of 105.6 Hz at 258 K.[55,56]

2.2.2. Kinetic Studies of the Conversion of $Ta(CH_2Bu^t)_5$ (1) to $(Bu^tCH_2)_3Ta{=}CHBu^t$ (2) and $Ta(CD_2Bu^t)_5$ (1-*d*$_{10}$) to $(Bu^tCD_2)_3Ta{=}CDBu^t$ (2-*d*$_7$)

The reaction of Bu^tCH_2Li with $(Bu^tCH_2)_4TaCl$ (**4**), prepared in situ from $(Bu^tCH_2)_3Ta{=}CHBu^t$ (**2**) and HCl,[50] yielded $Ta(CH_2Bu^t)_5$ (**1**).[55,56] Two methods were used to collect kinetic data for the α-H abstraction reaction of the short-lived $Ta(CH_2Bu^t)_5$ (**1**) at 273 K. In one method, the solution was maintained at 233 K until Bu^tCH_2Li disappeared.[55,56] Then the reaction $Ta(CH_2Bu^t)_5$ (**1**) $\rightarrow$ $(Bu^tCH_2)_3Ta{=}CHBu^t$ (**2**) was conducted at 273 K, and at the end of each time period the reaction was quenched by cooling the NMR tube containing the solution to 233 K. ^1H spectra were then taken at 233 K (Figure 2.3).[57] In another method, the reaction of Bu^tCH_2Li with $(Bu^tCH_2)_4TaCl$ (**4**) was conducted in an NMR tube at 273 K, and kinetic data were collected after $(Bu^tCH_2)_4TaCl$ (**4**) disappeared. These two methods were found to give similar kinetic plots.

The α-H abstraction reaction of $Ta(CH_2Bu^t)_5$ (**1**) to yield the alkylidene complex $(Bu^tCH_2)_3Ta{=}CHBu^t$ (**2**) was found to follow first-order kinetics. A plot of ln (C/C_0) vs t at 273 K is given in Figure 2.4. The rate constant for the α-H abstraction reaction at 273 K from the aforementioned two methods is k_H = 1.76(0.06) × 10^{-4} s^{-1} [half-life, $t_{1/2}$ = 66(2) min].

We reported earlier the observation of $Ta(CH_2SiMe_3)_5$ (**6**) and its conversion through α-H abstraction to alkylidene complex $(Me_3SiCH_2)_3Ta{=}CHSiMe_3$ (**7**) and then to bridging alkylidyne complex $(Me_3SiCH_2)_2Ta(\mu\text{-}CSiMe_3)_2Ta(CH_2SiMe_3)_2$ (**8**) (Scheme 2.3).[55,56] $Ta(CH_2SiMe_3)_5$ (**6**) and $(Me_3SiCH_2)_3Ta{=}CHSiMe_3$ (**7**) containing β-Si atoms are analogs of $Ta(CH_2CMe_3)_5$ (**1**) and $(Me_3CCH_2)_3Ta{=}CHCMe_3$ (**2**). Kinetic studies of the **6** → **7** conversion showed that it is much slower than the **1** → **2** conversion. The **6** → **7** conversion was investigated between 301.0 and 326.5 K yielding $\Delta H^{\neq}_H$ = 21.6(1.4) kcal/mol and $\Delta S^{\neq}_H$ = –5(5) eu.[55,56] The rate constants for the conversion of **6** → **7** range from 1.028(0.008) × 10^{-4} s^{-1} [$t_{1/2}$ = 112(1) min] at 301.0 K to 1.83(0.02) × 10^{-3} s^{-1} [$t_{1/2}$ = 6.3(0.1) min] at 326.5 K. Extrapolation of the rate constants at 301.0-326.5 K to 273 K using the Eyring equation yields a rate constant of 2.65 × 10^{-6} s^{-1} ($t_{1/2}$ = 4.36 × 10^3 min or 72.7 h) for the **6** → **7** conversion. Given the rate constant of 1.76(0.06) × 10^{-4} s^{-1} for the $Ta(CH_2Bu^t)_5$ (**1**) → $(Bu^tCH_2)_3Ta{=}CHBu^t$ (**2**) conversion, the α-H abstraction reaction of the neopentyl complex $Ta(CH_2CMe_3)_5$ (**1**) is about 66.4 times faster than that of its β-Si analog $Ta(CH_2SiMe_3)_5$ (**6**) at 273 K. This difference is perhaps not surprising given that $Ta(CH_2CMe_3)_5$ (**1**) is expected to be much more crowded than $Ta(CH_2SiMe_3)_5$ (**6**).

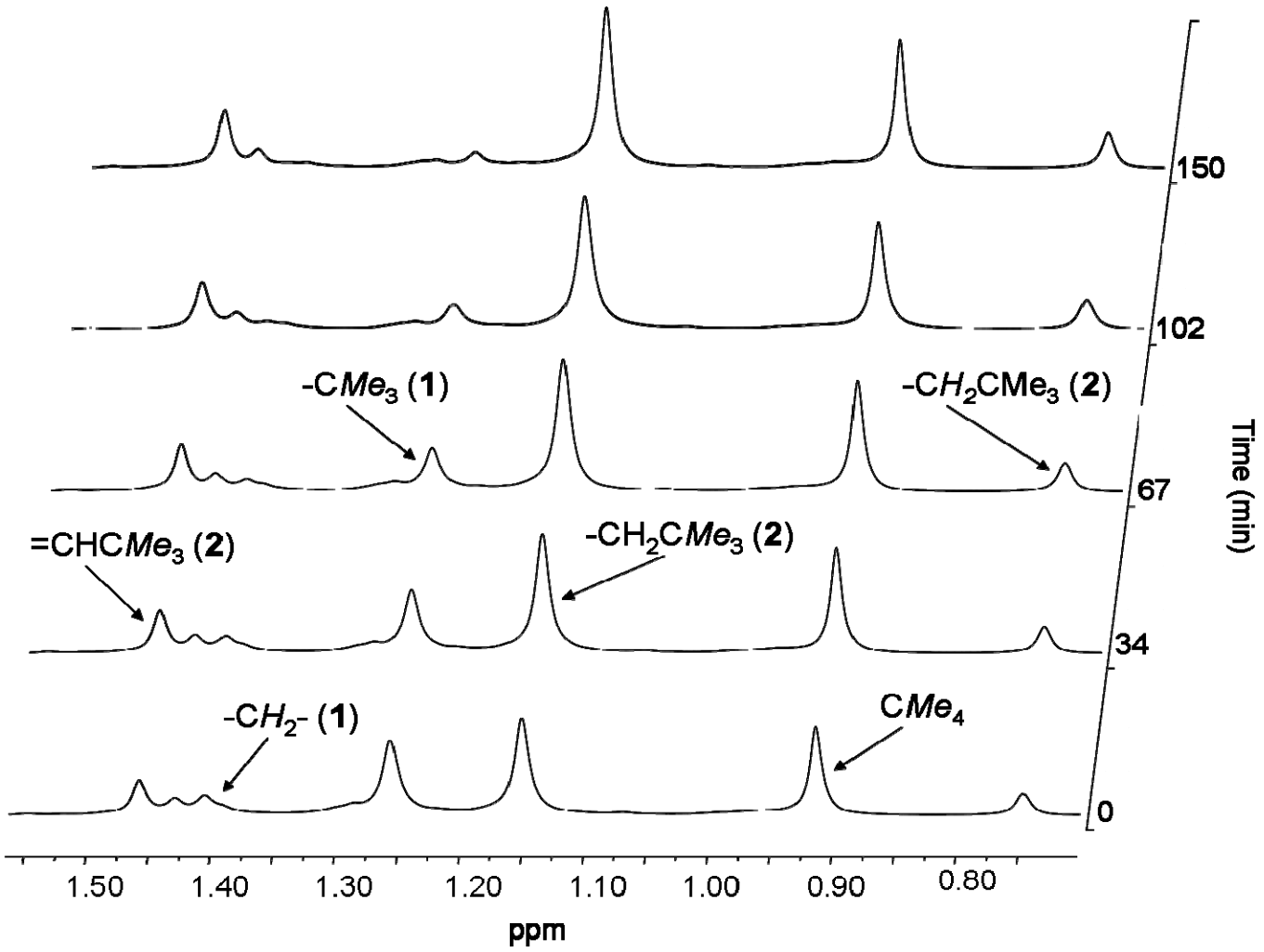

Figure 2.3. ^{1}H NMR spectra of the conversion of Ta(CH$_2$Bu^t)$_5$ (**1**) to (Bu^{t}CH$_2$)$_3$Ta=CHBu^t (**2**) in toluene-d_8 at 273 K.

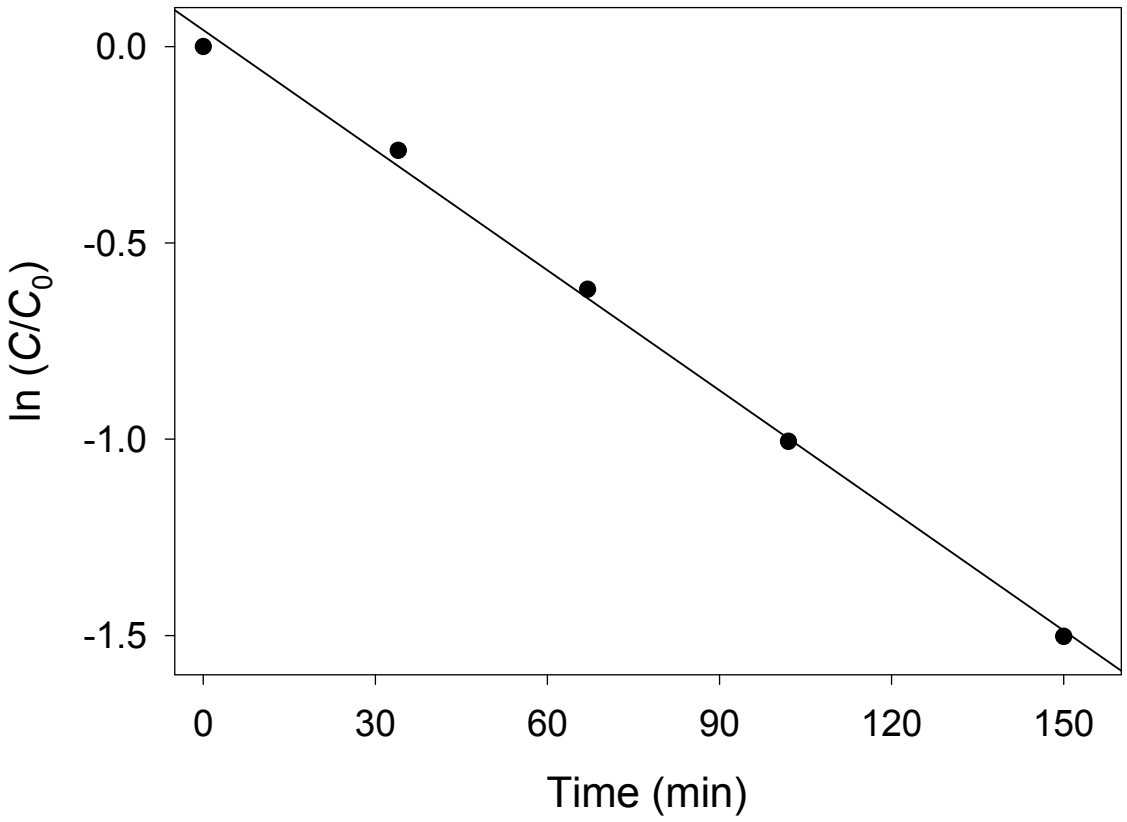

Figure 2.4. Kinetic plot of the conversion of $Ta(CH_2Bu^t)_5$ (**1**) to $(Bu^tCH_2)_3Ta{=}CHBu^t$ (**2**) at 273 K.

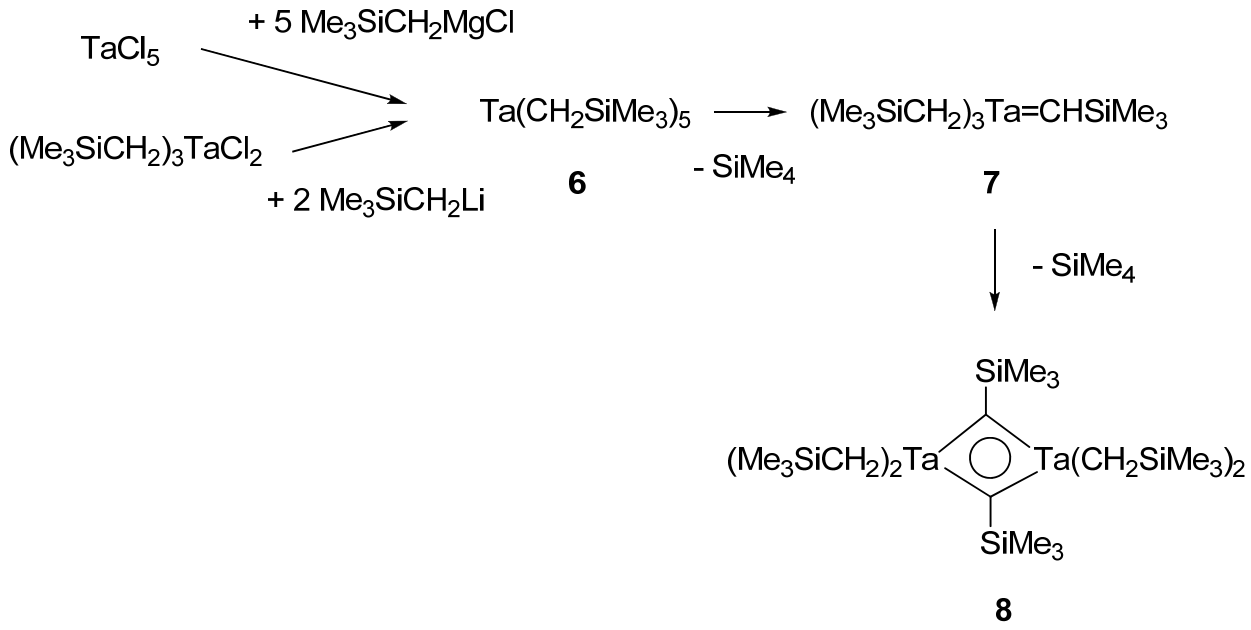

Scheme 2.3. $Ta(CH_2SiMe_3)_5$ (**6**) and its conversion to $(Me_3SiCH_2)_3Ta{=}CHSiMe_3$ (**7**) and then to $(Me_3SiCH_2)_2Ta(\mu\text{-}CSiMe_3)_2Ta(CH_2SiMe_3)_2$ (**8**).

A typical C-C bond length is 1.54 Å versus a typical C-Si bond length of 1.89 Å.

Decomposition of $Ta(CH_2Ph)_5$ (**9**), another pentaalkyl complex free of β-H atoms, has also been studied.[58] This decomposition leads to unknown species, and no NMR signal attributed to "$(PhCH_2)_3Ta{=}CHPh$" was observed in the decomposition process. Kinetic studies of the decomposition of $Ta(CH_2Ph)_5$ (**9**) at 313 K gave a rate constant of $3.8–4.3 \times 10^{-5}$ s^{-1} ($t_{1/2}$ = 269-304 min).[58] The decomposition of $Ta(CH_2Ph)_5$ (**9**) is about 10 times slower than that of $Ta(CH_2SiMe_3)_5$ (**6**) at 313 K. Kinetic studies of the decomposition involving $Ta(CH_2CMe_3)_5$ (**1**) were conducted at temperatures much lower than those involving $Ta(CH_2SiMe_3)_5$ (**6**) and $Ta(CH_2Ph)_5$ (**9**). Yet it is reasonable to show that decomposition rates of the three complexes are: $Ta(CH_2CMe_3)_5$ (**1**) > $Ta(CH_2SiMe_3)_5$ (**6**) > $Ta(CH_2Ph)_5$ (**9**).

The current work to observe $Ta(CD_2Bu^t)_5$ (**1-*d*$_{10}$**) and its conversion to $(Bu^tCD_2)_3Ta{=}CDBu^t$ (**2-*d*$_7$**) by ^1H and ^2H spectroscopy provides clear evidence that pentaneopentyltantalum (**1**) is an intermediate to the alkylidene complex **2**. The use of the D-labeled complex also offers the opportunity to further probe kinetics of the formation of the alkylidene complex $(Bu^tCD_2)_3Ta{=}CDBu^t$ (**2-*d*$_7$**) including kinetic isotope effect (KIE).

Kinetic studies of the conversion of $Ta(CD_2Bu^t)_5$ (**1-*d*$_{10}$**) to $(Bu^tCD_2)_3Ta{=}CDBu^t$ (**2-*d*$_7$**) were conducted after $(Bu^tCD_2)_4TaCl$ (**4-*d*$_8$**) and $(Bu^tCD_2)_3TaCl_2$ (**3-*d*$_6$**) had disappeared in ^1H NMR spectra. At this time, no more **1-*d*$_{10}$** was expected to form, and the time was counted as t = 0 min. The α-D abstraction reaction of $Ta(CD_2Bu^t)_5$ (**1-*d*$_{10}$**) to $(Bu^tCD_2)_3Ta{=}CDBu^t$ (**2-*d*$_7$**) was found to follow first-order kinetics. Plots of ln (C/C_0) vs. t at six different temperatures between 273 and 298 K are shown in

Figure 2.5. The rate constants at these temperatures are listed in Table 2.1. An Eyring plot of ln (k_D/T) vs. 1000/T is shown in Figure 2.6. The activation parameters derived for the conversion of **1-*d*$_{10}$** to **2-*d*$_7$** are $\Delta H^{\neq}_D$ = 21.1(1.5) kcal/mol, $\Delta S^{\neq}_D$ = -4(6) eu, and $\Delta G^{\neq}_{D,273K}$ = 22(3) kcal/mol. Near-zero or negative values for $\Delta S^{\neq}$ have been observed in C-H bond activation reactions where concerted four-center transition states, especially those involving cyclometalation, are proposed.[59-65] An example of such transition state is given in Scheme 2.4. A kinetic isotope effect (KIE) was calculated for the α-H/D abstraction of **1**/**1-*d*$_{10}$** at 273 K. Kinetics of the α-H abstraction in **1** was studied only at 273 K. At a higher temperature, the lifetime of **1** is too short to be measured accurately at the present time. At a lower temperature, the kinetics of decomposition of **1-*d*$_{10}$** is too slow. The rate constants at 273 K for the two abstraction reactions were k_H = 1.76 x 10^{-4} s^{-1} and k_D = 1.25 x 10^{-5} s^{-1}, giving the KIE (= k_H/k_D) of 14.1(0.8). $\Delta G^{\neq}_{H,273K}$ for the α-H abstraction reaction of $Ta(CH_2Bu^t)_5$ (**1**) may be estimated from the kinetic isotope effect and the Eyring equation: RT ln (k_H/k_D) = $\Delta G^{\neq}_D - \Delta G^{\neq}_H$, yielding $\Delta G^{\neq}_{H,273K}$ = 21(3) kcal/mol. In the calculation here, the C-H/C-D stretching frequency is assumed to disappear in the transition state to break the bond.[66] The activation free energy for the α-hydrogen abstraction reaction of $Ta(CH_2SiMe_3)_5$ (**6**), in comparison, is estimated to be $\Delta G^{\neq}_{H,273K}$ = 23(3) kcal/mol.[55,56]

The KIE in the current work is larger than usual. Average KIEs are found to be 4-7.[67] Large KIEs have been observed in hydrogen abstraction reactions[68-70] and electrophilic protonolysis of transition metal complexes.[71] A common contribution to a larger than normal KIE is a secondary KIE. Secondary KIE's are usually

considered when there is an isotopic substitution more than one bond away from the one being broken in the reaction.[67] In the reaction of **1-*d*$_{10}$** → **2-*d*$_7$** there are two deuterium atoms not involved in the bond breaking, but this contribution usually only increases the primary KIE by 1-2.[67] Larger KIE values have also been attributed to the tunneling effect for lighter H atoms, leading to the faster C-H bond breaking reaction.[68,71-75] The tunneling effect is reportedly more prominent for sterically crowded molecules.[75] Given the instability of $Ta(CH_2Bu^t)_5$ (**1**) and $Ta(CD_2Bu^t)_5$ (**1-*d*$_{10}$**) and limited experimental data in the current work, it is not feasible at present to obtain KIE values over a larger temperature range for the **1** → **2** conversion to study the tunneling effect.[76-78]

2.3. Concluding Remarks

Deuterium-labeled $Ta(CD_2Bu^t)_5$ (**1-*d*$_{10}$**) has been prepared from the reactions of $(Bu^tCD_2)_3TaCl_2$ (**3-*d*$_6$**) with 2 equivalents of Bu^tCD_2Li as well as $(Bu^tCD_2)_4TaCl$ (**4-*d*$_8$**) with 1 equivalent of Bu^tCD_2Li. Due to a kinetic isotope effect, $Ta(CD_2Bu^t)_5$ (**1-*d*$_{10}$**) has a much longer life than $Ta(CH_2Bu^t)_5$. In addition, there are fewer peaks in the ^1H NMR spectra of $Ta(CD_2Bu^t)_5$ (**1-*d*$_{10}$**). ^2H NMR spectroscopy could also be used to characterize **1-*d*$_{10}$**. These properties, along with ^{13}C NMR, provided an opportunity to identify and study **1-*d*$_{10}$** in detail. Kinetic studies of the $Ta(CD_2Bu^t)_5$ (**1-*d*$_{10}$**) → $(Bu^tCD_2)_3Ta{=}CDBu^t$ (**2-*d*$_7$**) and $Ta(CH_2Bu^t)_5$ (**1**) → $(Bu^tCH_2)_3Ta{=}CHBu^t$ (**2**) conversions yield a kinetic isotope effect (KIE) = 14.1(0.8) at 273 K. Even though this value is higher than generally observed, KIEs of such a magnitude or higher

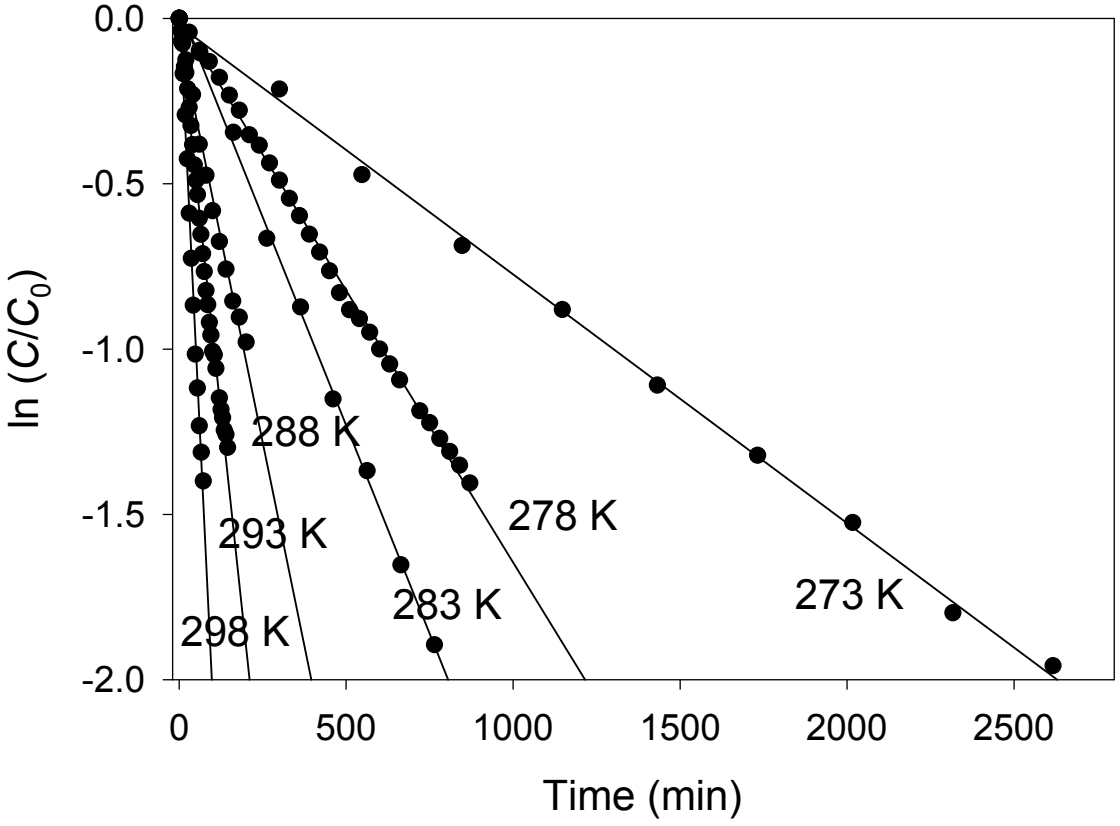

Figure 2.5. Kinetic plots of the conversion of **1-d_{10}** → **2-d_7**.

Table 2.1. Measured rate constants k for the **1-d_{10}** $\rightarrow$ **2-d_7** conversion.[a]

T (K)	$k \times 10^5$ (s^{-1})
273(1)	1.25(0.03)
278(1)	2.17(0.12)
283(1)	4.28(0.08)
288(1)	8.4(0.3)
293(1)	16.9(1.4)
298(1)	34.8(1.5)

[a] The total uncertainty $\delta k/k$ of 0.095 was calculated from $\delta k_{ran}/k$ = 0.081 and $\delta k_{sys}/k$ = 0.05.[79,80]

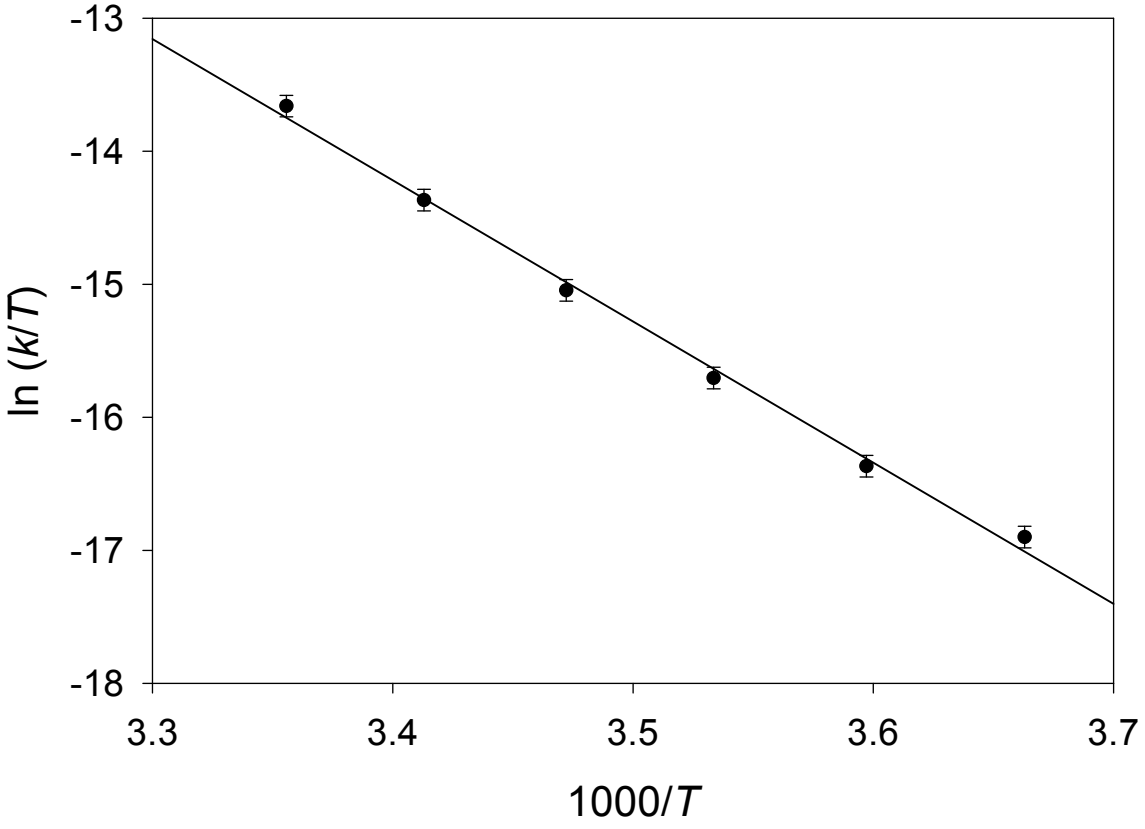

Figure 2.6. Eyring plot of the conversion of **1-d_{10}** → **2-d_7**.

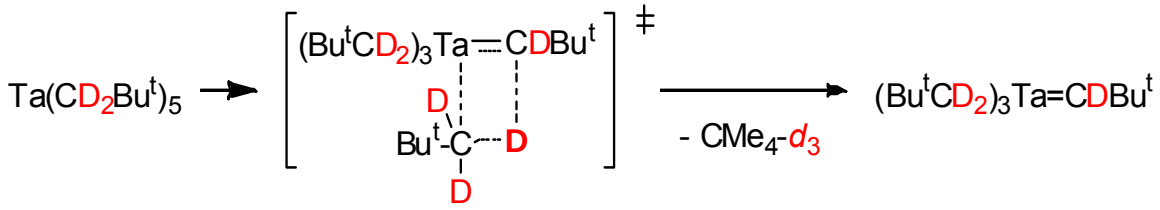

Scheme 2.4. Concerted four-center transition state in the conversion **1-*d*$_{10}$** → **2-*d*$_7$**.

conversions yield a kinetic isotope effect (KIE) = 14.1(0.8) at 273 K. Even though this value is higher than generally observed, KIEs of such a magnitude or higher have been reported.[68-75] In addition, kinetic studies of the **1-*d*$_{10}$** → **2-*d*$_7$** conversion at 273-298 K gave $\Delta H^{\neq}_{D}$ = 21.1(1.5) kcal/mol, $\Delta S^{\neq}_{D}$ = -4(6) eu, and $\Delta G^{\neq}_{D,273K}$ = 22(3) kcal/mol for the α-D abstraction reaction. $\Delta G^{\neq}_{H,273K}$ for the α-H abstraction reaction of $Ta(CH_2Bu^t)_5$ (**1**) was also calculated using the KIE value and the Eyring equation to give a value of 21(3) kcal/mol.

2.4. Experimental Section

All manipulations were preformed under a dry nitrogen or argon atmosphere with the use of either a drybox or standard Schlenk techniques. Ether, toluene and toluene-d_8 were dried over potassium/benzophenone, distilled and stored under N_2. Benzene-d_6 was dried over activated molecular sieves, stored under N_2, and used in the identification of several complexes after their synthesis. NMR spectra were recorded on a Bruker AMX-400 Fourier transform spectrometer and were referenced

to solvents. In the case of ^{2}H NMR spectra, a small amount of toluene-d_8 was added to toluene for reference. Bu^tCD_2Br,[50,65,81] $(Bu^tCD_2)_3TaCl_2$ (**3-d_6**),[50] and Bu^tCD_2Li[50] were prepared by the literature procedures. $ZnCl_2$ was dried by refluxing with $SOCl_2$.[50] $(Bu^tCH_2)_4TaCl$ (**4**) was prepared in situ from **2** and HCl.[50] DCl and HCl in ether (1.0 M) were purchased from Aldrich. They were each diluted to 0.10 M with ether before use.

The rate constants were the average of at least two separate experiments at each temperature. The *maximum* random uncertainty in the rate constants for each reaction was combined with the estimated systematic uncertainties, ca 5%.[79,80] The total uncertainties in the rate constants were used in the Eyring plots and in the following error propagation calculations. The estimated uncertainty in the temperature measurements for an NMR probe (used in the *k* determinations) was 1 K. The activation enthalpies ($\Delta H^{\neq}_D$) and entropies ($\Delta S^{\neq}_D$) were calculated from an unweighted nonlinear least-squares procedure contained in the SigmaPlot Scientific Graph System. The uncertainties in $\Delta H^{\neq}_D$ and $\Delta S^{\neq}_D$ were computed from the error propagation formulas derived from the Eyring equation by Girolami and coworkers.[82]

2.4.1. Preparation of $Zn(CD_2Bu^t)_2$

$Zn(CD_2Bu^t)_2$ was prepared earlier from Bu^tCD_2Li and $ZnCl_2$·dioxane.[50] In the current work, it was directly prepared from Bu^tCD_2MgBr and $ZnCl_2$. The Grignard reagent Bu^tCD_2MgBr was prepared by adding Bu^tCD_2Br (20.37 g, 133.1 mmol) dropwise to Mg turnings (3.251 g, 133.8 mmol) in ether (50 mL). Several drops of $BrCH_2CH_2Br$ were used to initiate the reaction, and the solution was refluxed for 20 h

at 45 °C. Filtration gave a solution of Bu^tCD_2MgBr in ether (75 mL, 0.95 M, 71 mmol, 53% yield). The concentration of the Grignard solution was determined by adding 1.0 mL of the solution into distilled water to form Mg(OH)Br and CMe_3CD_2H. Titration of the aqueous Mg(OH)Br solution using 0.096 M HCl gave the concentration of the Bu^tCD_2MgBr solution.

The solution of Bu^tCD_2MgBr was added slowly to $ZnCl_2$ (4.62 g) in ether (40 mL) at -20 °C, and stirred for two days at room temperature. Filtration, removal of ether, and distillation of the product yielded $Zn(CD_2Bu^t)_2$ (5.019 g, 23.74 mmol, 70% yield), which was then used to make $(Bu^tCD_2)_3TaCl_2$ (**3-*d*$_6$**) according to the literature procedures.[50]

2.4.2. In-situ Preparation of $Ta(CD_2Bu^t)_5$ (1-d_{10}) and Its Conversion to $(Bu^tCD_2)_3Ta{=}CDBu^t$ (2-d_7)

*Preparation of $Ta(CD_2Bu^t)_5$ (**1-d_{10}**) from the reaction between $(Bu^tCD_2)_3TaCl_2$ (**3**-d_6) and Bu^tCD_2Li.* $(Bu^tCD_2)_3TaCl_2$ (**3-*d*$_6$**) (40.0 mg, 0.0849 mmol) and Bu^tCD_2Li (17 mg, 0.21 mmol)[83] were each dissolved in toluene-d_8 at -78 °C. They were mixed in an NMR tube (total volume = 4.0 mL) at -78 °C, giving a dark yellow solution. The sample was kept at -78 °C until ready for use. ^{1}H NMR spectra of the solution were taken at 10 °C.

The reaction between $(Bu^tCD_2)_3TaCl_2$ (**3-*d*$_6$**) and Bu^tCD_2Li was conducted similarly in toluene containing a small amount of toluene-d_8. ^{2}H NMR spectra of the solution were collected using toluene-d_8 as internal standard. **1-*d*$_{10}$**: ^{1}H NMR (toluene-d_8, 399.7 MHz, 10 °C) δ 1.25 (s, 45H, Me_3CCD_2); ^{2}H NMR (toluene, 61.4

MHz, 10 °C) δ 1.39 (s, 10D, Me_3CCD_2); $^{13}C\{^1H\}$ NMR (toluene-d_8, 100.5 MHz, -5 °C) δ 114.8 (quintet, Me_3CCD_2, J_{C-D} = 15.9 Hz), 36.3 (Me_3CCD_2), 35.2 (Me_3CCD_2). **2-d_7**: ^1H NMR (toluene-d_8, 399.7 MHz, 10 °C) δ 1.44 (s, 9H, Me_3CCD=), 1.14 (s, 27H, Me_3CCD_2); ^2H NMR (toluene, 61.4 MHz, 10 °C) δ 1.90 (s, 1D, Me_3CCD=), 0.88 (s, 6D, Me_3CCD_2); $^{13}C\{^1H\}$ NMR (toluene-d_8, 100.5 MHz, -5 °C) δ 248.7 (t, Me_3CCD=, J_{C-D} = 14.1 Hz), 112.3 (quintet, Me_3CCD_2, J_{C-D} = 16.2 Hz), 47.0 (Me_3CCD=), 34.9 (Me_3CCD_2), 34.8 (Me_3CCD_2), 34.6 (Me_3CCD=).

*Preparation of $Ta(CD_2Bu^t)_5$ (**1-d_{10}**) from the reaction between $(Bu^tCD_2)_4TaCl$ (**4**-d_8) and Bu^tCD_2Li.* $(Bu^tCD_2)_4TaCl$ (**4-d_8**) was prepared from $(Bu^tCD_2)_3Ta{=}CDBu^t$ (**2-d_7**) and DCl (0.10 M, ether). $(Bu^tCD_2)_3Ta{=}CDBu^t$ (**2-d_7**, 30 mg, 0.064 mmol) was added to a flask in ether (10 mL). DCl (0.64 mL, 0.10 M, ether) was added slowly at -78 °C. The mixture was stirred for 30 min, and then solvent was removed. The solid was redissolved in toluene-d_8 and kept at -78 °C. An NMR tube was prepared with Bu^tCD_2Li (5.6 mg, 0.070 mmol)[83] in toluene-d_8 and cooled to -78 °C. The unstable $(Bu^tCD_2)_4TaCl$ (**4**-d_8) was quickly added to the NMR tube and the sample was kept at -78 °C until ready for use. ^1H NMR spectra of the solution were taken at 0 °C.

2.4.3. Kinetic Studies of the Conversion of $Ta(CD_2Bu^t)_5$ (1-d_{10}) to $(Bu^tCD_2)_3Ta{=}CDBu^t$ (2-d_7)

$(Bu^tCD_2)_3TaCl_2$ (**3-d_6**, 40.0 mg, 0.085 mmol) and Bu^tCD_2Li (17 mg, 0.21 mmol)[83] were dissolved in toluene-d_8 in separate NMR tubes. Bibenzyl (20-25 mg, an internal standard) was added to the solution of **3-d_6**. The samples were kept at -78 °C. The solution of **3-d_6**/bibenzyl was added to that of Bu^tCD_2Li, and kept at -78

°C until use. Initial NMR spectra were taken at 293 K until the peaks representing $(Bu^tCD_2)_3TaCl_2$ (**3-*d*$_6$**) and Bu^tCD_2Li had disappeared. Then ^1H NMR spectra were taken at the end of each time period at 273(1), 278(1), 283(1), 288(1), 293(1), and 298(1) K for kinetic measurements until the conversion of **1-*d*$_{10}$** to $(Bu^tCD_2)_3Ta{=}CDBu^t$ (**2-*d*$_7$**) was complete.

2.4.4. Kinetic Studies of the Conversion of $Ta(CH_2Bu^t)_5$ (1) to $(Bu^tCH_2)_3Ta{=}CHBu^t$ (2)

In the first method, $(Bu^tCH_2)_4TaCl$ (**4**)[50] in toluene-d_8 at -78 °C was mixed with Bu^tCH_2Li in toluene-d_8 at -78 °C. The solution was kept in the pre-cooled NMR spectrometer at -40 °C until Bu^tCH_2Li disappeared.[55,56] The reaction was then conducted at 0.0 °C in a circulation bath and quenched at -40 °C at the end of each time period to take ^1H spectra. After **4** disappeared, subsequent ^1H spectra and the peaks of $Ta(CH_2Bu^t)_5$ (**1**) were used in the kinetic studies.[57]

In the second method, **4**, prepared in situ from **2** (60.0 mg, 0.129 mmol) and HCl (1.40 mL, 0.10 M, ether) at -78 °C,[50] was redissolved in toluene-d_8 at -78 °C and then added to a solution of Bu^tCH_2Li (12 mg, 0.15 mmol) and bibenzyl (20 mg, internal standard) in toluene-d_8 at -78 °C. The NMR tube containing the mixture was then placed into an NMR spectrometer pre-cooled to 0 °C. The reaction was conducted at 0 °C and ^1H spectra were taken directly at this temperature and were used for kinetic studies.

Chapter 3

Tantalum Neopentyl and Neopentylidene Complexes. Isotopic Shifts and Conformational Studies

3.1. Introduction

The previous chapter of this dissertation focuses on the mechanism and kinetics of the formation of $(Bu^tCH_2)_3Ta{=}CHBu^t$ (**2**) using deuterated analogs. This chapter focuses on studies of the compounds themselves. First, chemical shift differences observed in the NMR between the deuterated and non-deuterated compounds are reported. Second, the structural conformation of the intermediate, $Ta(Bu^tCD_2)_5$ (**1-*d*$_{10}$**), and the starting material, $(Bu^tCD_2)_3TaCl_2$ (**3-*d*$_6$**), are studied using NMR. $TaEt_5$ (**10**) was used as a model in the conformational studies using DFT.

3.1.1. Isotopic Shifts in NMR

It has been shown that isotope substitution can affect the chemical shifts of compounds.[84-95] An NMR shift is based on the specific magnetic and chemical environment of an atom in a molecule. When one atom in the molecule is substituted with an isotope there are subtle changes in the electronic and magnetic structure of the molecule. The shielding of a nucleus is a function of the bond lengths in the molecule.[86] With the substitution of an isotope, bond lengths can change leading to a

change in chemical shift.[94] When an atom in a compound is substituted by a heavier isotope containing more neutrons, other nuclei in the molecule experience an increase in magnetic shielding by the neutrons in the heavier isotope, resulting in an upfield NMR shift.[84] The size of the shift is dependent on the distance of the nuclei in question to the isotopic substitution. The greater the number of bonds between the nuclei, the smaller the magnitude of the shift .[84]

The isotopic substitution leads to a change in the vibrational zero-point energy.[84] The C-H and C-D bonds have different zero-point energies. This energy for the C-D bond is lower than that for the corresponding C-H bond. Thus kinetic barriers for isotopomers are different. This is also the basis for the kinetic isotope effect, which is discussed in the previous chapter of this dissertation.

In this chapter, NMR experiments were preformed to determine the effect that substituting deuterium for hydrogen at the alpha position in $(Bu^tCH_2)_3TaCl_2$ (**3**), $(Bu^tCH_2)_5Ta$ (**1**), and $(Bu^tCH_2)_3Ta{=}CHBu^t$ (**2**) has on the chemical shifts of the other hydrogen and carbon atoms in the compounds.

3.1.2. Conformational Studies

Binary alkyl metal complexes have been the subject of many studies, starting in 1959 with the synthesis of $TiMe_4$.[96] Early transition metal alkyl complexes decompose quickly through β-hydrogen elimination. The binary alkyl complexes do not contain β-hydrogen atoms, and thus were found to be more stable. Following the synthesis of $TiMe_4$, many other d^0 metal complexes have been synthesized, including MMe_x (M = Zr, Ta, Nb, W), MPh_x (M = Ti, Zr, V), $M(CH_2Ph)_x$ (M = Ti, Zr, Hf, Ta), and

$M(CH_2SiMe_3)_x$ (M = Ti, Zr, Hf, V, Ta).[55,97-102] As discussed in Chapter 2, attempts to synthesize $Ta(CH_2Bu^t)_5$ (**1**, as well as the Nb analog) resulted in the discovery of the first alkylidene complex by Schrock.[3]

The molecular structures of a few tantalum pentaalkyl complexes have been published.[103-105] The question has been posed as to whether the compounds adopt a trigonal bipyramidal or a square pyramidal structure (Figure 3.1). The bulkiness of the ligands in **1** is expected to lead to trigonal bipyramidal structures, but in the cases cited above, all three compounds were found to be square pyramidal.[103-105] Work done by Haaland and coworkers[104] elucidated the structure of $TaMe_5$ and $SbMe_5$. They stated that this was the first structural determination of any pentaalkyl complex. They found that $TaMe_5$ adopts a square pyramidal structure, but $SbMe_5$ has a

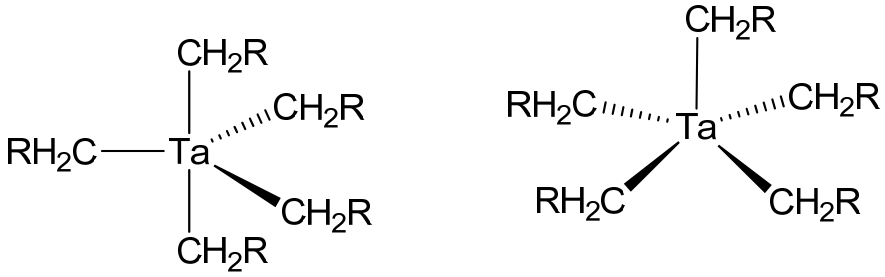

Figure 3.1. Predicted structures of tantalum pentaalkyl complexes.

trigonal bipyramidal structure. They explain this finding by the fact that d orbitals are more involved in the formation of $TaMe_5$, and their orientation around the metal favors square pyramidal over trigonal bipyramidal. These results agree with previous theoretical calculations as well.[106,107]

We have shown in previous work that the precursor to **1**, $(Bu^tCH_2)_4TaCl$ (**4**), has a trigonal bipyramidal structure at -40 °C.[55] The data regarding the structure of $(Bu^tCH_2)_3TaCl_2$ (**3**) are inconclusive because its NMR spectrum shows only one resonance at -40 °C.[55] This is also true for $Ta(CH_2Bu^t)_5$ (**1**) which is too unstable to study in detail. The purpose of this chapter is to probe further, through NMR and DFT studies, the structure of the intermediate, $Ta(CH_2Bu^t)_5$ (**1**), to the Schrock carbene through the use of the deuterated analog. Also given is an NMR study of the conformation of $(Bu^tCH_2)_3TaCl_2$ (**3**).

3.2. Results and Discussion

3.2.1. Isotopic Shifts of $(Bu^tCD_2)_3TaCl_2$ (3-d_6), $Ta(CD_2Bu^t)_5$ (1-d_{10}), and $(Bu^tCD_2)_3Ta{=}CDBu^t$ (2-d_7) versus Their Non-Deuterated Counterparts

^1H and ^{13}C NMR were taken of solutions containing $(Bu^tCH_2)_3TaCl_2$ (**3**) and $(Bu^tCD_2)_3TaCl_2$ (**3-d_6**), $(Bu^tCH_2)_5Ta$ (**1**) and $(Bu^tCD_2)_5Ta$ (**1-d_{10}**), and $(Bu^tCH_2)_3Ta{=}CHBu^t$ (**2**) and $(Bu^tCD_2)_3Ta{=}CDBu^t$ (**2-d_7**), respectively. The chemical shifts of each are listed in Table 3.1.

Table 3.1. Chemical shifts of **3**, **3-*d*$_6$**, **1**, **1-*d*$_{10}$**, **2**, and **2-*d*$_7$**.

	^{1}H[a]			^{13}C{^{1}H}[a]		
	E = D	E = H	Difference in ppm	E = D	E = H	Difference in ppm
$(\mathit{Me}_3CCE_2)_3TaCl_2$	1.228	1.233	0.005	34.903	34.926	0.023
$(Me_3\mathit{C}CE_2)_3TaCl_2$	n.a.[c]	n.a.	n.a.	34.342	34.589	0.247
$(Me_3C\mathit{CE}_2)_3TaCl_2$	n.a.	n.a.	n.a.	113.355	114.908	1.553
$Ta(CE_2C\mathit{Me}_3)_5$	1.273	1.284[b]	0.011	35.135	35.152[b]	0.017
$Ta(CE_2\mathit{C}Me_3)_5$	n.a.	n.a.	n.a.	36.290	36.520[b]	0.230
$Ta(\mathit{C}E_2CMe_3)_5$	n.a.	n.a.	n.a.	114.750	115.641[b]	0.891
$(\mathit{Me}_3CCE_2)_3Ta{=}CECMe_3$	1.138	1.140	0.002	34.903	34.931	0.028
$(Me_3\mathit{C}CE_2)_3Ta{=}CECMe_3$	n.a.	n.a.	n.a.	35.308	35.310	0.002
$(Me_3C\mathit{C}E_2)_3Ta{=}CECMe_3$	n.a.	n.a.	n.a.	112.356	113.664	1.308
$(Me_3CCE_2)_3Ta{=}\mathit{C}ECMe_3$	n.a.	n.a.	n.a.	249.127	249.857	0.730
$(Me_3CCE_2)_3Ta{=}CE\mathit{C}Me_3$	n.a.	n.a.	n.a.	47.007	47.039	0.032
$(Me_3CCE_2)_3Ta{=}CEC\mathit{Me}_3$	1.431	1.431	0	34.644	34.670	0.026

[a] Spectra were taken on a 400 MHz NMR spectrometer and the samples were dissolved in toluene-d_8.

[b] Chemical shifts were taken from previous work.[55]

[c] n.a. = not applicable

In the ^{1}H NMR spectra of $(Bu^tCH_2)_3TaCl_2$ (**3**) and $(Bu^tCD_2)_3TaCl_2$ (**3-*d*$_6$**) (Figure 3.2), the difference between the methyl resonances of the complexes is 0.005 ppm. This is similar to results found in other neopentyl chloride complexes.[108] Among the three different carbon signals in the ^{1}H-decoupled ^{13}C NMR spectra (Figure 3.3), the chemical shift difference between the corresponding carbons in the two isotopomers decreases the farther the carbon atom is from the deuterium atom. For the $-CH_2-/-CD_2-$ peaks, the $-CH_2-$ is a singlet because the experiment is ^{1}H-decoupled, but the $-CD_2-$ is a quintet as a result of deuterium coupling to carbon. Deuterium has a nuclear spin of 1, and the ^{13}C peak splitting is five according to the spin-spin splitting equation, $2I + 1$, where I is the sum of the nuclear spins of the coupled atoms. The separation of 1.55 ppm between the $-CH_2-$ and $-CD_2-$ peaks is the largest of the three resonances. This is because the carbon atom is in closest proximity to the deuterium atoms. The quaternary carbon is two bonds away from the deuterium, and there is a reduction in the separation of the peaks to 0.25 ppm. The final carbon resonance is from the three methyl carbons, and the separation between these peaks is 0.03 ppm.

Isotopic shifts were also observed in the ^{1}H and ^{13}C NMR spectra of $Ta(CD_2Bu^t)_5$ (**1-*d*$_{10}$**) and $Ta(CH_2Bu^t)_5$ (**1**). These compunds were difficult to compare, because the conversion of **1** to **2** occurs very quickly and the intermediate has a very short lifetime [$t_{1/2}$ = 66(2) min at 0 °C]. In addition, both isotopomers are prepared in situ from $(Bu^tCE_2)_3TaCl_2$ and Bu^tCE_2Li (E = H or D). For these reasons, placing both isotopomers in the same NMR sample is nearly impossible. Instead, NMR spectra from previous work on $(Bu^tCH_2)_5Ta$ (**1**) at -40 °C[55] were used. New spectra of

$(Bu^tCD_2)_5Ta$ (**1-*d*$_{10}$**) were taken at -40 °C for comparison. The two spectra were superimposed using the NMR analysis program Mestrenova, version 6.1. These spectra are given in Figures 3.4 and 3.5. It should be noted that the differences are not as accurate as they would be if they were recorded at the same time and in the same sample. In the ^{1}H NMR, the difference of the methyl resonances is 0.011 ppm. This is larger than the difference in Figure 3.2 for **3/3-*d*$_6$** or Figure 3.6 for **2/2-*d*$_7$,** and is probably due to the NMR spectra not being taken in the same sample. In the ^{13}C NMR spectra, the three resonances follow the same trend as the other complexes: chemical shift separations increase with increasing proximity to the isotope atoms.

Finally, isotopic shifts were observed for the carbene compounds, $(Bu^tCH_2)_3Ta{=}CHBu^t$ (**2**), and $(Bu^tCD_2)_3Ta{=}CDBu^t$ (**2-*d*$_7$**). Similar to the two previous samples, the farther the carbon atoms are from the deuterium atoms in the compound, the less the isotopic shift is. In the ^{1}H NMR spectrum, a shift of 0.002 ppm was observed for the methyl groups in the neopentyl ligands. No distinguishable shift was observed for the methyl groups of the carbene ligand, but the peak was broader than expected. This is probably because the carbene ligand only has one deuterium atom while the neopentyl ligands have two deuterium atoms each. Since the methyl carbon is three bonds from the deuterium, it is expected to exhibit only a small shift. With only one deuterium, however, the shift becomes less distinguishable on 400 MHz NMR. Increasing the NMR field strength to 600 MHz did not improve the resolution. The ^{1}H NMR spectra are given in Figure 3.6.

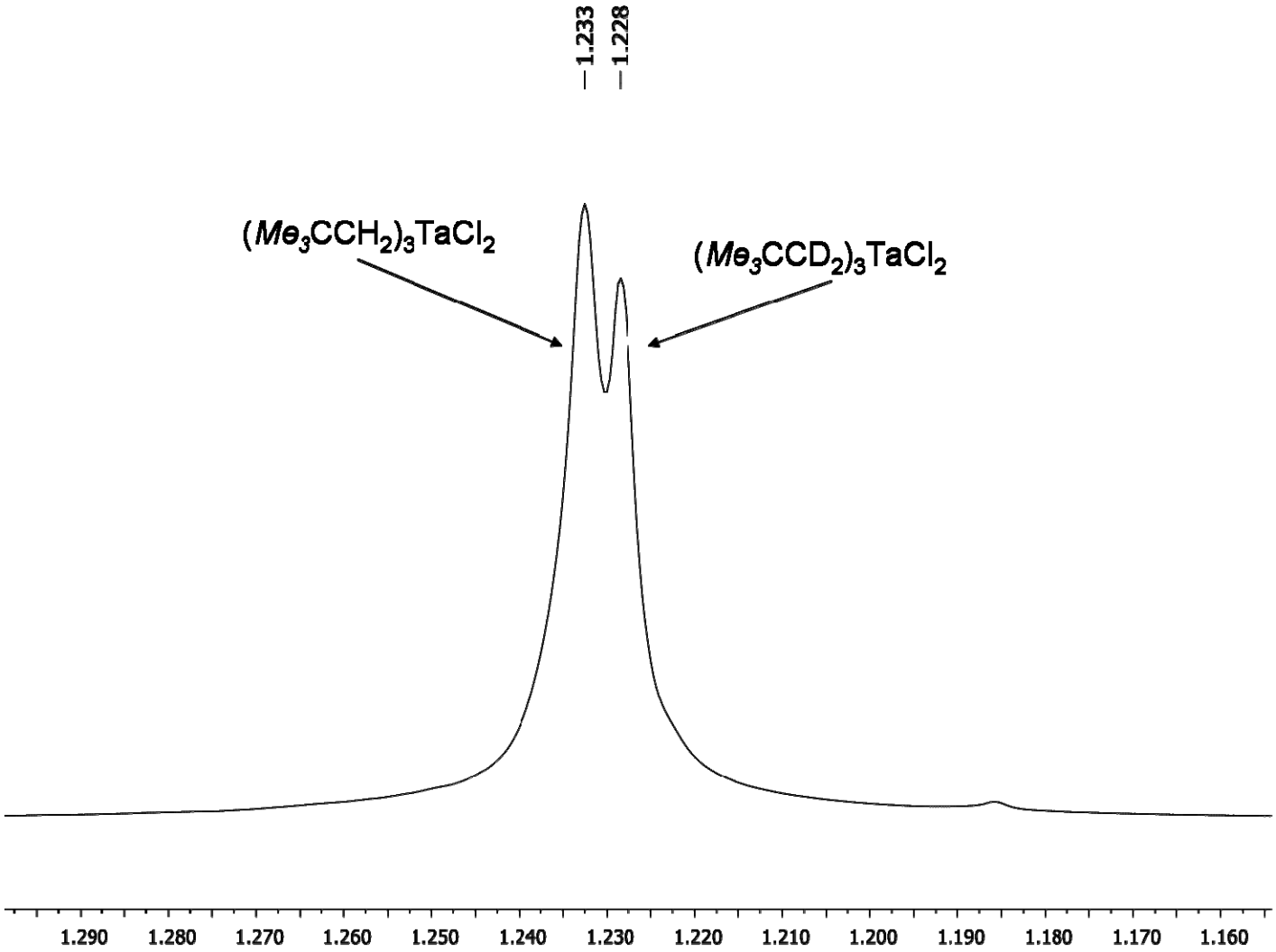

Figure 3.2. ^{1}H NMR spectrum of $(Bu^{t}CH_2)_3TaCl_2$ (**3**) and $(Bu^{t}CD_2)_3TaCl_2$ (**3-*d*$_6$**).

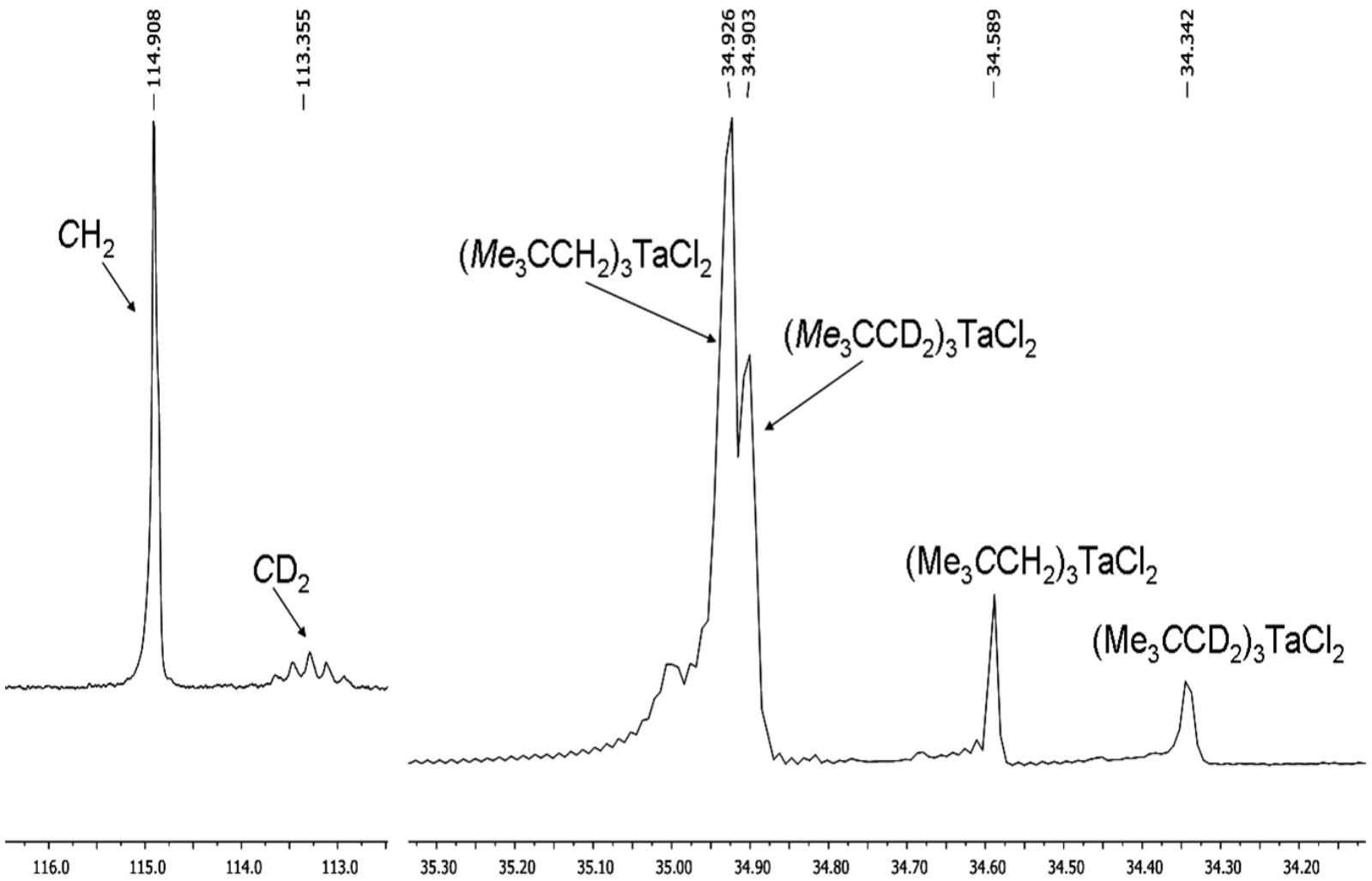

Figure 3.3. ^{13}C NMR spectrum of $(Bu^tCH_2)_3TaCl_2$ (**3**) and $(Bu^tCD_2)_3TaCl_2$ (**3-*d*$_6$**).

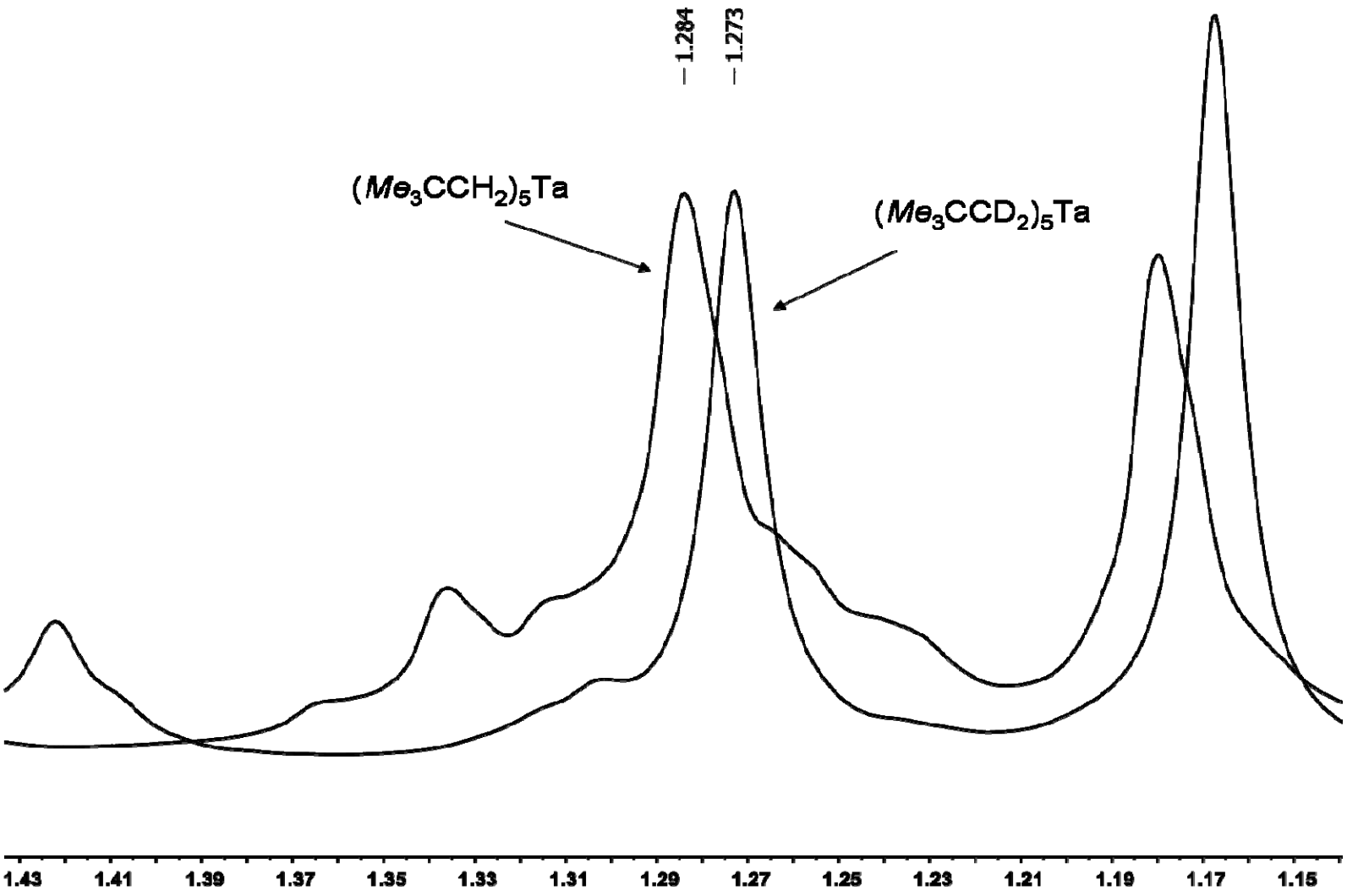

Figure 3.4. ^{1}H NMR spectrum of $(Bu^{t}CH_2)_5Ta$ (**1**) and $(Bu^{t}CD_2)_5Ta$ (**1-*d*$_{10}$**).

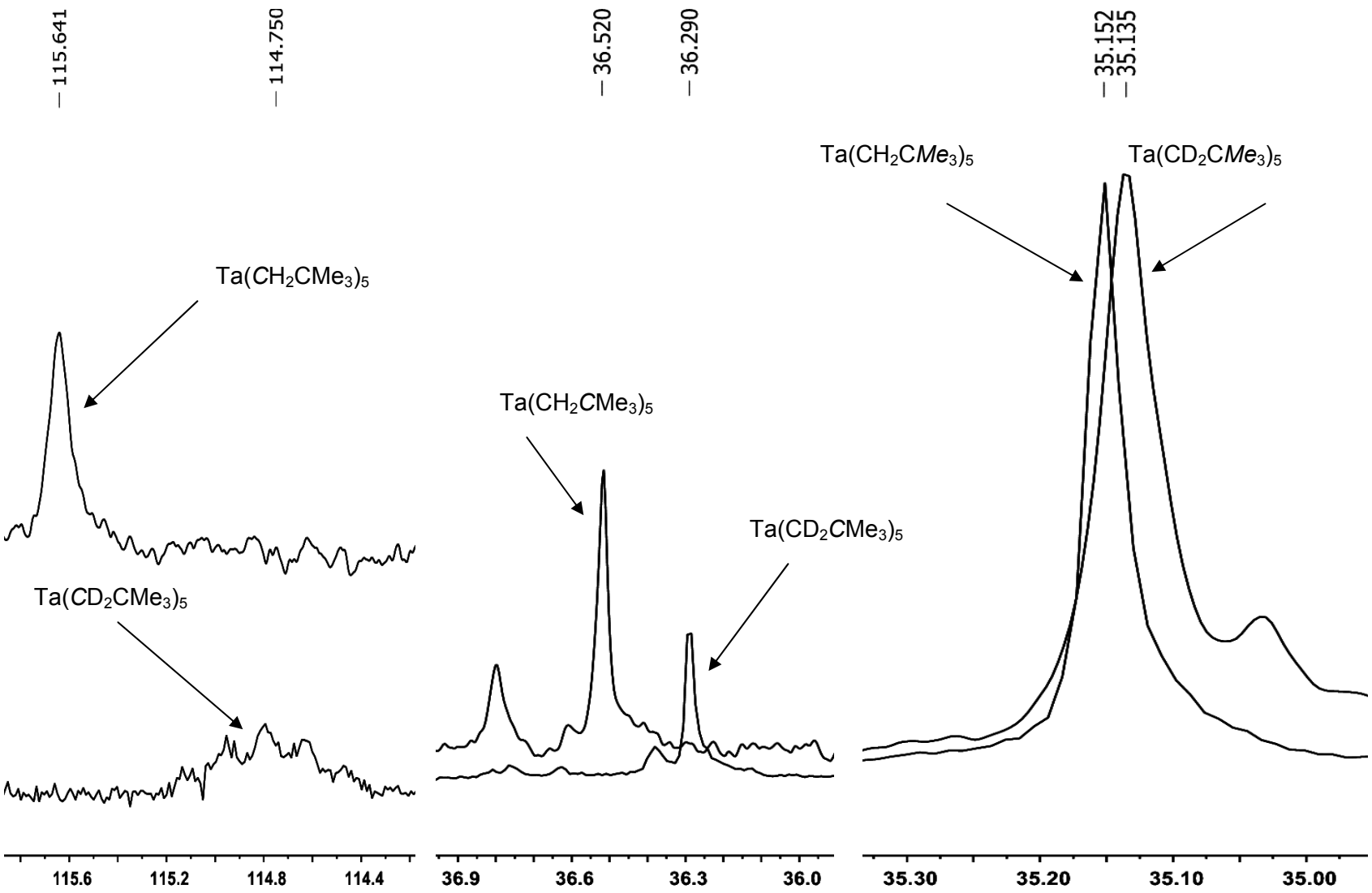

Figure 3.5. ^{13}C NMR spectrum of $(Bu^tCH_2)_5Ta$ (**1**) and $(Bu^tCD_2)_5Ta$ (**1-*d*$_{10}$**).

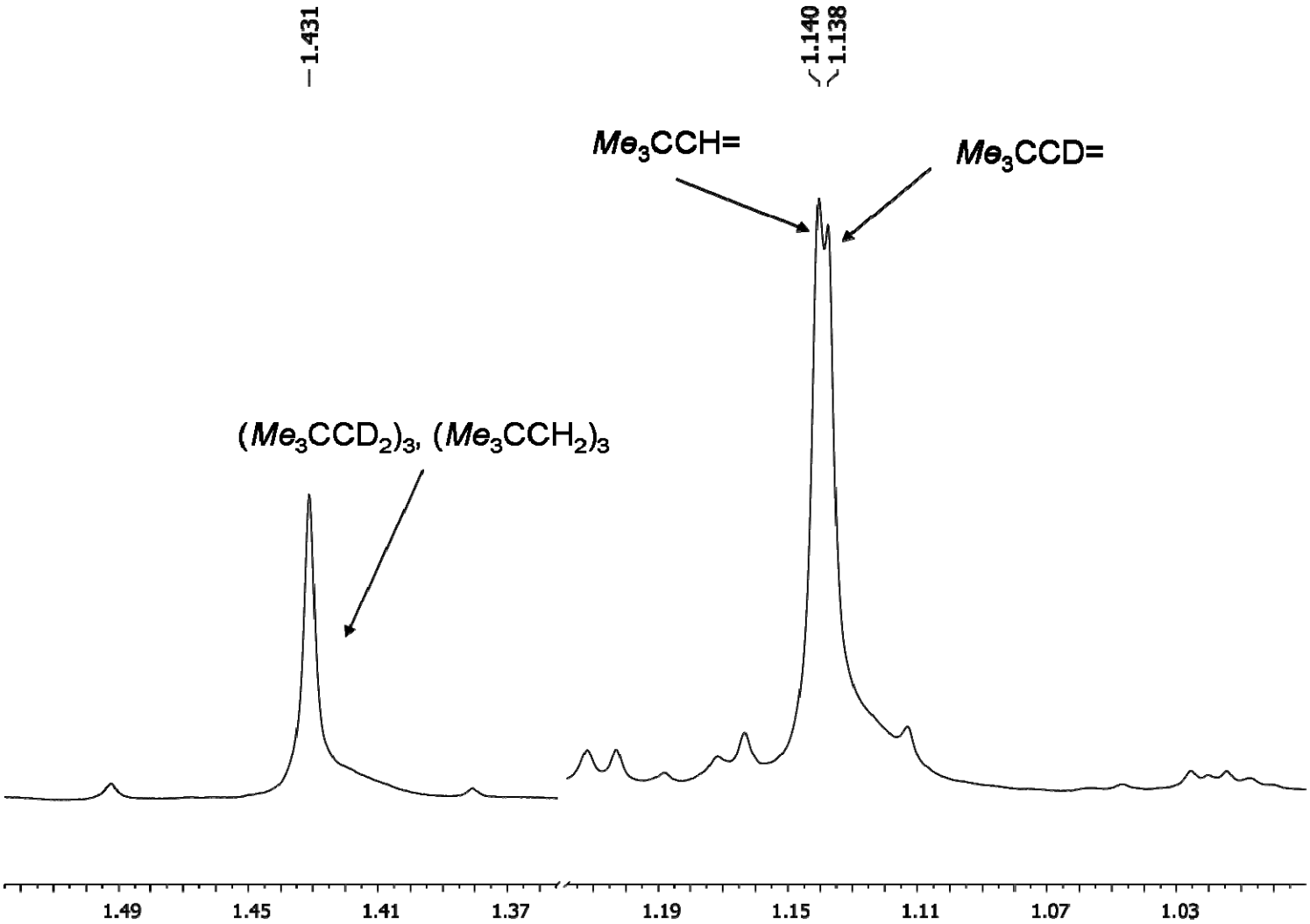

Figure 3.6. ^{1}H NMR spectrum of $(Bu^{t}CH_2)_3Ta{=}CHBu^{t}$ (**2**) and $(Bu^{t}CD_2)_3Ta{=}CDBu^{t}$ (**2-*d*$_7$**).

In the ^{13}C NMR spectrum of **2**/**2-*d*$_7$**, shifts could be detected for all carbon atoms. Portions of the ^{13}C NMR spectrum are given in Figures 3.7a and 3.7b. The carbene carbon shift is difficult to see, because of low intensity and high signal to noise ratio. The non-deuterated singlet appears at 249.857 ppm. The deuterated complex shows a triplet due to C-D coupling at 249.127 ppm giving an isotopic shift of 0.73 ppm. The peaks for the $-CD_2-$ and $-CH_2-$ resonances show up as a singlet at 113.664 ppm for the $-CH_2-$ group and a quintet at 112.356 ppm for the $-CD_2-$ group. This is a shift of 1.308 ppm. This is a greater isotopic shift (almost double) than that observed in the carbene carbons because the carbon is in close proximity to the two deuterium atoms instead of one as in the =CD– group. The Me_3CCH=/Me_3CCD= peaks appear at 47.039 ppm and 47.007 ppm, respectively. This difference of 0.032 ppm fits the trend of decreasing chemical shift difference with increasing distance from the deuterium. The tertiary carbon of the carbene ligand shows weak resonances at 35.310 and 35.275 ppm for the non-deuterated and deuterated compounds, respectively. This is a difference of 0.035 ppm, which is much smaller than the other carbon atoms in the compound. The methyl groups of the neopently ligand appear at 34.931 ppm (non-deuterated) and 34.903 ppm (deuterated) giving a shift of 0.028 ppm. The methyl groups of the neopentene show a difference of 0.021 ppm, the smallest of all the resonances.

While experimental studies of isotopic shifts, especially in organometallic compounds, are rare, some examples have been reported for other compounds containing neopentyl ligands.[65.108] Hughes and Kingsley synthesized deuterated and non-deuterated titanium and zirconium neopentyl chloro complexes,

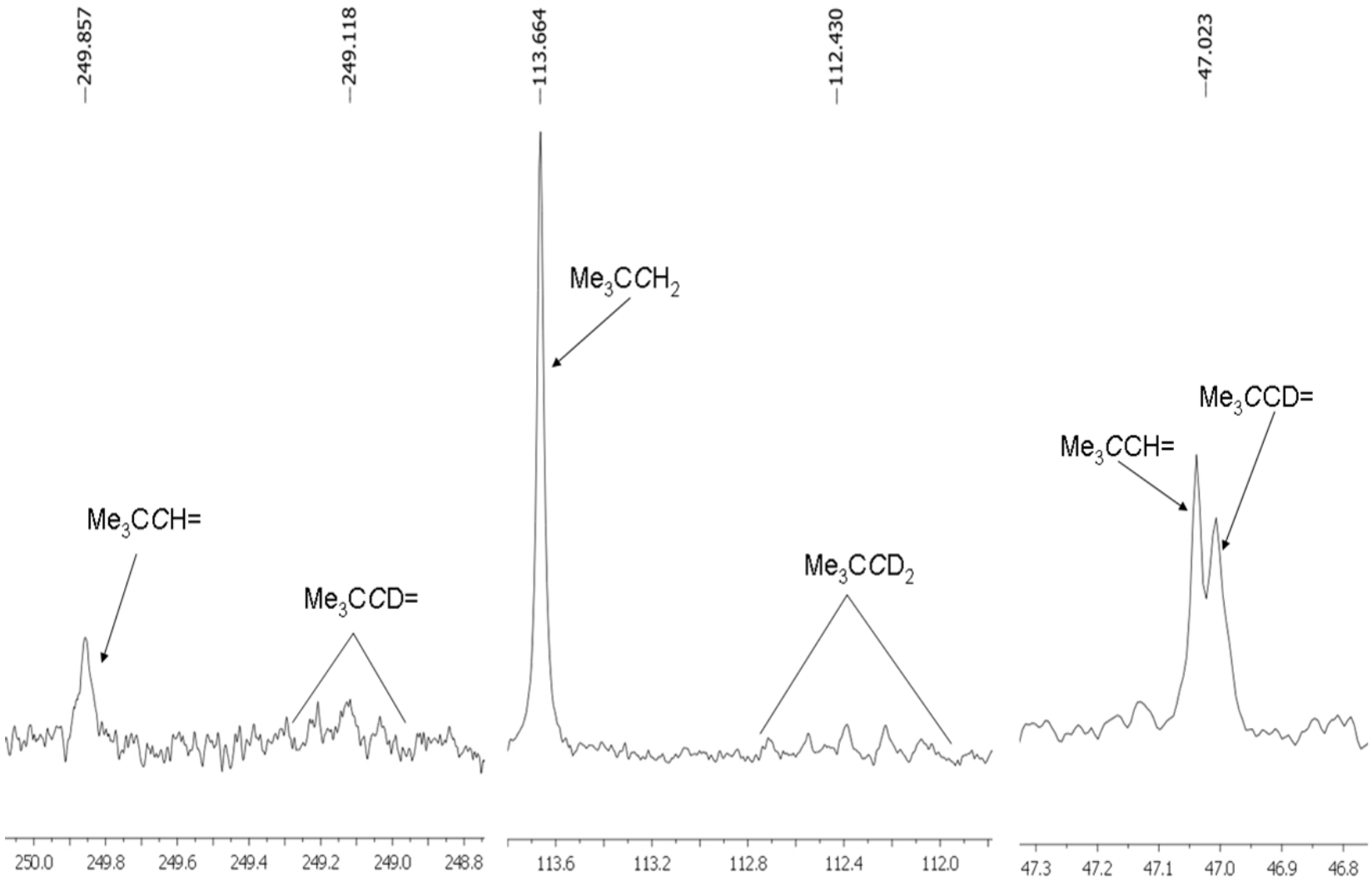

Figure 3.7a. Downfield portions of the ^{13}C NMR spectrum of $(Bu^tCH_2)_3Ta{=}CHBu^t$ (**2**) and $(Bu^tCD_2)_3Ta{=}CDBu^t$ (**2-*d*$_7$**).

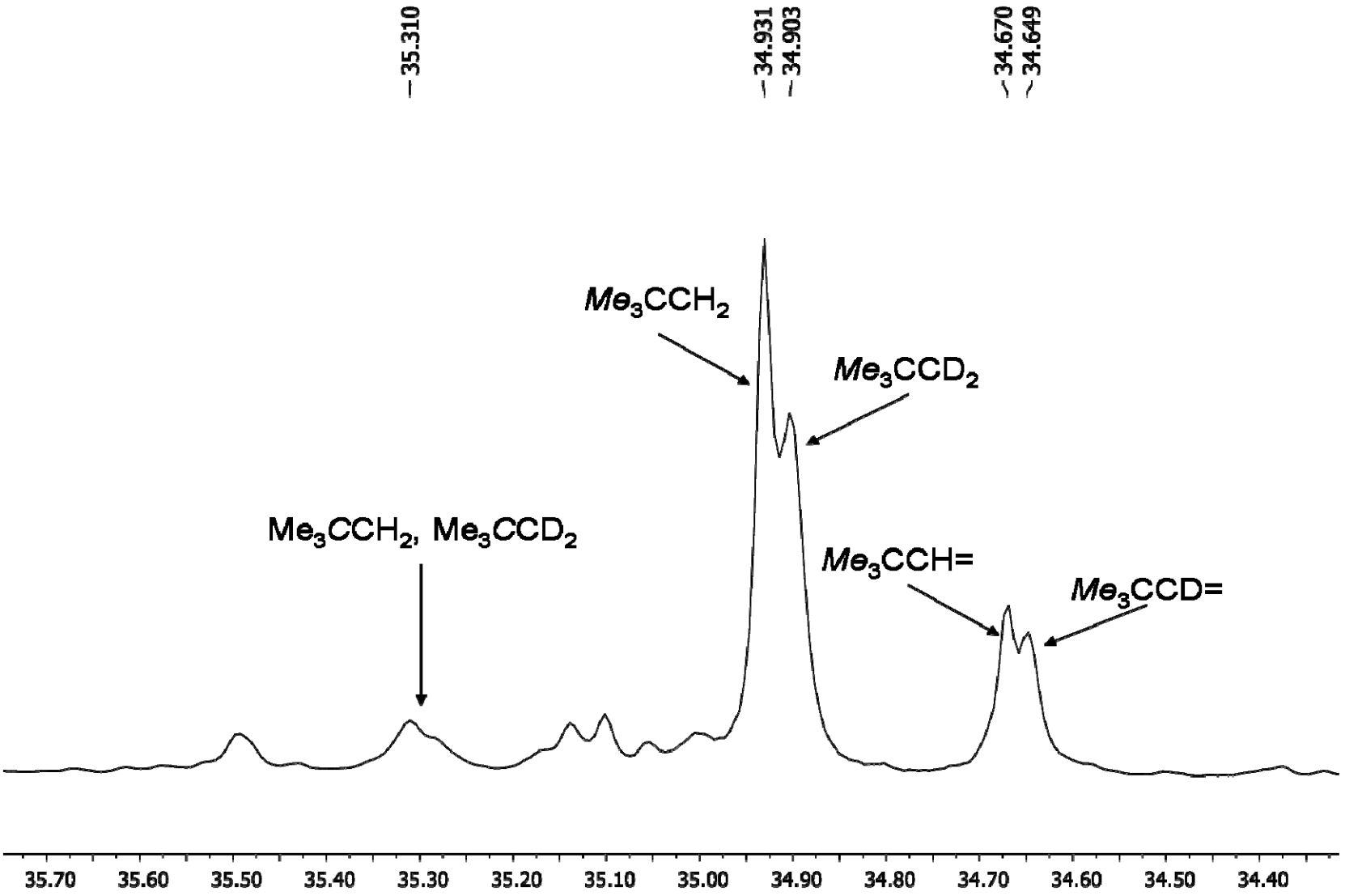

Figure 3.7b. Upfield portion of the ^{13}C NMR spectrum of $(Bu^tCH_2)_3Ta{=}CHBu^t$ (**2**) and $(Bu^tCD_2)_3Ta{=}CDBu^t$ (**2-*d*$_7$**).

$M(CE_2CMe_3)_xCl_{4-x}$ (E = H, D).[108] They found that with all variations of ligands, the isotopic shifts in the ^{1}H NMR for the methyl groups of the neopentyl ligands were less than 0.1 ppm. Caulton and coworkers recorded isotopic shifts for a tungsten neopentyl compound, $(Me_3CCH_2)_3W{\equiv}CSiMe_3$, and its deuterated analog.[65] They found isotopic shifts of 0.003-0.004 ppm in the ^{1}H NMR for the methyl resonance of the neopentyl ligands. For the methyl resonances of the neopentyl ligands mentioned in this chapter, all three isotopic shifts were less than 0.011 ppm.

3.2.2. Conformational Studies of $(Bu^tCH_2)_3TaCl_2$ (3) and $Ta(Bu^tCH_2)_5$ (1)

It was shown in previous work[55] that an intermediate, $(Bu^tCH_2)_4TaCl$ (**4**), in the formation of $(Bu^tCH_2)_3Ta{=}CHBu^t$ (**2**), has a trigonal bipyramidal structure. This was observed by ^{1}H NMR at -40 °C as two distinct resonance peaks, one for equatorial and one for axial with a 3:1 ratio. This was also observed in the deuterated analog.[109] Both the starting material, $(Bu^tCH_2)_3TaCl_2$ (**3**) and the intermediate, $Ta(CH_2Bu^t)_5$ (**1**), show only one resonance peak at -40 °C in previous studies.[55] This indicates that the rate of conversion of the ligands in the compounds is faster than the NMR time scale. To test this further, variable-temperature ^{1}H NMR spectra of the two deuterated analogs, **3-*d*$_6$** and **1-*d*$_{10}$**, were taken at -75 °C (198 K, Figures 3.8 and 3.9). Neither compound showed any separation of peaks, even at these very low temperatures. Thus, the structure of the compounds could not be determined by NMR at -75 °C.

To further study the structures of $Ta(CD_2Bu^t)_5$ (**1-*d*$_{10}$**) and $Ta(CH_2Bu^t)_5$ (**1**), DFT calculations were preformed on a similar compound by Prof. Zhenyang Lin and

Peng Yuan at the Hong Kong University of Science and Technology. $Ta(CH_2CH_3)_5$ (**10**) was chosen because the smaller ligand simplified the calculations. This compound is naturally unstable, and has not been prepared successfully. The DFT studies showed the ground state of **10** to be distorted square pyramidal (Figure 3.10), very similar to the ground state of $TaMe_5$.[104,106,107]

The VT NMR studies showed that $Ta(CH_2Bu^t)_5$ (**1**) is a highly fluxional molecule,[55] likely through rotation of the Bu^t groups around the Ta-C bonds as well as exchange of the apical-basal ligands. A pathway was calculated to model the fluxional behavior based on the ground state of **10** as a representation of **1** (Figure 3.11). Interestingly, the free energy difference from the ground state to the highest energy state is only 6.1 kcal/mol. This is very small compared to other ligand exchange processes.[110] The small energy difference could explain why no separation of the peaks was seen in the NMR of $Ta(CD_2CMe_3)_5$ (**1-*d*$_{10}$**), even at very low temperatures. DFT studies also showed the transition state with the highest energy (TS_{DG}, Figure 3.12) is related to a ligand exchange process, and the transition state adopts an approximate trigonal bipyramidal structure. The other transition states (TS_{AB}, TS_{BD}, and TS_{GA}) represent rotations of the Me groups, leaving the overall geometry as square pyramidal. The other conformers, **1A**, **1B**, **1D**, and **1G**, are given in Figure 3.13.

While the DFT calculations preformed are for an analog of $Ta(CH_2Bu^t)_5$ (**1**), the results reflect what is probably true for **1** as well, although there may be small differences in the actual ground state. With these calculations and with information about other pentaalkyl tantalum complexes, it can be stated that the highest

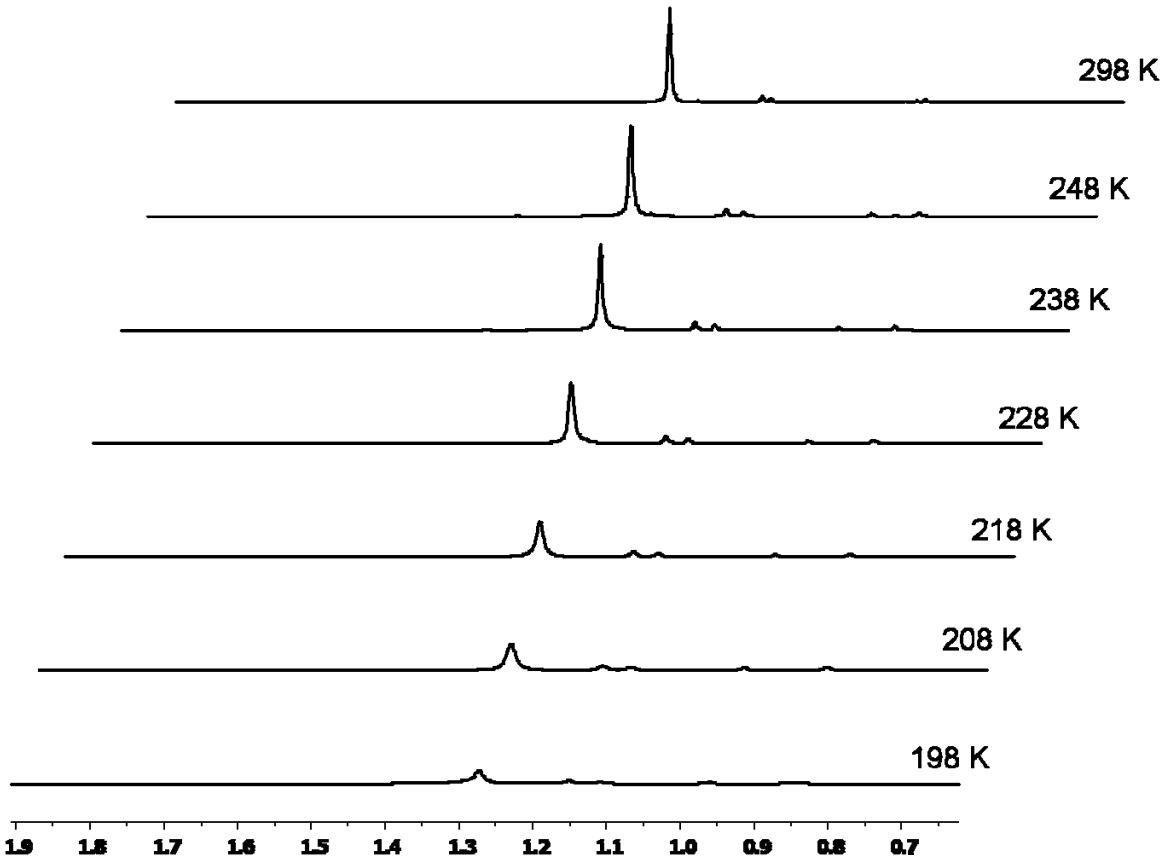

Figure 3.8. Variable-Temperature NMR spectra of $(Bu^tCD_2)_3TaCl_2$ (**3-*d*$_6$**).

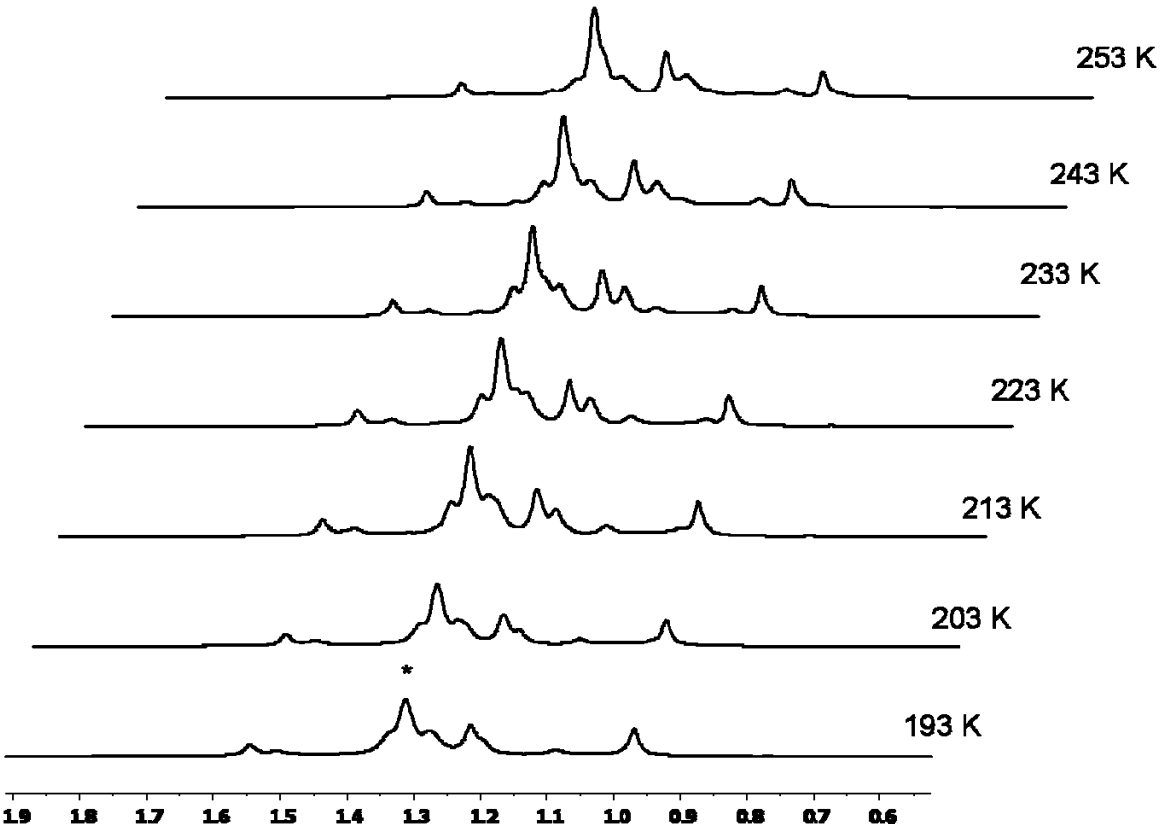

Figure 3.9. Variable-Temperature NMR spectra of $Ta(CD_2Bu^t)_5$ (**1-*d*$_{10}$**).

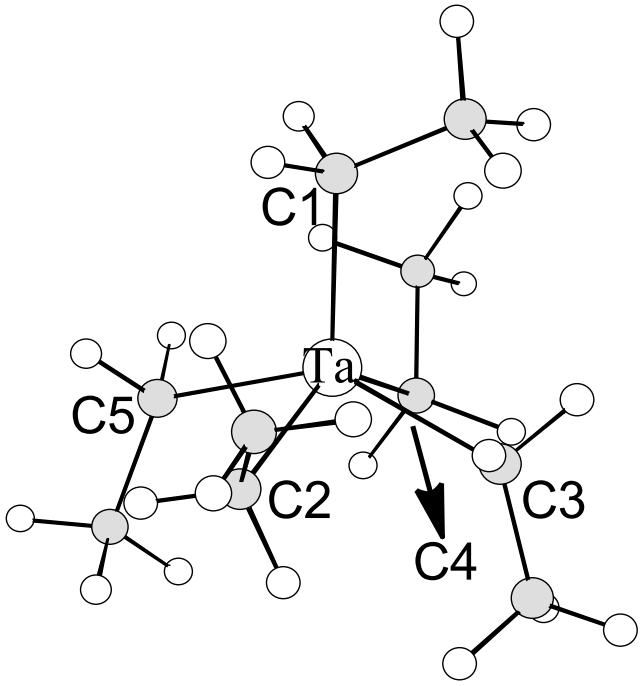

Figure 3.10. Ground state structure of $TaEt_5$ (**10**).

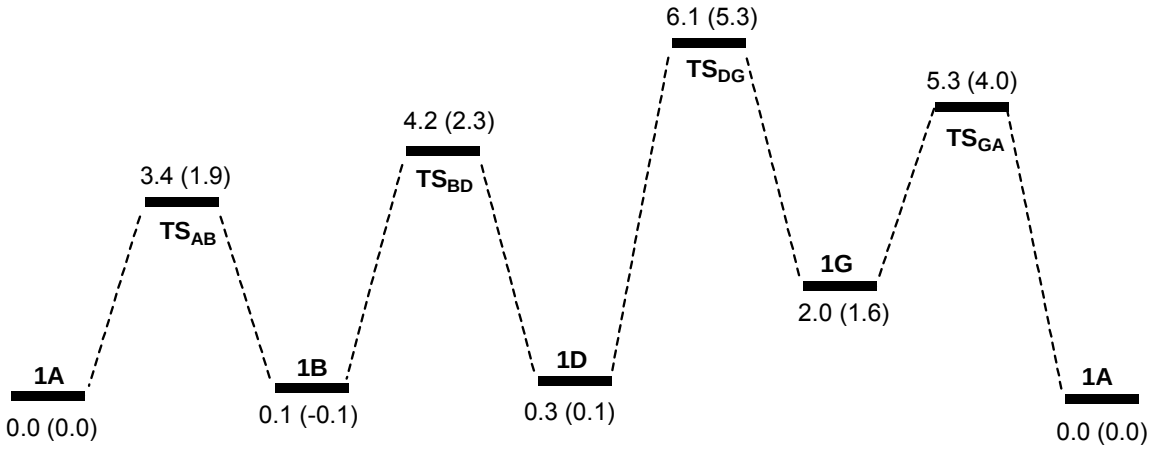

Figure 3.11. Energy profile connecting different conformers of $TaEt_5$ (**10**).

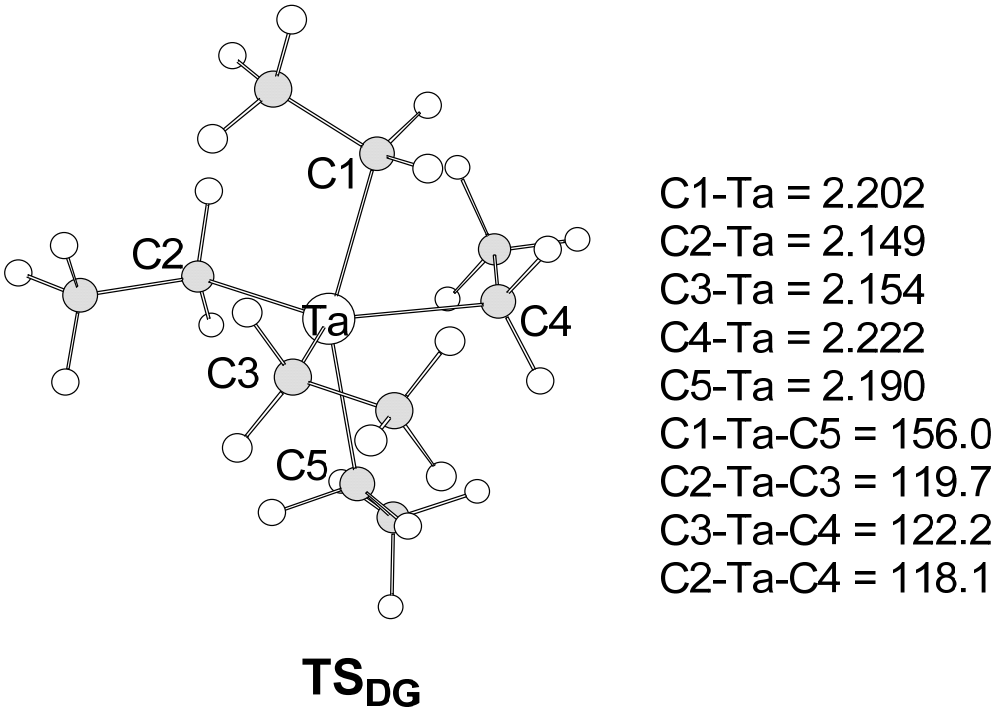

Figure 3.12. The transition state structure that corresponds to an apical-basal ligand exchange process in $TaEt_5$ (**10**).

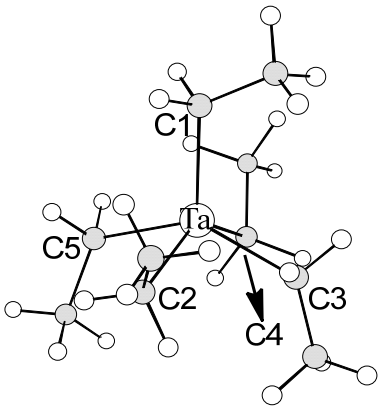

C1-Ta-C2 = 112.8
C1-Ta-C3 = 110.5
C1-Ta-C4 = 112.1
C1-Ta-C5 = 107.9
Ta-C2 = 2.201
Ta-C3 = 2.169
Ta-C4 = 2.203
Ta-C5 = 2.170

1A

0.0 (0.0)

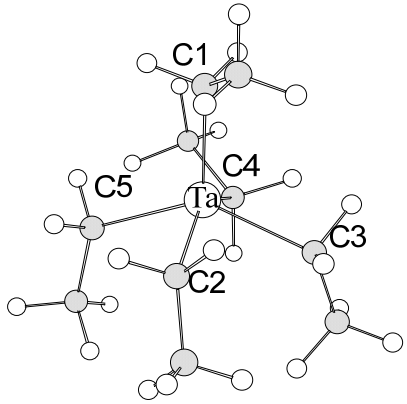

C1-Ta-C2 = 108.5
C1-Ta-C3 = 111.0
C1-Ta-C4 = 108.7
C1-Ta-C5 = 110.9
Ta-C2 = 2.179
Ta-C3 = 2.189
Ta-C4 = 2.203
Ta-C5 = 2.170

1B

0.1 (-0.1)

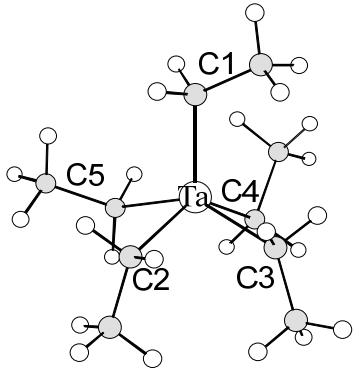

C1-Ta-C2 = 110.7
C1-Ta-C3 = 107.7
C1-Ta-C4 = 115.6
C1-Ta-C5 = 107.1
Ta-C2 = 2.172
Ta-C3 = 2.165
Ta-C4 = 2.211
Ta-C5 = 2.195

1D

0.3 (0.1)

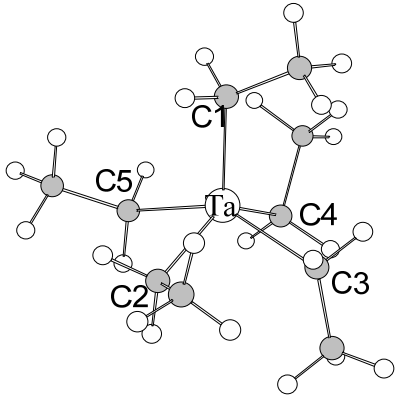

C1-Ta-C2 = 111.1
C1-Ta-C3 = 108.8
C1-Ta-C4 = 115.2
C1-Ta-C5 = 108.6
Ta-C2 = 2.179
Ta-C3 = 2.159
Ta-C4 = 2.215
Ta-C5 = 2.201

1G

2.0 (1.6)

Figure 3.13. Calculated structural conformers of $TaEt_5$ (**10**) together with their relative energies.

probability ground state of **1** is square pyramidal. Through the NMR studies of **1-*d*$_{10}$** and the energy diagram of **10**, it seems likely that **1** is a highly fluxional compound.

3.3. Concluding Remarks

In this chapter, the effect of isotopic substitution on NMR chemical shifts is discussed. In the ^{13}C NMR spectra of $(Bu^tCD_2)_3TaCl_2$ (**3-*d*$_6$**), $Ta(CD_2Bu^t)_5$ (**1-*d*$_{10}$**), and $(Bu^tCD_2)_3Ta{=}CDBu^t$ (**2-*d*$_7$**) with their non-deuterated analogs, the farther the carbon atoms reside from the α-deuterium atoms, the smaller the chemical shift difference is between the two compounds. Also discussed was the conformation of the intermediate, $Ta(CH_2Bu^t)_5$ (**1**), which likely adopts a square pyramidal structure. A variable-temperature NMR study was inconclusive as only one resonance was observed down to -75 °C. DFT studies of an analog, $TaEt_5$ (**10**), showed the ground state to be square pyramidal. It also showed that an energy difference of only 6 kcal/mol exists between the ground state and the highest energy transition state, possibly explaining why only one resonance was observed in the ^{1}H NMR spectra of $Ta(CH_2Bu^t)_5$ (**1**) and **1-*d*$_{10}$**. It is believed that $Ta(CH_2Bu^t)_5$ (**1**) likely takes a square pyramidal conformation in its ground state.

3.4. Experimental Section

All manipulations were preformed under a dry nitrogen atmosphere with the use of either a drybox or standard Schlenk techniques. Toluene-d_8 was dried over activated molecular sieves and stored under N_2. NMR spectra were recorded on a Bruker AMX-400 Fourier transform spectrometer and were referenced to solvents.

3.4.1. Isotopic Shifts

A mixture of $(Bu^tCH_2)_3TaCl_2$ (**3,** 30.0 mg, 0.0645 mmol) and $(Bu^tCD_2)_3TaCl_2$ (**3-*d*$_6$,** 30.0 mg, 0.0637 mmol) was dissolved in toluene-d_8 in a J. Young tube. ^{1}H and ^{13}C NMR spectra were taken at 298 K.

$(Bu^tCH_2)_3TaCl_2$ (**3,** 20.0 mg, 0.0430 mmol) and Bu^tCH_2Li (10.0 mg, 0.128 mmol) were added to a J. Young tube. $(Bu^tCD_2)_3TaCl_2$ (**3-*d*$_6$**, 20.0 mg, 0.0424 mmol) and Bu^tCD_2Li (10.0 mg, 0.124 mmol) were added to a second J. Young tube. Both were allowed to react at 23 °C, and were monitored by NMR. When $(Bu^tCH_2)_3Ta{=}CHBu^t$ (**2**) and $(Bu^tCD_2)_3Ta{=}CDBu^t$ (**2-*d*$_7$**) had formed, the solution from the two samples was transferred to a clean J. Young tube in order to remove LiCl that had formed and settled to the bottom of each tube. ^{1}H and ^{13}C NMR spectra were taken on both a 400 and a 600 MHz NMR spectrometer at 298 K.

$Ta(CD_2Bu^t)_5$ (**1-*d*$_{10}$**) was prepared according to literature methods.[109] The sample was dissolved in toluene-d_8 in a J. Young tube. ^{1}H and ^{13}C NMR spectra of $Ta(CD_2Bu^t)_5$ (**1-*d*$_{10}$**) were taken at 233 K. This was compared with spectra of $Ta(CH_2Bu^t)_5$ (**1**) taken in a previous study.[55]

3.4.2. Variable-Temperature NMR Studies

$(Bu^tCD_2)_3TaCl_2$ (**3-*d*$_6$**, 30.0 mg, 0.0637 mmol) was dissolved in toluene-d_8 in a J. Young tube. ^{1}H NMR spectra of the solution were taken from 298 to 198 K, in 5 K increments. To the J. Young tube, Bu^tCD_2Li (10.0 mg, 0.124 mmol) was added. The solution was allowed to react at 288 K until the intermediate compound, $Ta(CD_2Bu^t)_5$

(**1-*d*$_{10}$**), was reached and all starting compounds were gone. ^{1}H NMR spectra were then taken from 298 to 193 K, in 5 K increments.

3.4.3. DFT Calculations[111]

Molecular geometries of Ta(Et)$_5$ (**10**), its different comformers, and the transition-state structure in the ligand exchange process were optimized without constraints via DFT calculations using the Becke3LYP (B3LYP) functional.[112-115] The effective core potentials (ECPs) of Hay and Wadt with a double-ζ valence basis set (LanL2DZ)[116-118] were used in describing Ta, whereas the 6-31G basis set was used for all other atoms.[119-121] In the calculations of the α-H abstraction processes, the 6-311G* basis set was used for those C and H atoms involved in the processes. Frequency calculations at the same level of theory were also performed to identify all the stationary points as minima (zero imaginary frequencies) or transition states (one imaginary frequency) and to provide free energies at 298.15 K, which include entropic contributions by taking into account the vibrational, rotational, and translational motions of the species under consideration. Transition states were located using the Berny algorithm. Intrinsic reaction coordinates (IRC)[122,123] were calculated for the transition states to confirm that such structures indeed connect two relevant minima. All calculations were performed with the Gaussian 03 software package.[124]

Chapter 4

Synthesis of Guanidinate Imide Complexes $Ta(NMe_2)(=NSiMe_3)[RNC(NMe_2)NR]_2$ (R = Cy, Pr^i). Formation of an Imide through Unprecedented α-$SiMe_3$ Abstraction by an Amide Ligand

4.1. Introduction

Transition metal imide complexes have been actively studied[125-132] and used as catalysts[133-136] and precursors in chemical vapor deposition (CVD) of microelectronic materials.[137-140] A variety of methods have been developed to prepare imide ligands, utilizing both intermolecular and intramolecular reactions.[125] Intermolecular syntheses are more common and include imidinations with primary amines, imines, nitriles, and a variety of other nitrogen-containing compounds. Examples include the synthesis of $Bu^tN=OsO_3$ through the treatment of OsO_4 with Bu^tNH_2,[141] $PhN=MoCl_2(S_2CNEt_2)_2$ from the reaction of $MoOCl_2(S_2CNEt_2)_2$ with $PhNPPh_3$,[142] and $PhN=ReCl_3(PPh_3)_2$ from the reaction of $ReOCl_3(PPh_3)_2$ with PhN=CHNHPh.[143] Intramolecular imidination is less common, and in these reactions, an imido ligand is formed through 1,2-elimination of, usually, Me_3SiCl or interligand transfer (Scheme 4.1). The treatment of $TiCl_3[N(SiMe_3)_2]$ with pyridine,[144] e.g., leads to 1,2-elimination of Me_3SiCl and formation of $Me_3SiN=TiCl_2(py)_2$. In the reaction of

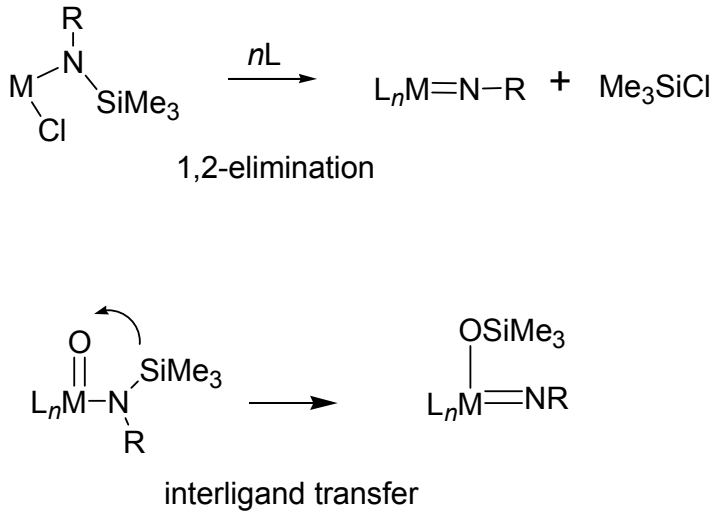

Scheme 4.1. Examples of the two main types of intramolecular imidation.[125]

$VOCl_3$ with 3 equivalents of $NaN(SiMe_3)_2$, a $–SiMe_3$ group migrates to the oxo ligand forming the imide $Me_3SiN=V(OSiMe_3)[N(SiMe_3)_2]_2$.[145]

Early transition metal complexes with nitrogen-containing ligands are currently studied as precursors to metal oxide thin films in CVD and atomic layer deposition (ALD) processes.[146-159] Guanidinate complexes are among the actively studied precursors.[146-150,160-162] Guanidinate is a bidentate ligand (Figure 4.1), as are the N-containing amidinate[163] and triazenate[164] ligands (Figure 4.1). The guanidinate ligand is the least studied of the three, in part because it was first thought to bind only in a mono-dentate manner.[165] However, in the mid-1990s it was found that guanidinate compounds could bind in a bidentate manner as well.[166,167] Since then, studies have been conducted to synthesize different complexes with guanidinate ligands. Guanidinate complexes have also been prepared using Group 4,[137,149,160]

Group 5,[137,146-148] and Group 6[168-170] metals. Guanidinate imide complexes have also been reported.[146-148] In the previous preparations of guanidinate imide complexes, an amide imide is formed first, followed by carbodiimide insertion into the M-amide bond to form the guanidinate ligands (Scheme 4.2).[146-148] In our studies of the reactions between amide complex $Ta(NMe_2)_4[N(SiMe_3)_2]$ (**13**) and carbodiimides RN=C=NR (R = Cy, Pr^i), we were surprised to find elimination of $Me_3Si\text{-}NMe_2$ (**14**) and the formation of the guanidinate imides, $Ta(NMe_2)(=NSiMe_3)[RNC(NMe_2)NR]_2$ (R = Cy, **11**; Pr^i, **12**; Scheme 4.3). To our knowledge, elimination of $Me_3Si\text{-}NMe_2$ (**14**) in the formation of an imide ligand has not been reported. Herein, our studies of the reactions and characterization of **11** and **12** are reported.

4.2. Results and Discussion

4.2.1. Preparation of $Ta(NMe_2)(=NSiMe_3)[CyNC(NMe_2)NCy]_2$ (11)

The guanidinate ligand exists in two resonance forms[161] (Figure 4.2), due to the delocalization of the lone pair from the uncoordinated nitrogen atom throughout the ligand π system. In the work described here, the ligands are represented by the anion form.

Two basic pathways have been used in the formation of metal guanidinate complexes. The first method proceeds through a salt metathesis in which metal halides are treated with a lithium or sodium guanidinate.[149-151] In the second method, a carbodiimide is reacted with a metal amide, and the guanidinate is formed through an insertion of the carbodiimide into one of the M-amide bonds.[146,152,160,168,171] The

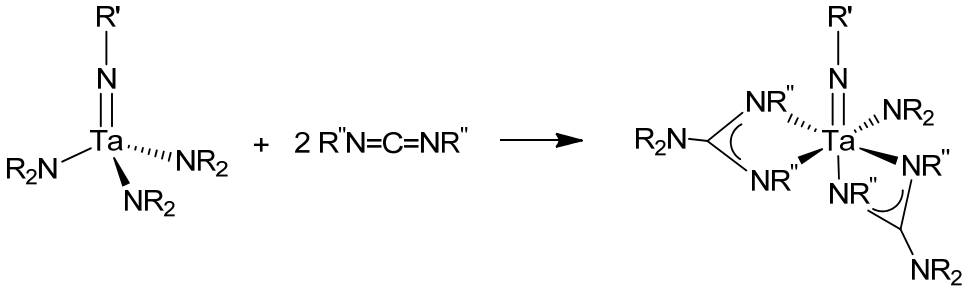

Scheme 4.2. Previous synthesis of guanidinate amide imide complexes.

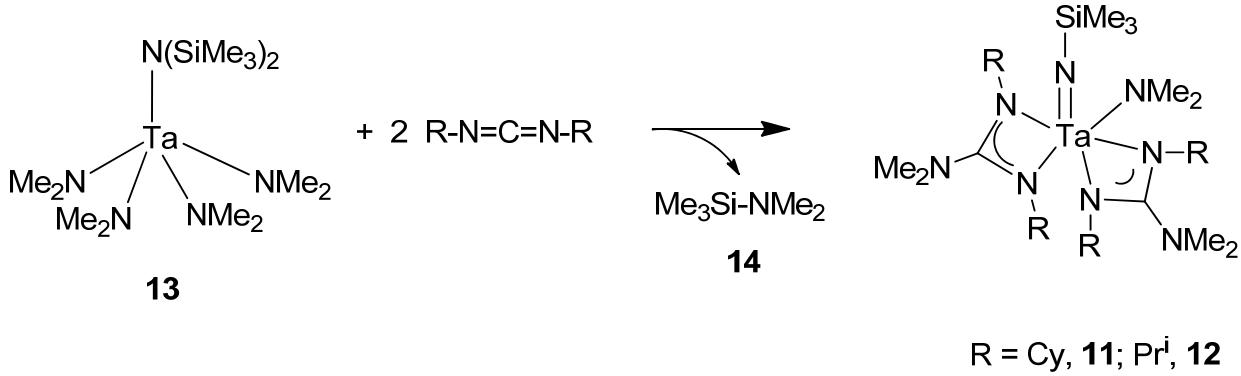

Scheme 4.3. Formation of **11** and **12**.

second pathway was employed in this work because of the simplicity of using commercial carbodiimides. There are also few byproducts, and the process requires minimal purification.

In reported syntheses of guanidinate complexes,[149,152,171] the metal amide or chloride is mixed with the guanidinate source at room temperature and stirring at this temperature for 24 h was adequate to complete the reactions. This procedure was

initially employed in the current work, but no reaction was observed between $Ta(NMe_2)_4[N(SiMe_3)_2]$ (**13**) and CyN=C=NCy at 23 °C. The reaction vessel (a J. Young NMR tube or Schlenk flask) containing **13** and 2 equivalents of CyN=C=NCy was heated to 60 °C and stirred for six days (Scheme 4.3). This procedure gave **11** in 48% yield. This heating may have helped facilitate the insertion of the carbodiimide and the amide to imide conversion.

One dimensional ^{1}H and ^{13}C NMR spectra of **11** (Figures 4.3 and 4.4) are complex. Only through two dimensional NMR experiments and the single crystal diffraction was the complete structure of the compound identified, and the NMR peaks assigned. These are discussed below. $Me_3Si\text{-}NMe_2$ (**14**) was directly observed in the product mixture when the reaction was followed by NMR in a J.

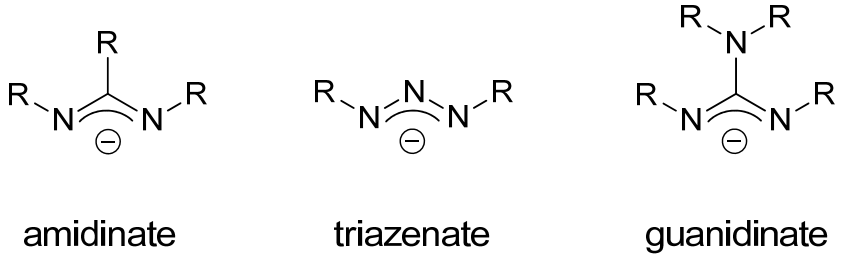

Figure 4.1. Common types of bidentate N-containing ligands.

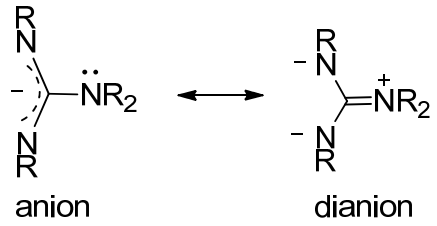

Figure 4.2. The two resonance forms of the guanidinate ligand.

Young tube. The NMR spectra of **14** in the mixture match those reported in the literature (Figure 4.5).[172-174] Upon evacuation of the volatiles from the product mixture under vacuum, $Me_3Si\text{-}NMe_2$ (**14**) was removed along with the solvent.

$Ta(NMe_2)(=NSiMe_3)[CyNC(NMe_2)NCy]_2$ (**11**) is inert to O_2 at one atmosphere. Over an extended period of time, it is mostly inert to air. When reacted with H_2O, though, an insoluble material was formed. This is likely a polymeric material, but due to its insolubility, no further characterization was performed.

4.2.2. X-ray Crystal Structure of 11

The crystal structure of **11** is shown in Figure 4.6. Select crystallographic data and bond distances and angles are given in Tables 4.1 and 4.2, respectively. The Ta center is in a distorted-octahedral environment, surrounded by the four N atoms of

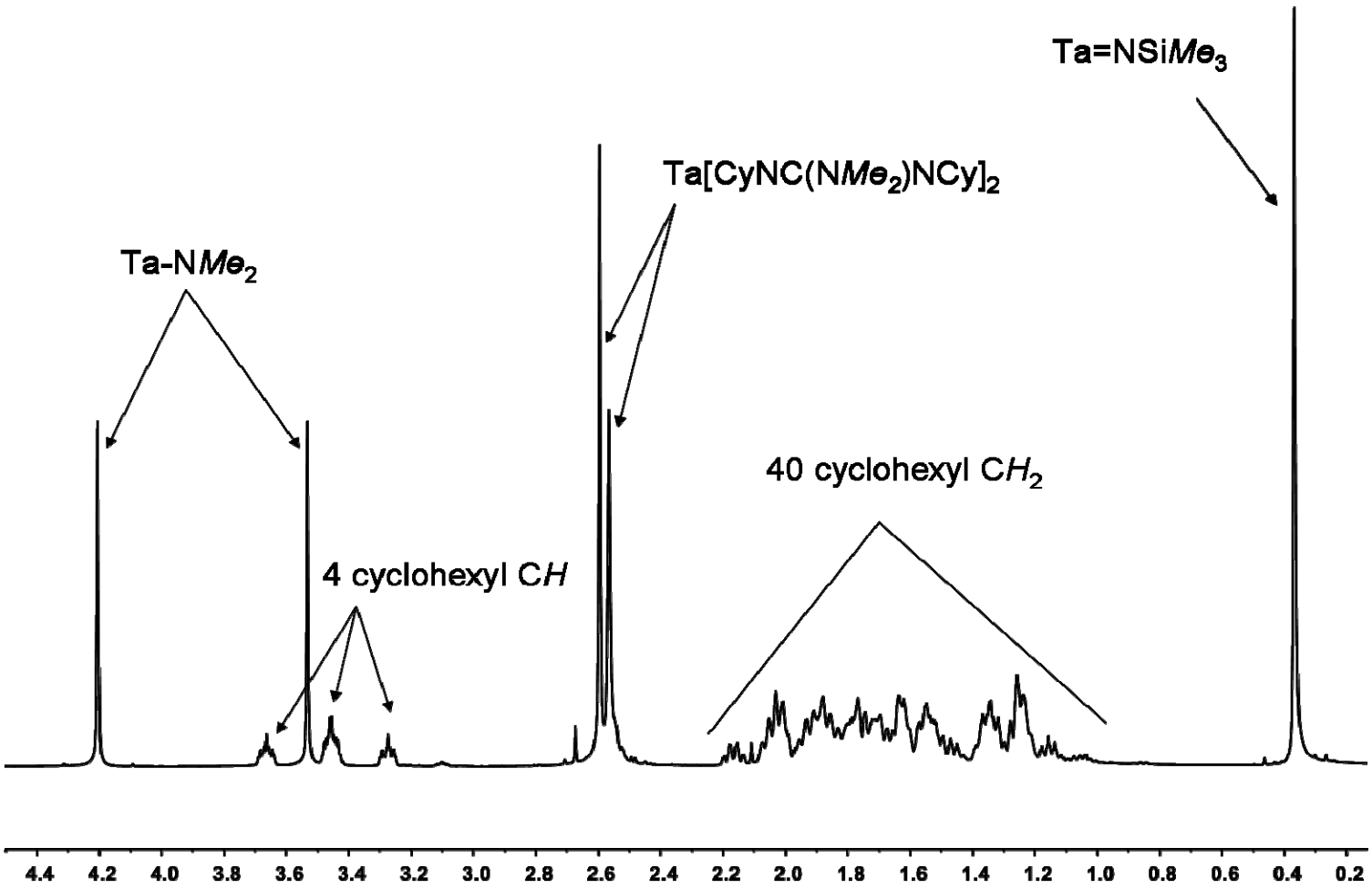

Figure 4.3. ^{1}H NMR spectrum of Ta(NMe$_2$)(=NSiMe$_3$)[CyNC(NMe$_2$)NCy]$_2$ (**11**).

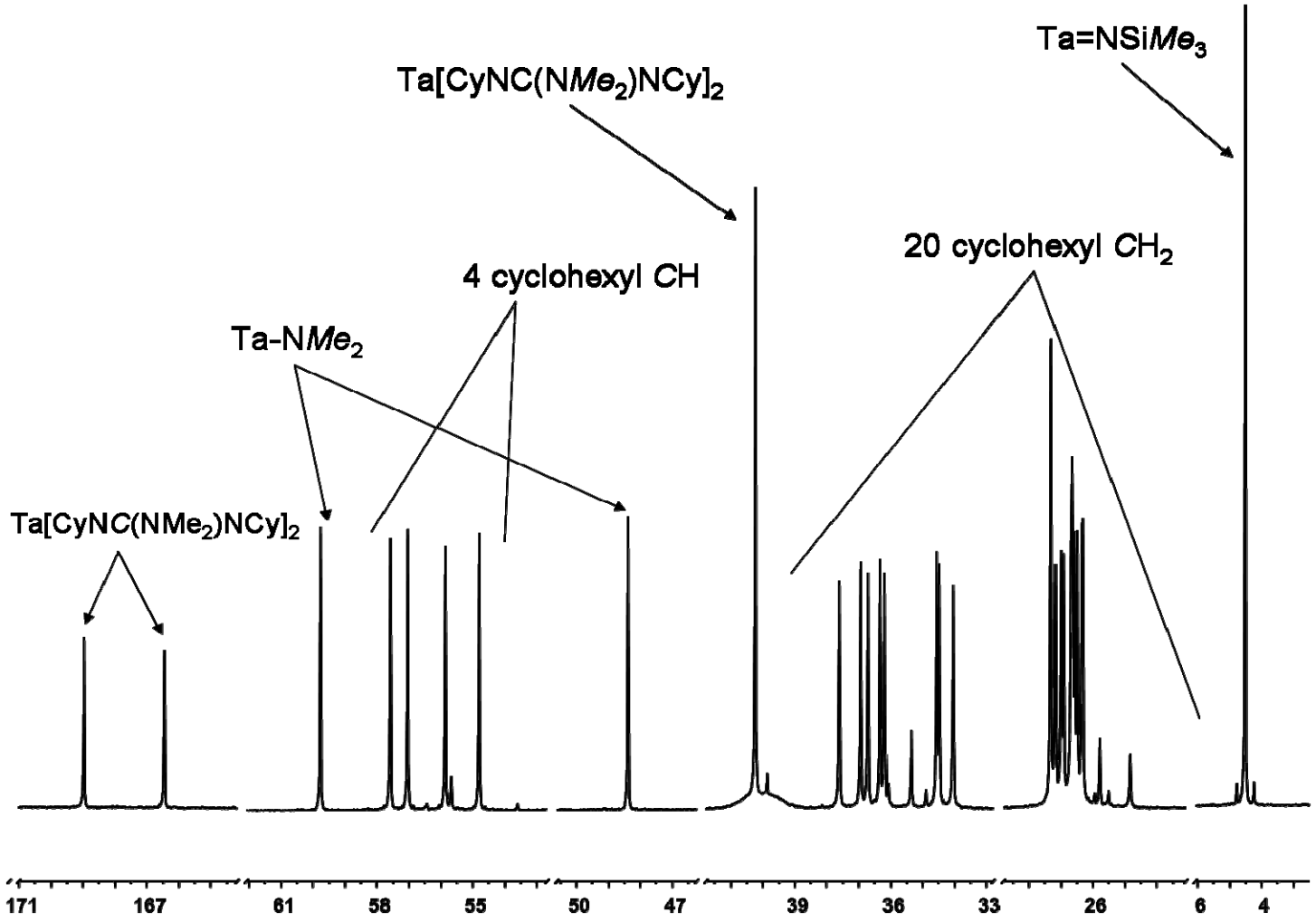

Figure 4.4. ^{13}C NMR spectrum of $Ta(NMe_2)(=NSiMe_3)[CyNC(NMe_2)NCy]_2$ (**11**).

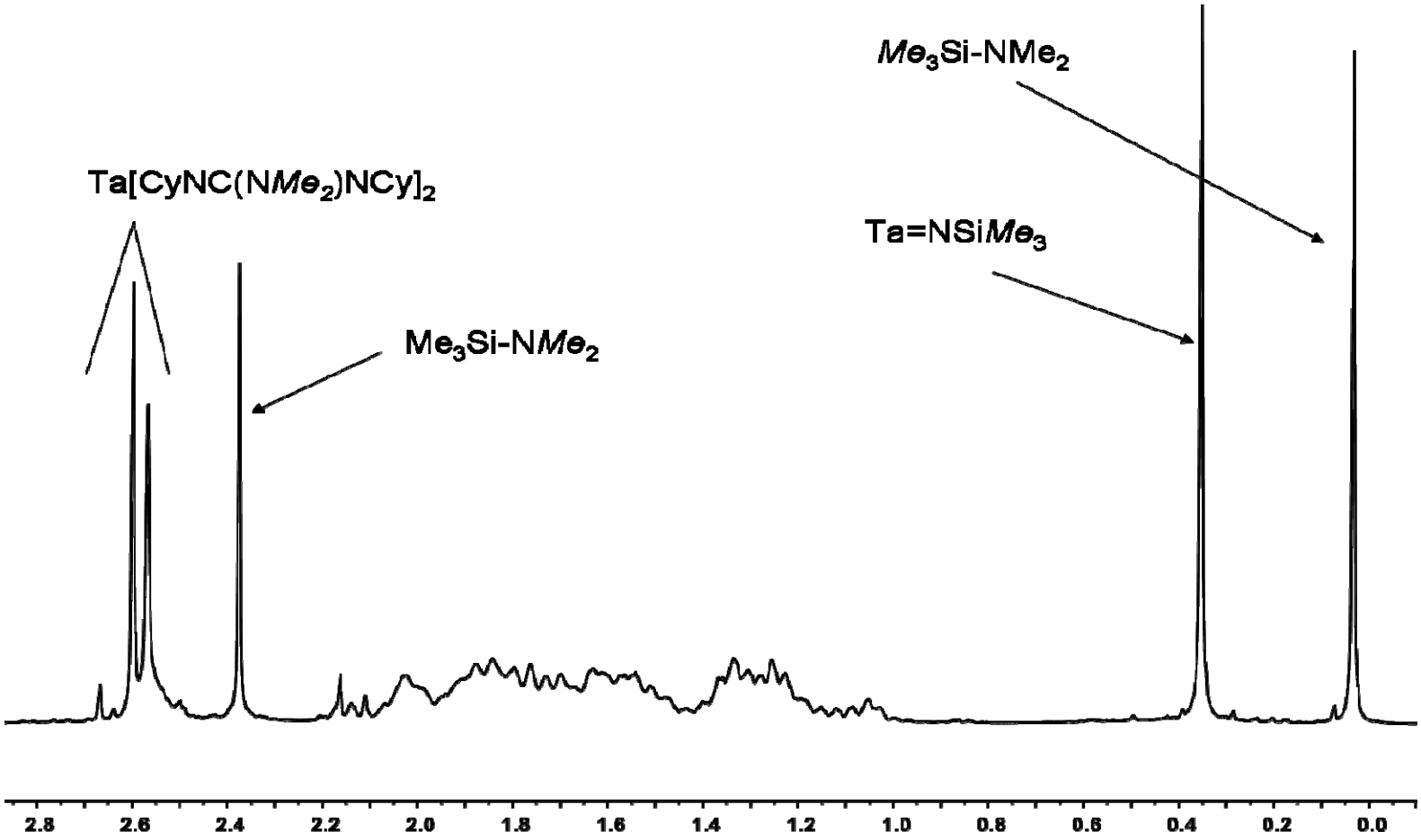

Figure 4.5. Portion of the ^{1}H NMR spectrum of the reaction mixture showing **11** and $Me_3Si\text{-}NMe_2$ (**14**).

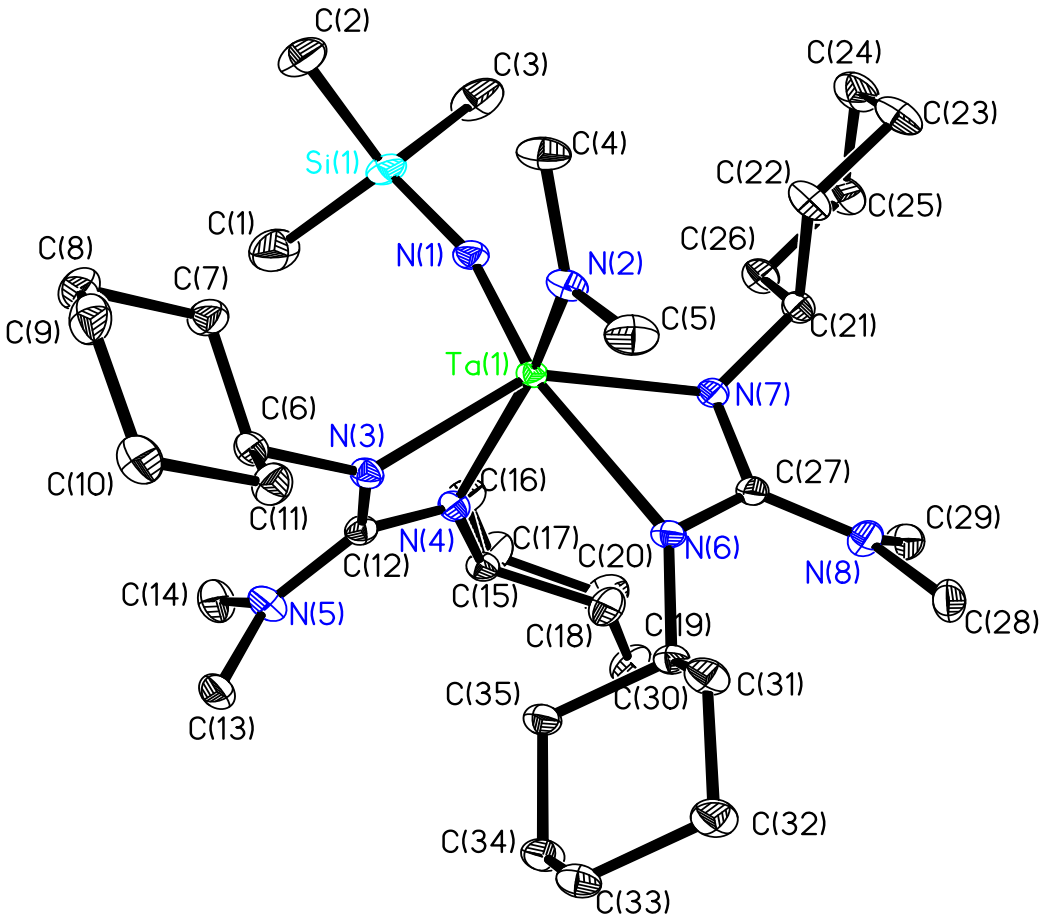

Figure 4.6. ORTEP view of $Ta(NMe_2)(=NSiMe_3)[CyNC(NMe_2)NCy]_2$ (**11**).

Table 4.1. X-ray crystallographic data for **11**.

Formula	$C_{35}H_{71}N_8SiTa$
Formula weight	813.04
Temperature (K)	173(2)
Crystal system, Space group	Monoclinic, *P*2(1)/n
a (Å)	11.2599(15)
b (Å)	23.957(3)
c (Å)	14.892(2)
β (°)	93.496(3)
V (Å^3)	4009.8(9)
Z	4
D_{calc} (g/cm^3)	1.347
Crystal size (mm^3)	0.20 x 0.20 x 0.30
θ range (°)	1.61 to 27.22
Reflections collected	54129
Independent reflections	8902 [*R*(int) = 0.0527]
Completeness to *θ* (°)	99.3%, 27.22
GOF on F^2	0.742
Final *R* indices [$I > 2\sigma(I)$][a]	*R*1 = 0.0251, w*R*2 = 0.0820
R indices (all data)	*R*1 = 0.0365, w*R*2 = 0.0964

[a] $R = \Sigma\ ||F_o| - |F_c|| / \Sigma|F_o|$; $R_w = (\Sigma[w(F_o^2 - F_c^2)^2] / \Sigma[w(F_o^2)^2])^{1/2}$

Table 4.2. Selected bond lengths (Å) and angles (°) in **11**.

Ta(1)-N(1)	1.814(3)	N(6)-C(27)	1.312(4)
Ta(1)-N(2)	2.008(3)	N(7)-C(27)	1.366(4)
Ta(1)-N(3)	2.163(3)	N(1)-Ta(1)-N(2)	97.27(12)
Ta(1)-N(4)	2.279(3)	N(3)-Ta(1)-N(4)	59.57(10)
Ta(1)-N(6)	2.424(3)	N(7)-Ta(1)-N(6)	58.09(9)
Ta(1)-N(7)	2.119(3)	Si(1)-N(1)-Ta(1)	165.79(19)
Si(1)-N(1)	1.710(3)	C(14)-N(5)-C(13)	115.7(3)
N(3)-C(12)	1.347(4)	C(29)-N(8)-C(28)	114.4(3)
N(4)-C(12)	1.321(4)	C(5)-N(2)-C(4)	108.5(3)

the two guanidinate ligands, one $-NMe_2$ ligand, and one $=NSiMe_3$ ligand. The difference in the bond lengths of Ta-N(1) [1.814(3) Å] and Ta-N(2) [2.008(3) Å] suggest that Ta-N(1) is a double bond, and Ta-N(2) is a single bond. The bond lengths found in **11** are similar to other reported compounds.[146,147] Fischer *et al*. synthesized a related tantalum complex,[147] $Ta(NMe_2)(=NBu^t)[CyNC(NMe_2)NCy]_2$. They found that the Ta-N(imido) bond length is 1.786(6) Å, slightly shorter than 1.814(3) Å in **11**. The Ta-NMe_2 bond lengths are similar in the two complexes: 2.005(5) Å versus 2.008(3) Å in **11**. Another compound by Fischer *et al*, $Ta(NMe_2)(=NBu^t)[(Pr^iNC(NMe_2)NPr^i)]_2$,[146] also shows similar bond lengths for the types of two Ta-N bonds at 1.785(5) Å for the imido, and 2.014 (5) Å for the amido ligand. It is interesting to note that in **11**, the four Ta-N (guanidinate) bond lengths of 2.163(3), 2.279(3), 2.424(3), and 2.119 (3) Å are fairly different. A similar phenomenon was observed by Fischer *et al* in their two complexes.[146,147] The difference in bond lengths contributes to the difference in the NMR chemical shifts for the guanidinate ligands in **11** discussed below.

4.2.3. 2D NMR Characterization of 11

To help understand and decipher the complex 1D ^1H and ^{13}C NMR spectra, several two dimensional NMR experiments have been conducted. Heteronuclear Single Quantum Coherence (HSQC, Figure 4.7) gives the correlation between ^1H and ^{13}C atoms directly bound to each other. The HSQC spectrum showed a correlation peak between each of the four ipso carbon atoms on the cyclohexyl rings, as pentets, in the ^1H NMR spectrum at 3.28, 3.45 (2 overlapping), and 3.67 ppm, and

the four single peaks on the ^{13}C NMR at 54.79, 55.87, 57.04, and 57.59 ppm, respectively. The HSQC also showed a correlation between the ^{1}H and ^{13}C peaks for the two inequivalent CH_3 groups on the $–NMe_2$ ligand.

Heteronuclear Multiple Bond Correlation (HMBC, Figure 4.8) shows the ^{1}H-^{13}C correlations that occur through two or more bonds. With this experiment, the correlation between the tertiary carbon and the methyl groups in the guanidinate ligands were observed.

The ^{1}H NMR spectrum of **11** shows two singlets at 3.53 ppm and 4.21 ppm (Figure 4.3). These peaks are assigned to the two methyl groups of the amide ligand, indicating that they are inequivalent. This has been observed in other similar compounds.[137,146,147] This type of inequivalence has been well studied, especially in *N*,*N*-dimethylformamide (DMF),[175-179] as a result of a hindered rotation due to the π-bonding between the carbon and nitrogen atoms. When the temperature of the system is raised enough to overcome the energy barrier of the rotation, the two peaks coalesce, giving a single resonance.[175,176]

In **11**, the nitrogen of the amide ligand donates its lone pair of electrons to the tantalum atom to reduce the electron deficiency at the metal center (Figure 4.9). The restricted rotation of the d-p π bond leads to different chemical environments for the two methyl groups. One methyl group is much closer to the $–NSiMe_3$ ligand than the other, as shown in the partial crystal structure of **11** (Figure 4.10). It is interesting to note that, in DMF, the difference in the two peaks is only about 10 Hz[175] at room temperature, while in **11** the difference is about 265 Hz, indicating a larger difference in chemical environments between the two methyl groups of the $–NMe_2$ ligand in **11**.

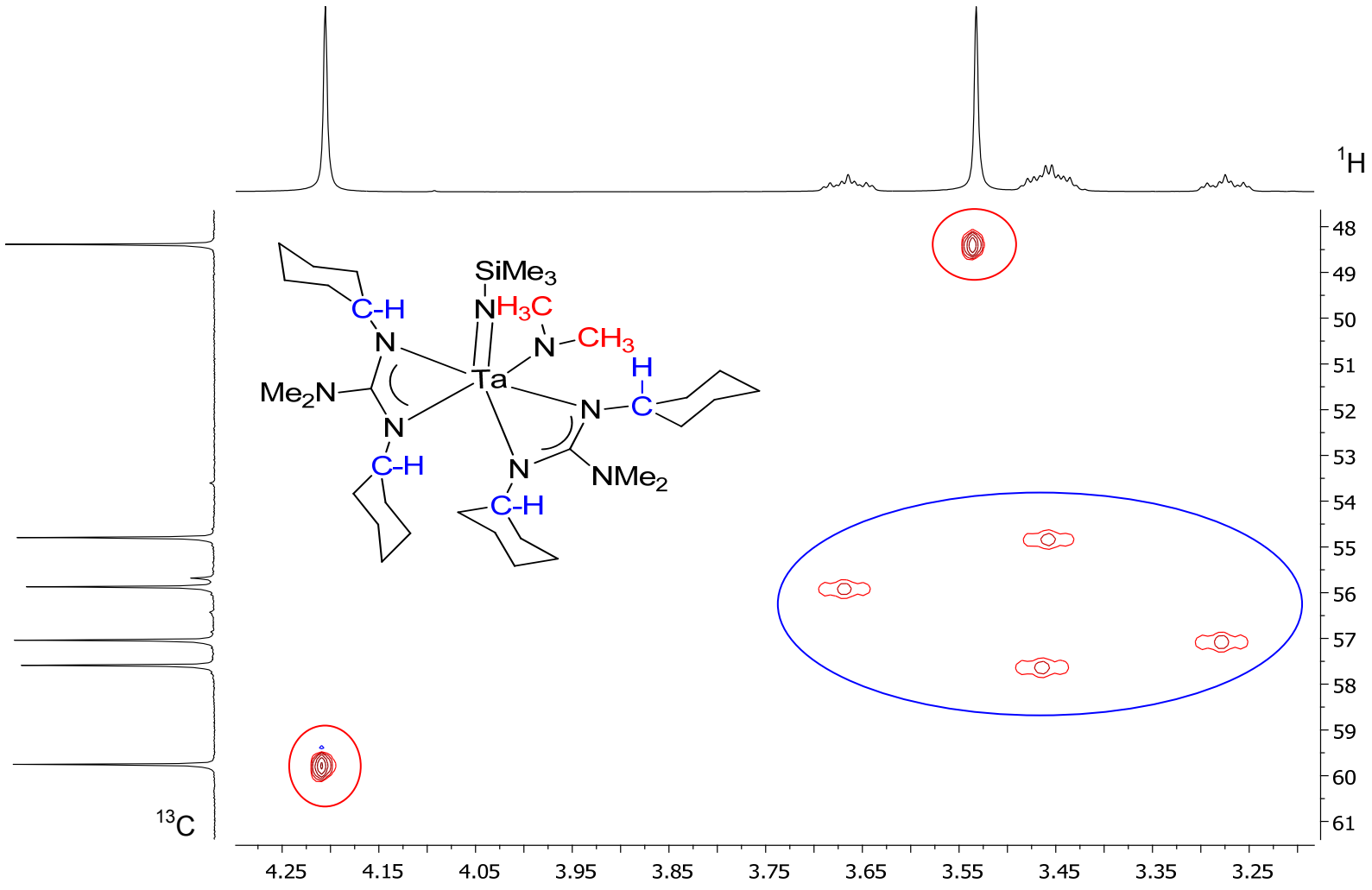

Figure 4.7. HSQC spectrum of **11** at room temperature.

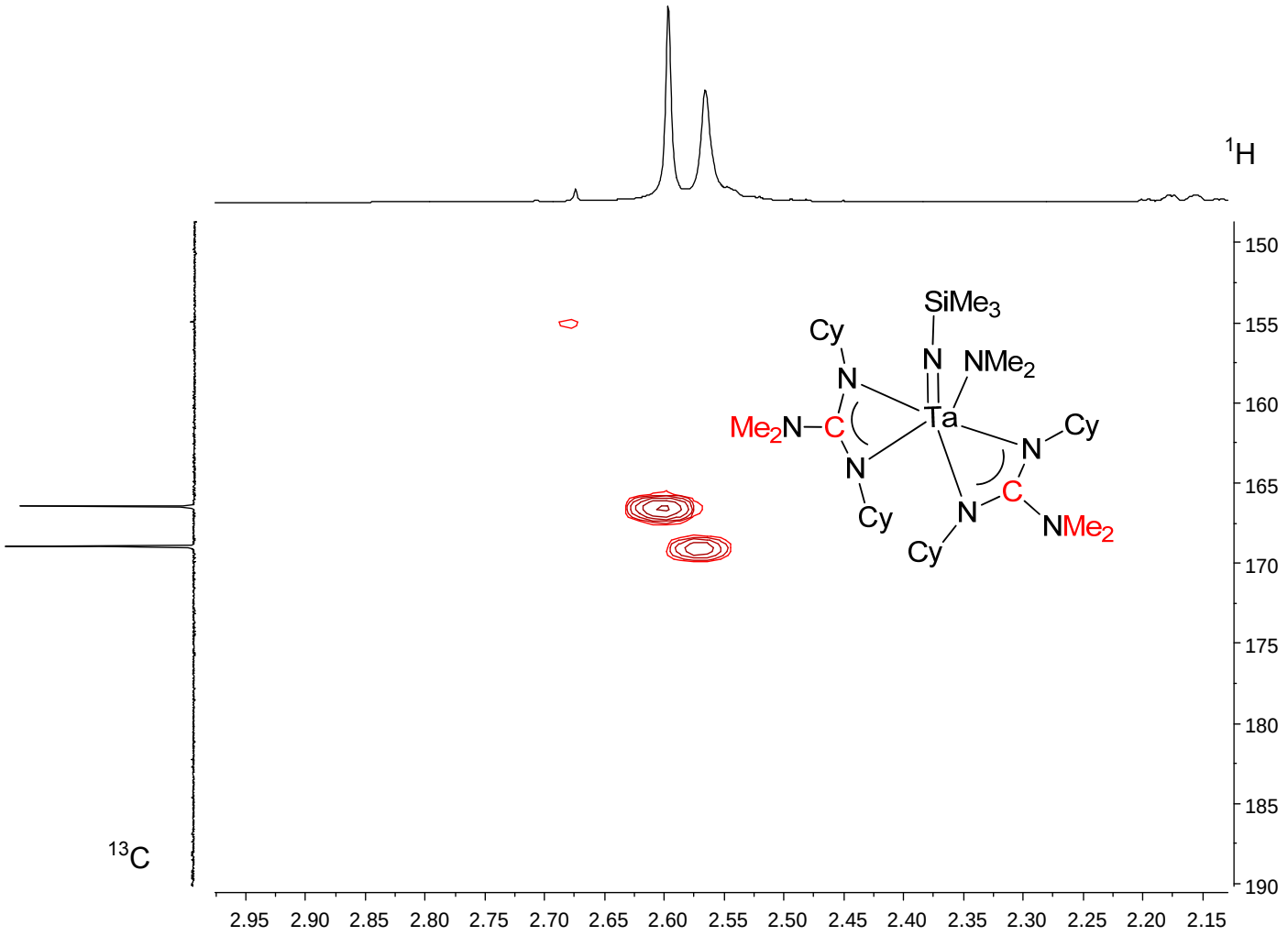

Figure 4.8. HMBC spectrum of **11** at room temperature.

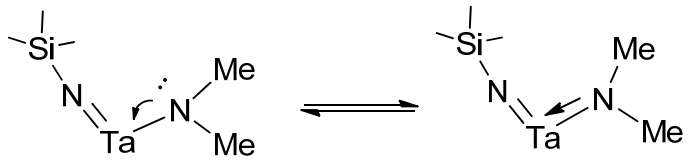

Figure 4.9. d-p π bond between Ta and N atoms in **11**.

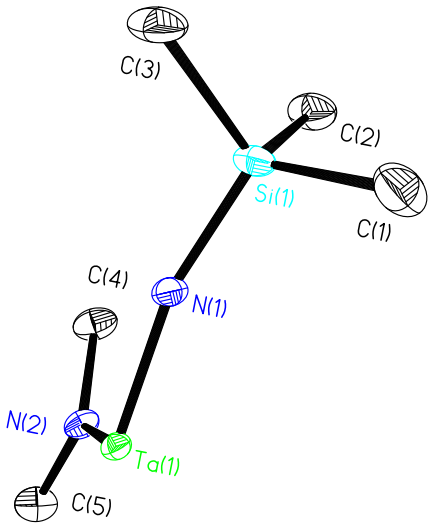

Figure 4.10. Portion of the ORTEP view of **11**.

A Nuclear Overhauser Enhancement Spectroscopy (NOESY) experiment was conducted to characterize the inequivalent methyl groups in the $-NMe_2$ ligand. A NOESY experiment shows the ^1H-^1H correlation between two atoms through space. The fact that one methyl group in the amide group is closer to the imide ligand through space should be visible in the NOESY spectrum by a stronger correlation peak at one methyl group than at the other in relation to the methyl peak of the $=NSiMe_3$ ligand. The NOESY spectrum (Figure 4.11) indeed confirms that one methyl group of the amide ligand (at 4.21 ppm in ^1H NMR) is closer than the other (3.53 ppm) to the imide ligand.

4.2.4. Variable-Temperature NMR Studies of 11

It is expected that at higher temperatures, the two methyl peaks of the $-NMe_2$ ligand coalesce as the compound overcomes the barrier of rotation and breaks the π bond between the nitrogen and the tantalum, leading to coalescence of the peaks.[5] To determine when this coalescence occurs, variable-temperature NMR studies were preformed (Figure 4.12). The coalescence temperature was found to be 120 °C (393 K), which is approximately the same as that in DMF.[175,176] It was also found that the slow exchange limit, or the temperature at which the two peaks no longer move apart is 70 °C (343 K).[180,181] Attempts were made to calculate the rate constants for this interconversion at various temperatures using Eq. 4.1.

$$k = \pi\sqrt{2(\Delta\nu_0^2 - \Delta\nu^2)} \qquad \text{Eq. 4.1}$$

(where $\Delta\nu_0$ and $\Delta\nu$ are the frequency differences (Hz) between the site of the slow exchange limit and the exchange-broadened site at temperature *T*, respectively[182-185]).

Unfortunately, due to significant peak overlaps of the upfield methyl resonance with other peaks, as shown in Figure 4.12, this calculation could not be performed with good accuracy. The rate constant was thus calculated only at the coalescence temperature, when in Eq. 4.1, $\Delta\nu = 0$. This rate was found to be 1182 s^{-1}.

4.2.5. Preparation and Characterization of $Ta(NMe_2)(=NSiMe_3)$-$[Pr^iNC(NMe_2)NPr^i]_2$ (12)

12 was synthesized by reacting $Ta(NMe_2)_4[N(SiMe_3)_2]$ (**13**) with two equivalents of $Pr^iN=C=NPr^i$ (Scheme 4.3). The mixture was heated to 60 °C and stirred for six days to complete the reaction. The ^1H and ^{13}C NMR spectra (Figures 4.13 and 4.14) are similar to those of **11**, except that one –CH– peak in the ^{13}C NMR spectrum overlaps with a peak of the $–NMe_2$ ligand. This was confirmed by an HSQC experiment. The HSQC spectrum (Figure 4.15) showed that one –CH– peak (3.90 ppm) and one peak of the $–NMe_2$ ligand (3.51 ppm) in the ^1H NMR spectrum overlap in the ^{13}C NMR spectrum at 48.35 ppm. While no crystal structure was obtained, NMR evidence indicates that the compound is isostructural with **11**.

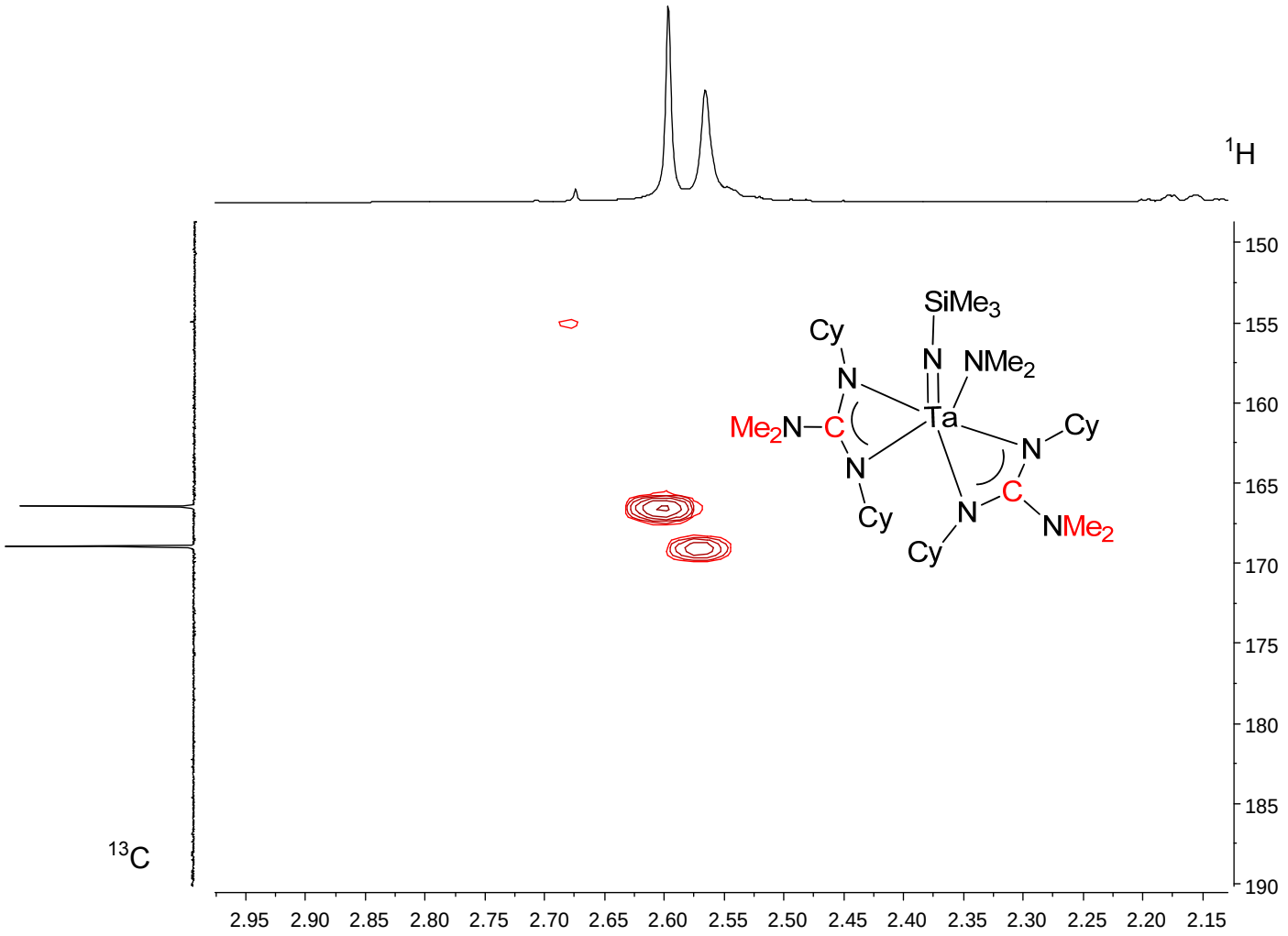

Figure 4.8. HMBC spectrum of **11** at room temperature.

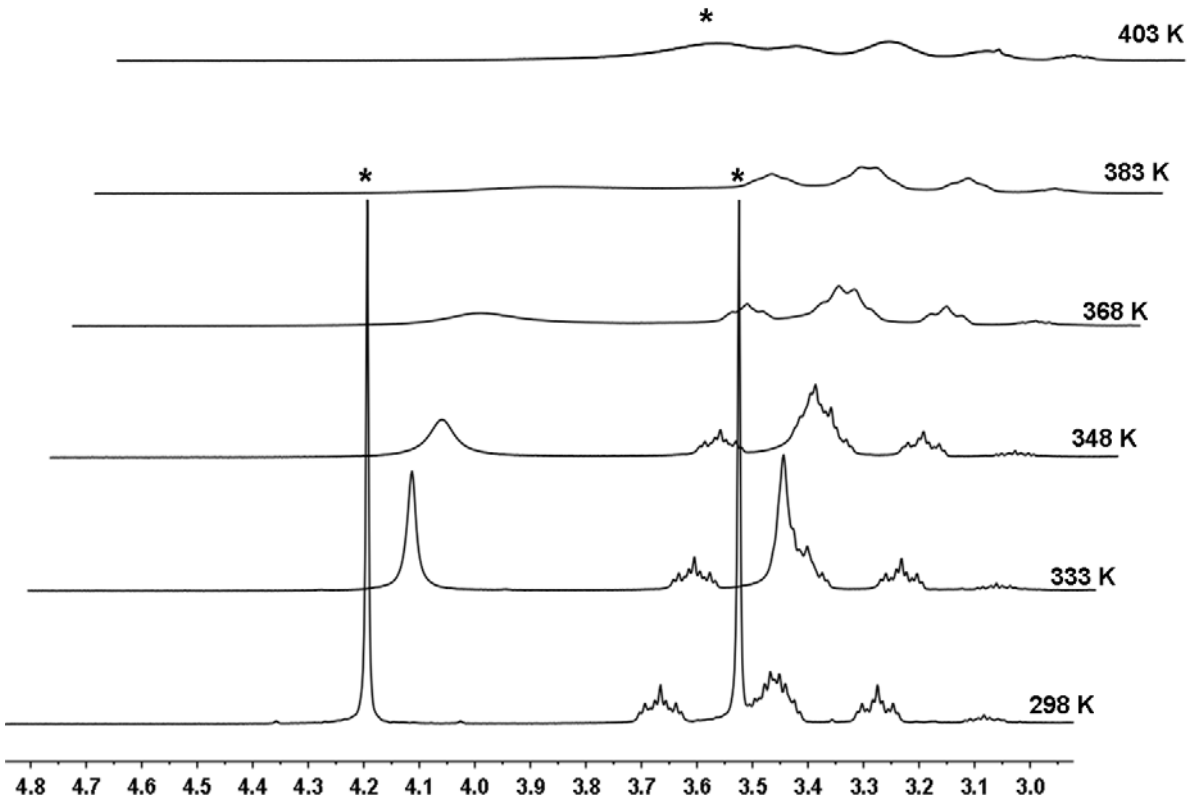

Figure 4.12. VT ^{1}H NMR spectra showing the coalescence of the two methyl groups in the amide ligand (–NMe_2) of **11** as the temperature increases.

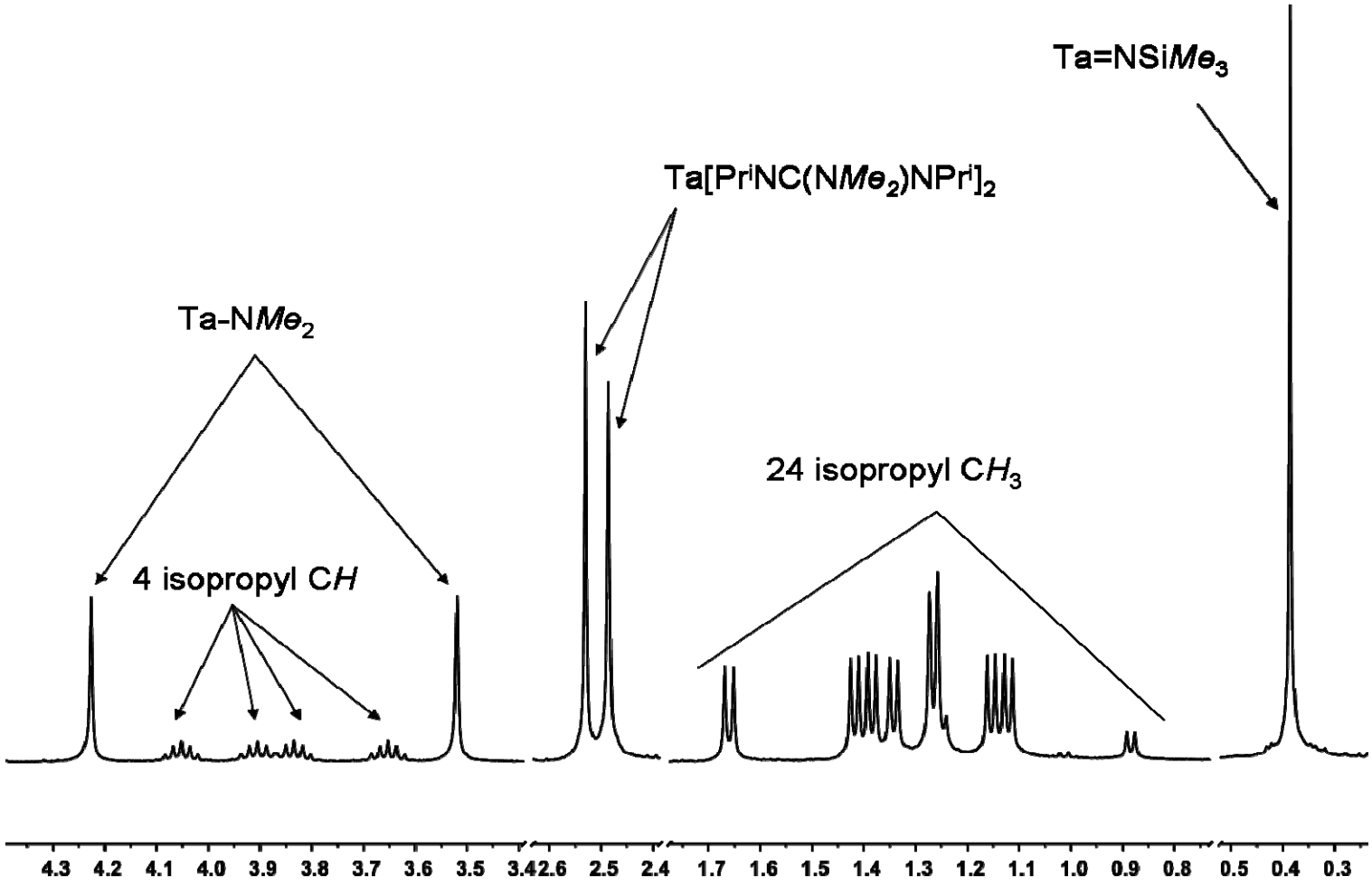

Figure 4.13. ^{1}H NMR spectrum of $Ta(NMe_2)(=NSiMe_3)[Pr^iNC(NMe_2)NPr^i]_2$ (**12**).

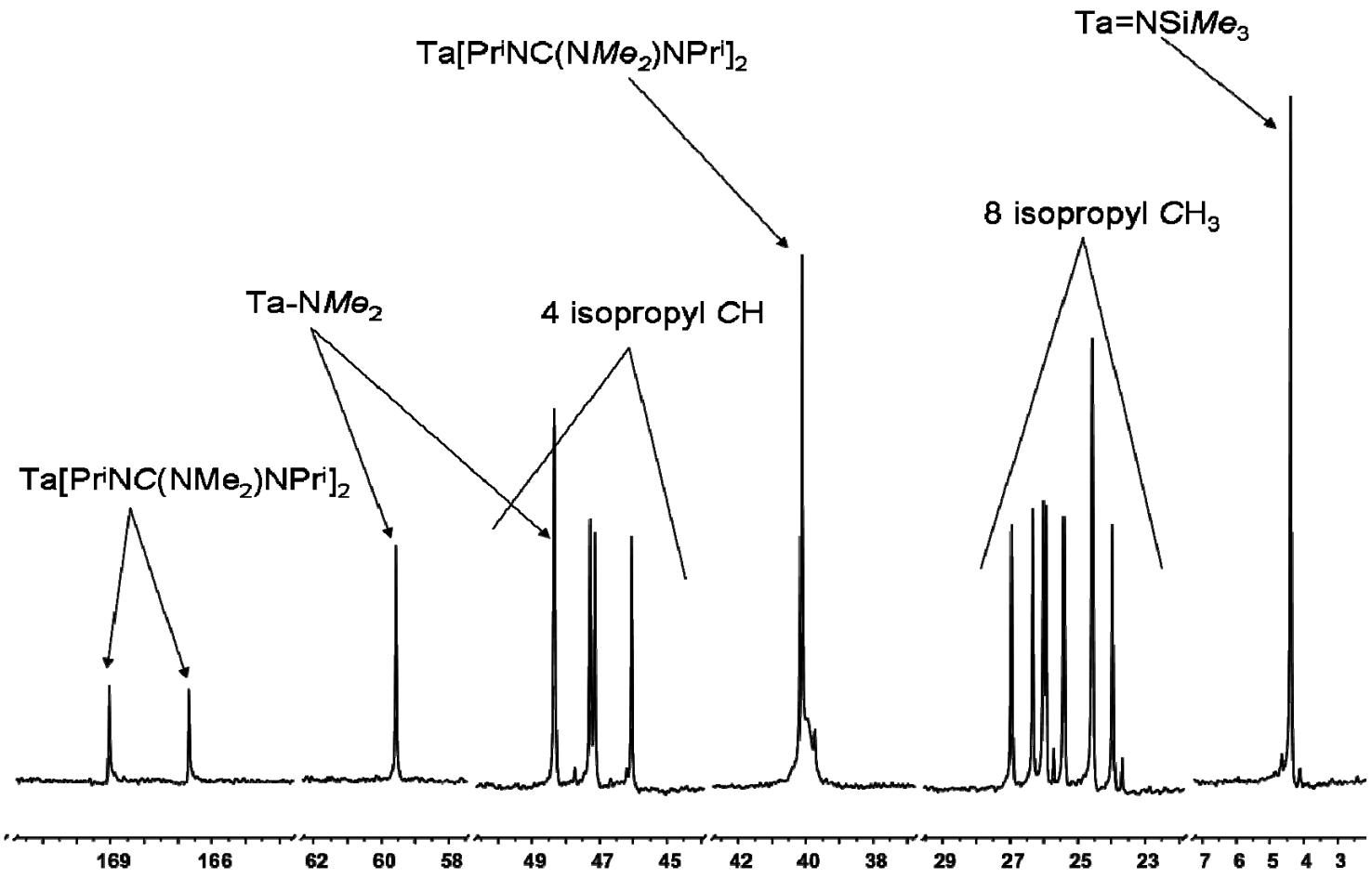

Figure 4.14. ^{13}C NMR spectrum of $Ta(NMe_2)(=NSiMe_3)[Pr^iNC(NMe_2)NPr^i]_2$ (**12**).

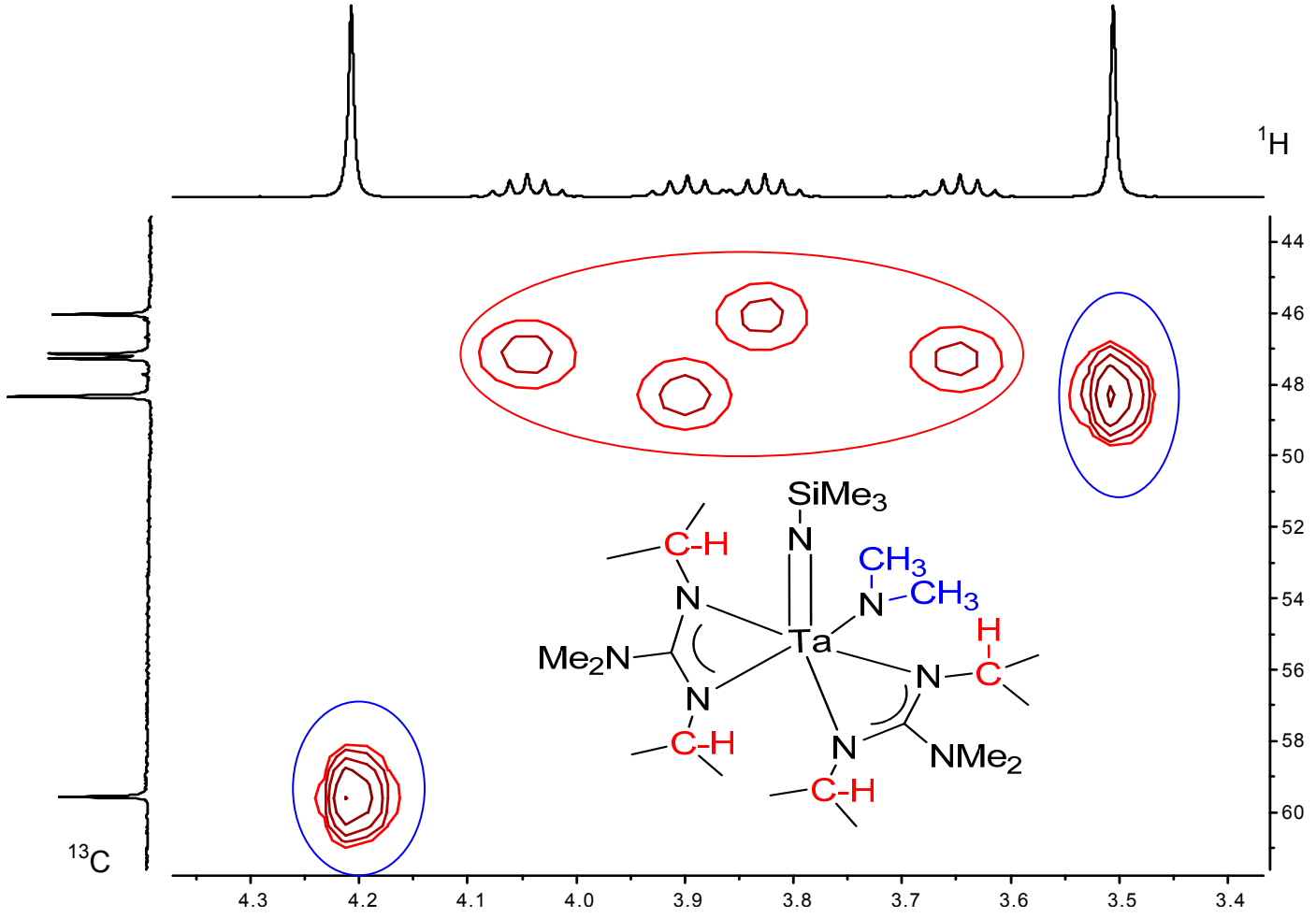

Figure 4.15. HSQC spectrum of **12**.

4.2.6. Mechanistic Studies of the Formation of 11

The formation of **11** has been investigated. A possible mechanistic pathway in the formation of **11** is given in Scheme 4.4. Imide formation from $Ta(NMe_2)_4[N(SiMe_3)_2]$ (**13**) occurs, once heating begins, giving the unstable compound $Ta(NMe_2)_3(=NSiMe_3)$ (**15**). A carbodiimide then coordinates to the metal, followed by a migratory insertion into an amide ligand, forming the intermediate **16**. A second carbodiimide insertion gives the final product **11**.

Studies were performed to identify the intermediate(s) in the reaction. In the first experiment, the starting material, **13**, was heated at 85 °C for a total of 50 h. After 2 h, peaks of $Me_3Si\text{-}NMe_2$ (**14**) were observed as well as unidentified peaks that were assigned to be those of **15** in ^1H, ^{13}C, and ^{29}Si NMR (Figures 4.16-4.18). After 24 h, **15** and **13** were no longer present, and only **14** was observed in the ^1H NMR spectrum. The observations indicated that **15** is thermally unstable, and only with the addition of the carbodiimide is the imide product stablized. This experiment shows that the formation of the imide through elimination of **14** is an intrinsic property of $Ta(NMe_2)_4[N(SiMe_3)_2]$ (**13**). The insertion of the carbodiimides apparently does not lead to the formation of the imide **15**, but, by capturing it to form the guanidinate, **11**, it stabilizes the intermediate, **15**.

To confirm the pathway after the formation of **15**, 1 equivalent of CyN=C=NCy was added to **13** in benzene-d_6 and the solution was heated at 60 °C. The reaction was monitored by ^1H and ^{13}C spectroscopy. As the reaction proceeded, peaks representing **11** and **14** were observed in ^1H and ^{13}C NMR spectra. In addition, ^1H and ^{13}C NMR peaks consistent with the intermediate $Ta(NMe_2)_2(=NSiMe_3)$-

[CyNC(NMe_2)NCy] (**16**) were also observed in the spectra. The ^{1}H and ^{13}C NMR spectra at the end of the reaction are given Figures 4.19 and 4.20a-b, respectively, which show the peaks of all three compounds, the intermediate **16** as well as **11** and **14**. To further confirm the identity of the intermediate **16**, ^{29}Si NMR spectroscopy was also used to monitor the reaction. A new peak at -13.128 ppm (Figure 4.21) was assigned to that of the imide ligand =$NSiMe_3$ in **16**. As expected, the chemical shift of this imide peak is closer to that of the imide ligand =$NSiMe_3$ in **11** (-16.349 ppm) than that of the amide ligand –$N(SiMe_3)_2$ in $Ta(NMe_2)_4[N(SiMe_3)_2]$ (**13**) (-4.514 ppm).

Direct Analysis in Real Time (DART) mass spectrometry (MS) was also used to identify the intermediate **16** as well as other species in the reaction mixture. No peak representing the mass of any of the compounds in the sample was observed. This is likely due to fragmentation of the compounds during the acquisition process. During the acquisition, the sample was briefly exposed (<5 s) to air. Air sensitivity of the compounds in the sample may lead to their decomposition prior to the sample reaching the MS. This scenario seems unlikely, though, as the sample was exposed to air for 1.5 h with no significant decomposition.

Since heating at 60 °C was also used to make $Ta(NMe_2)_2(=NSiMe_3)[Pr^iNC(NMe_2)NPr^i]_2$ (**12**), it is likley that its formation follows a pathway similar to that in the formation of its bulkier analog **11**.

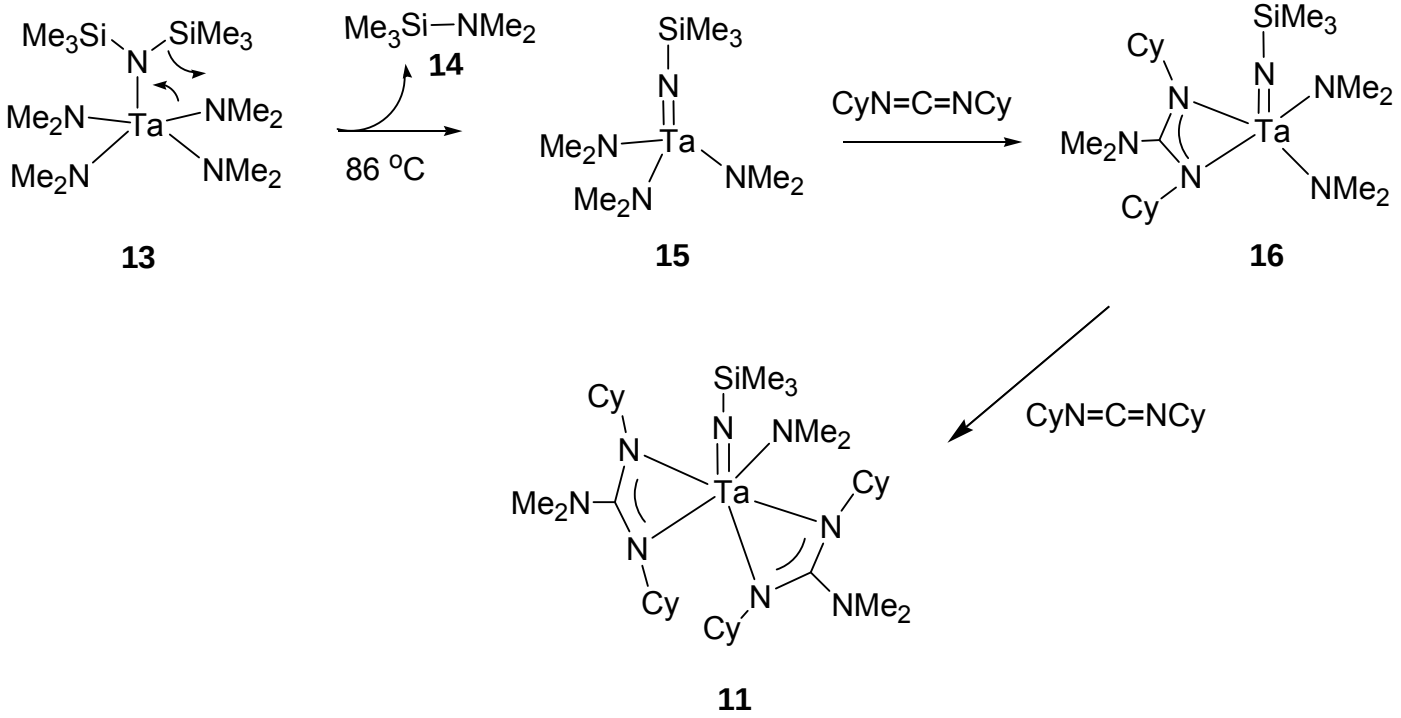

Scheme 4.4. Proposed pathway in the formation of **11**.

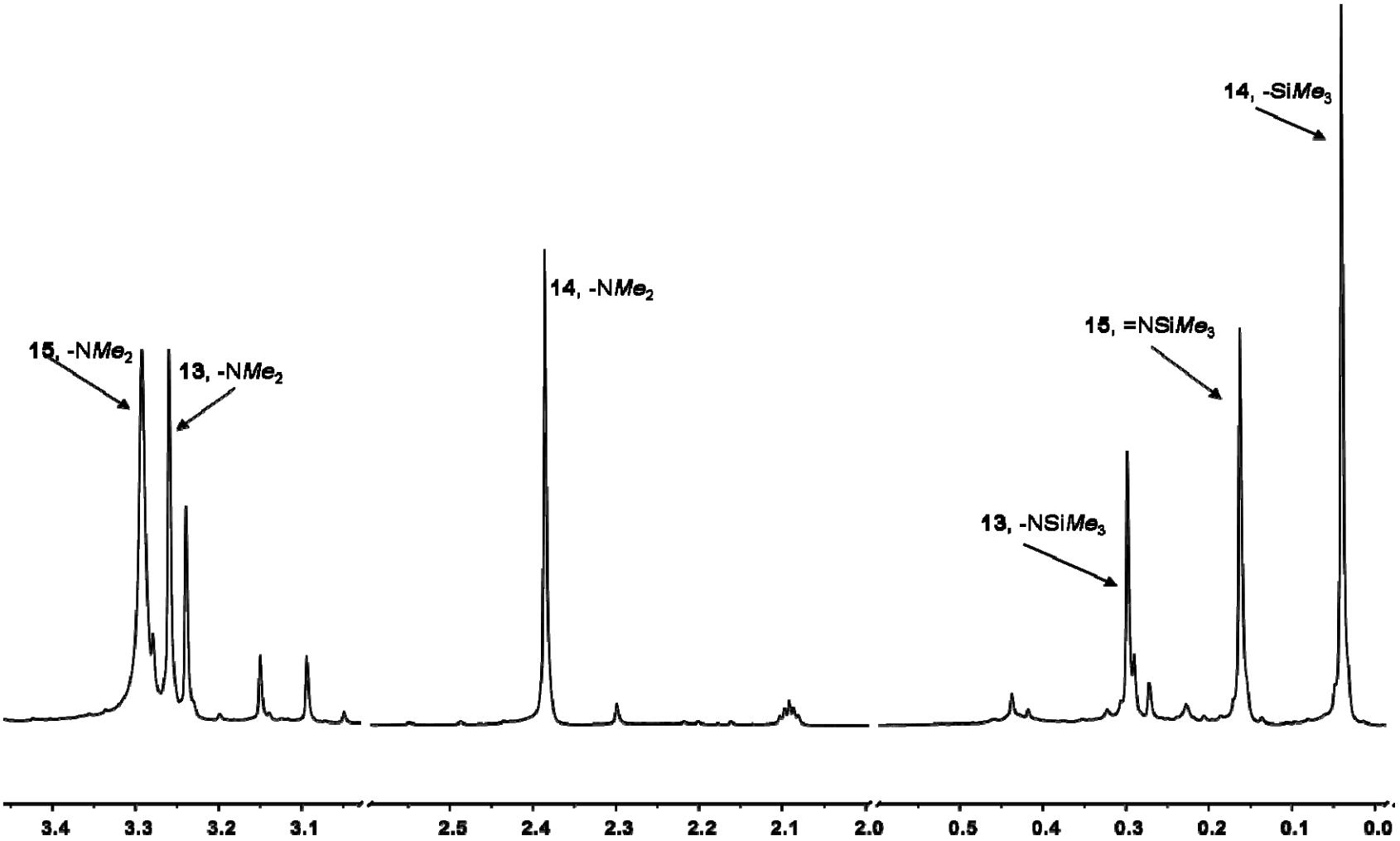

Figure 4.16. ^{1}H NMR spectrum after heating **13** for 2 h at 85 °C.

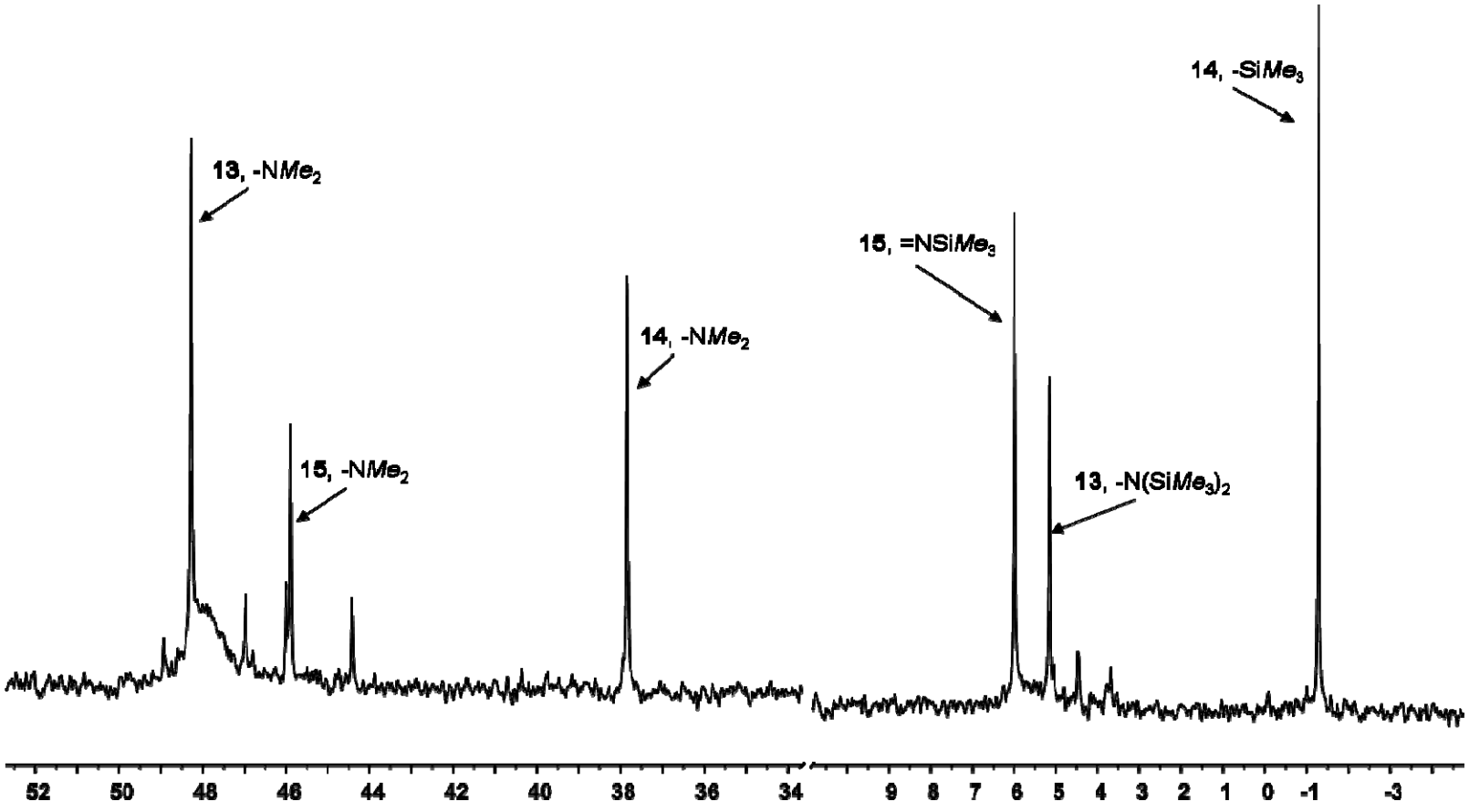

Figure 4.17. ^{13}C NMR spectrum after heating **13** for 2 h at 85 °C.

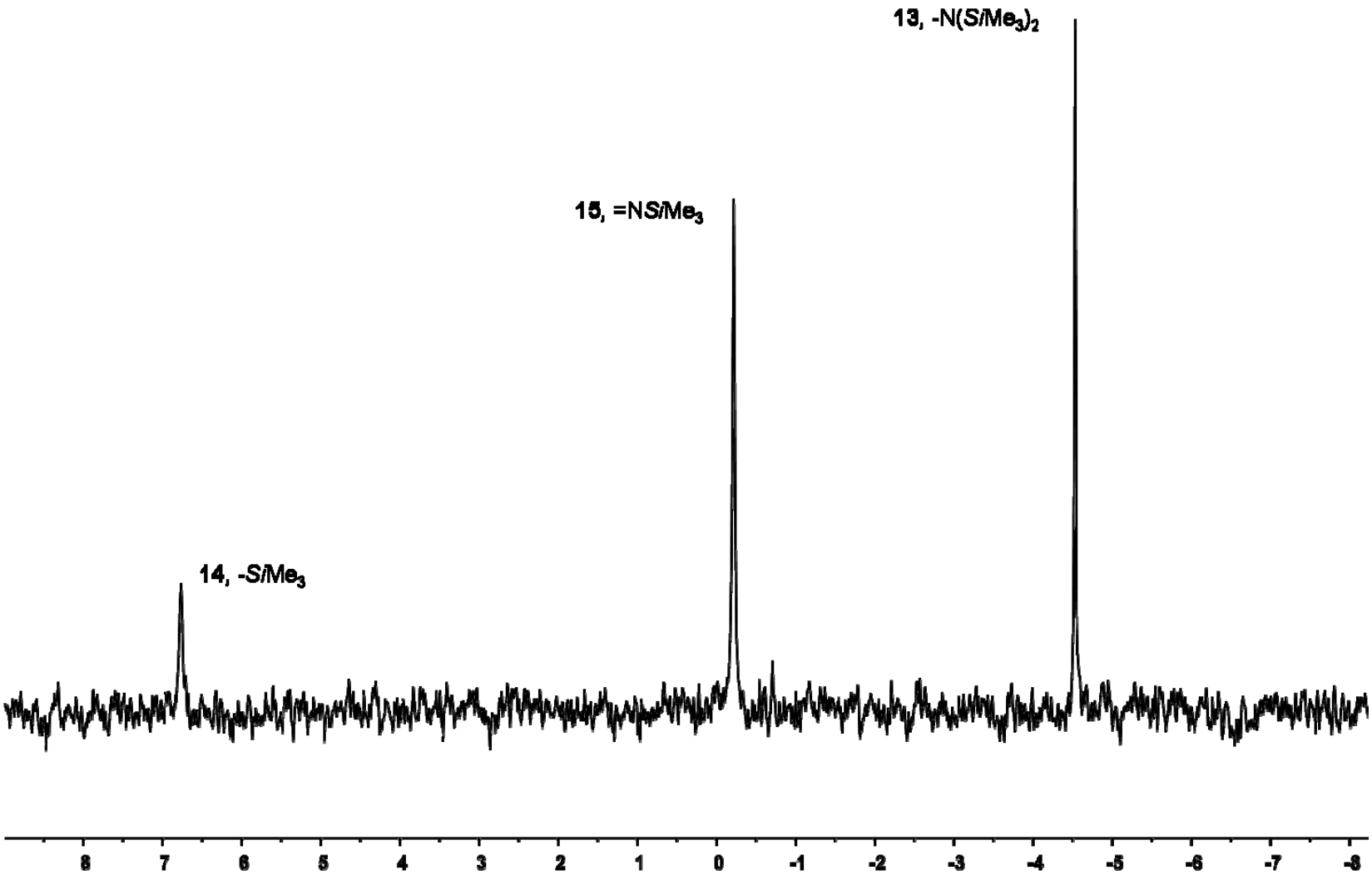

Figure 4.18. ^{29}Si NMR spectrum after heating **13** for 2 h at 85 °C

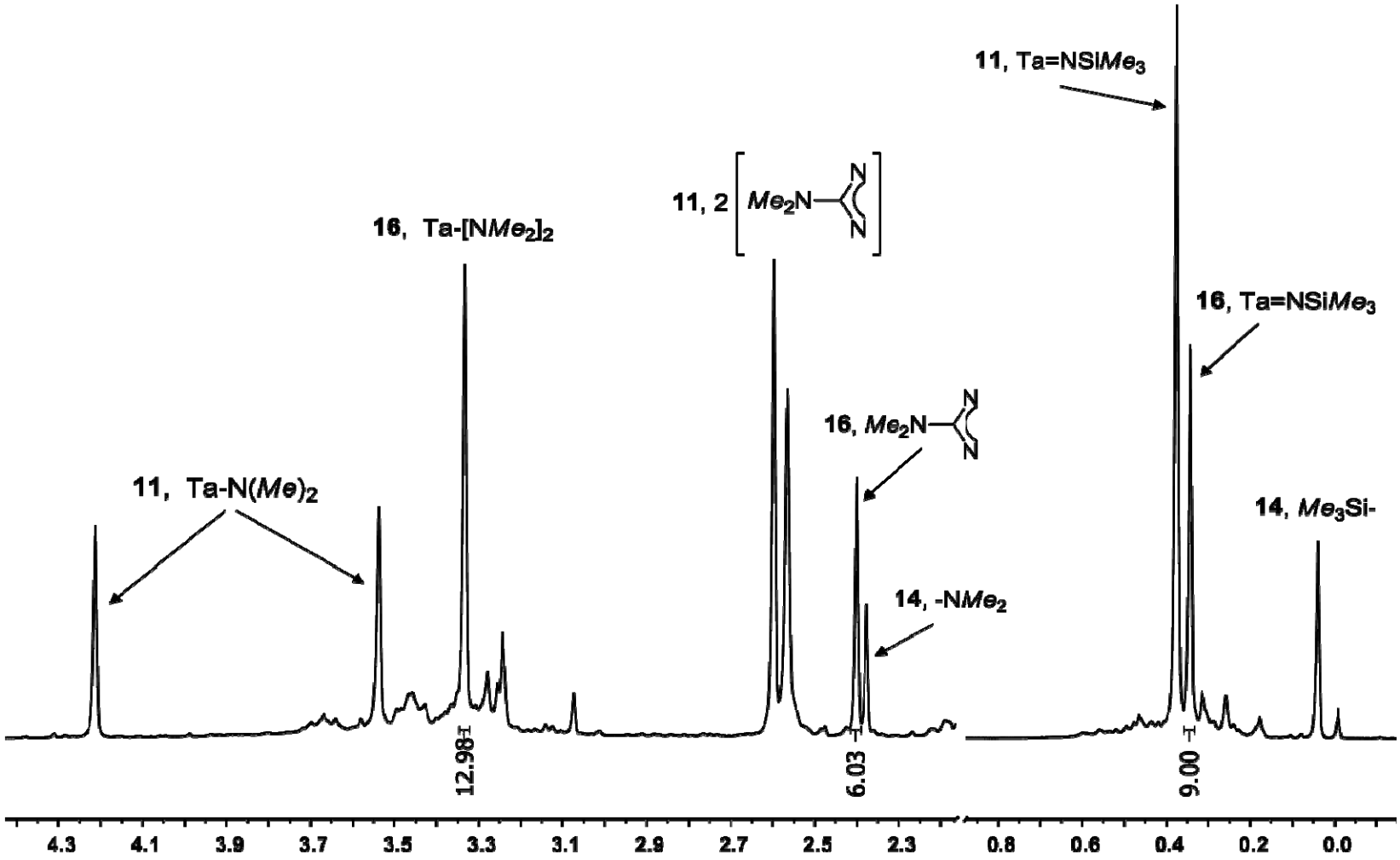

Figure 4.19. ^{1}H NMR spectrum of the reaction between **13** and 1 equivalent of CyN=C=NCy.

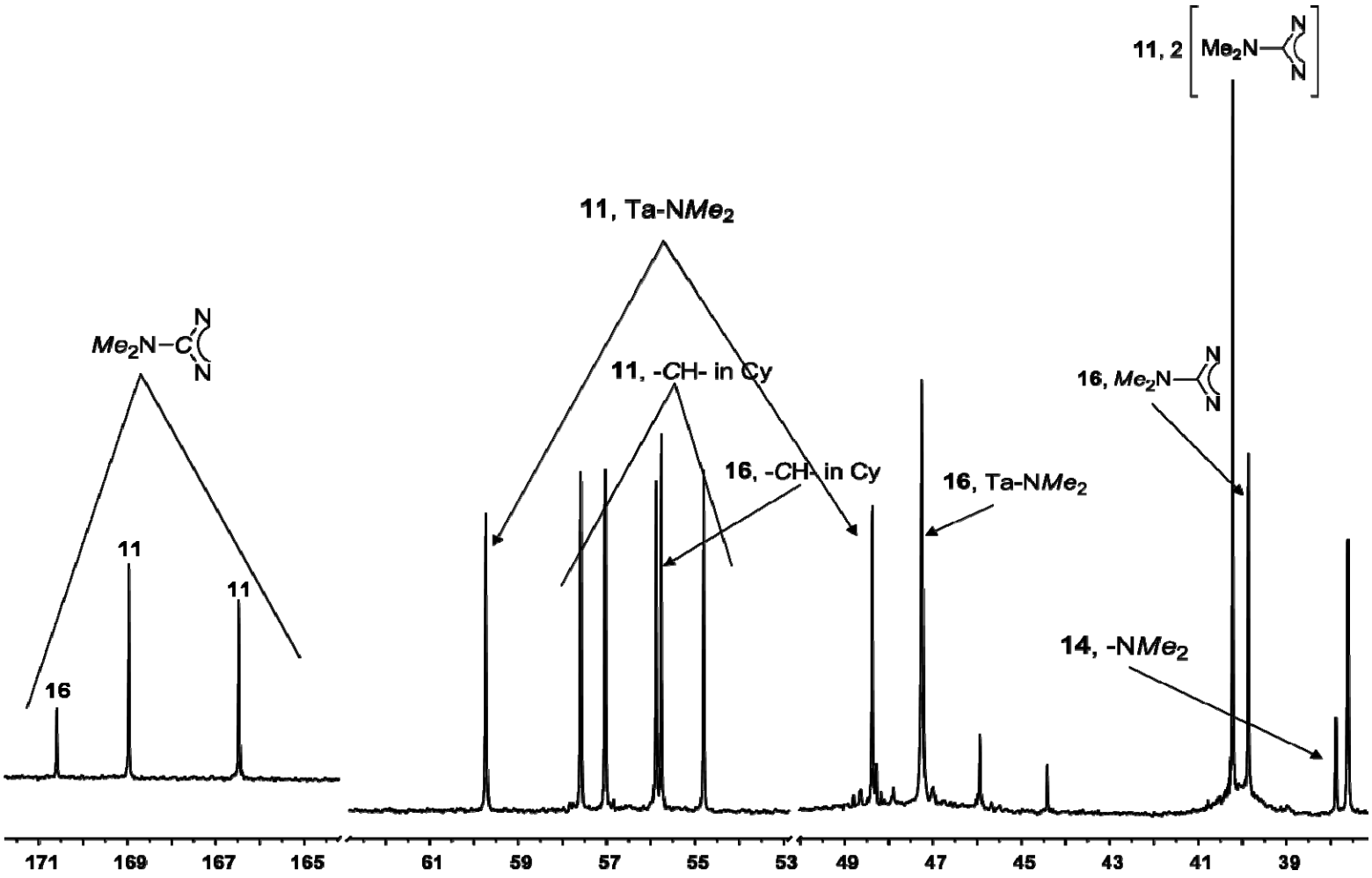

Figure 4.20a. ^{13}C NMR spectrum (downfield portion) of the reaction between **13** and 1 equivalent of CyN=C=NCy.

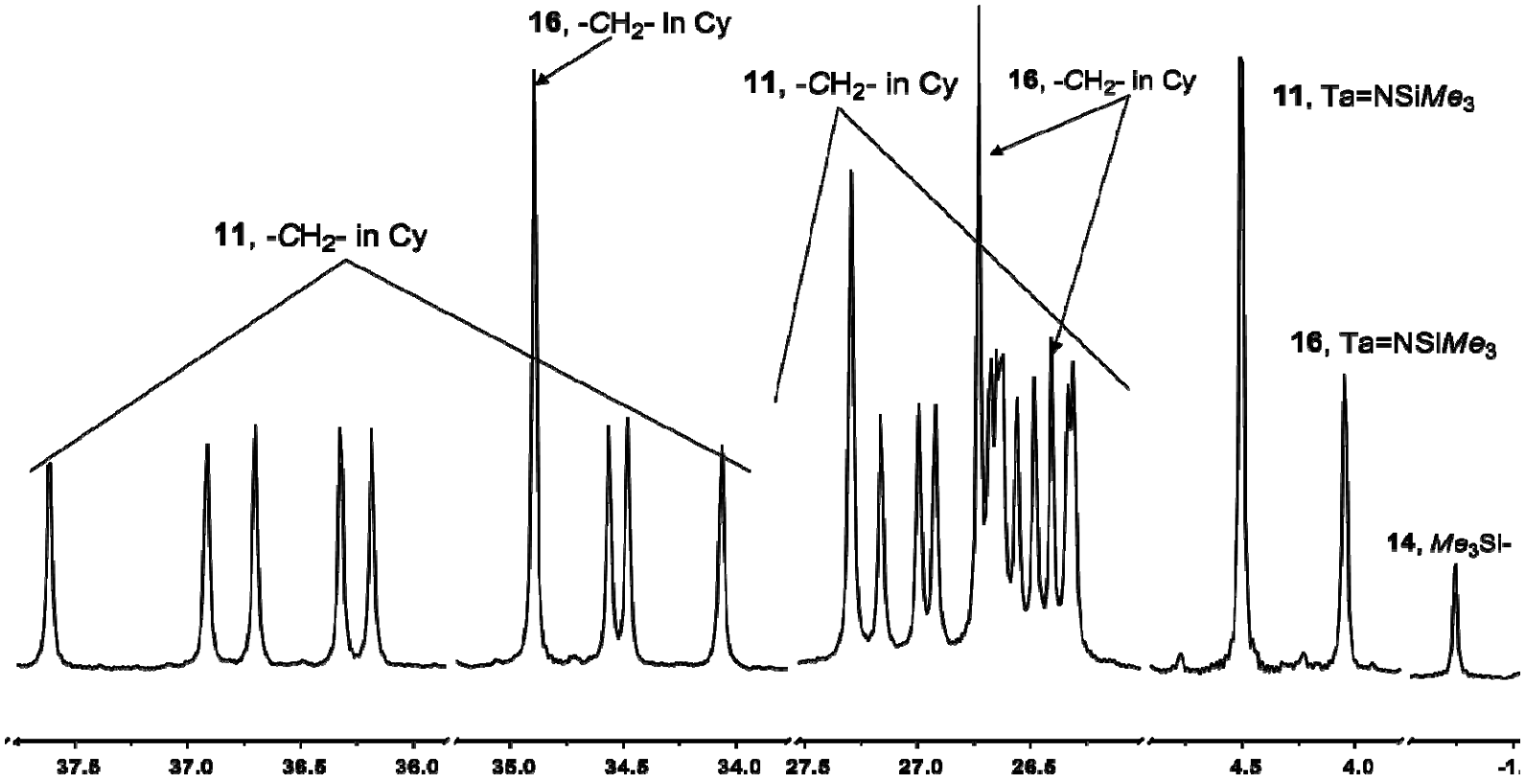

Figure 4.20b. ^{13}C NMR spectrum (upfield portion) of the reaction between **13** and 1 equivalent of CyN=C=NCy.

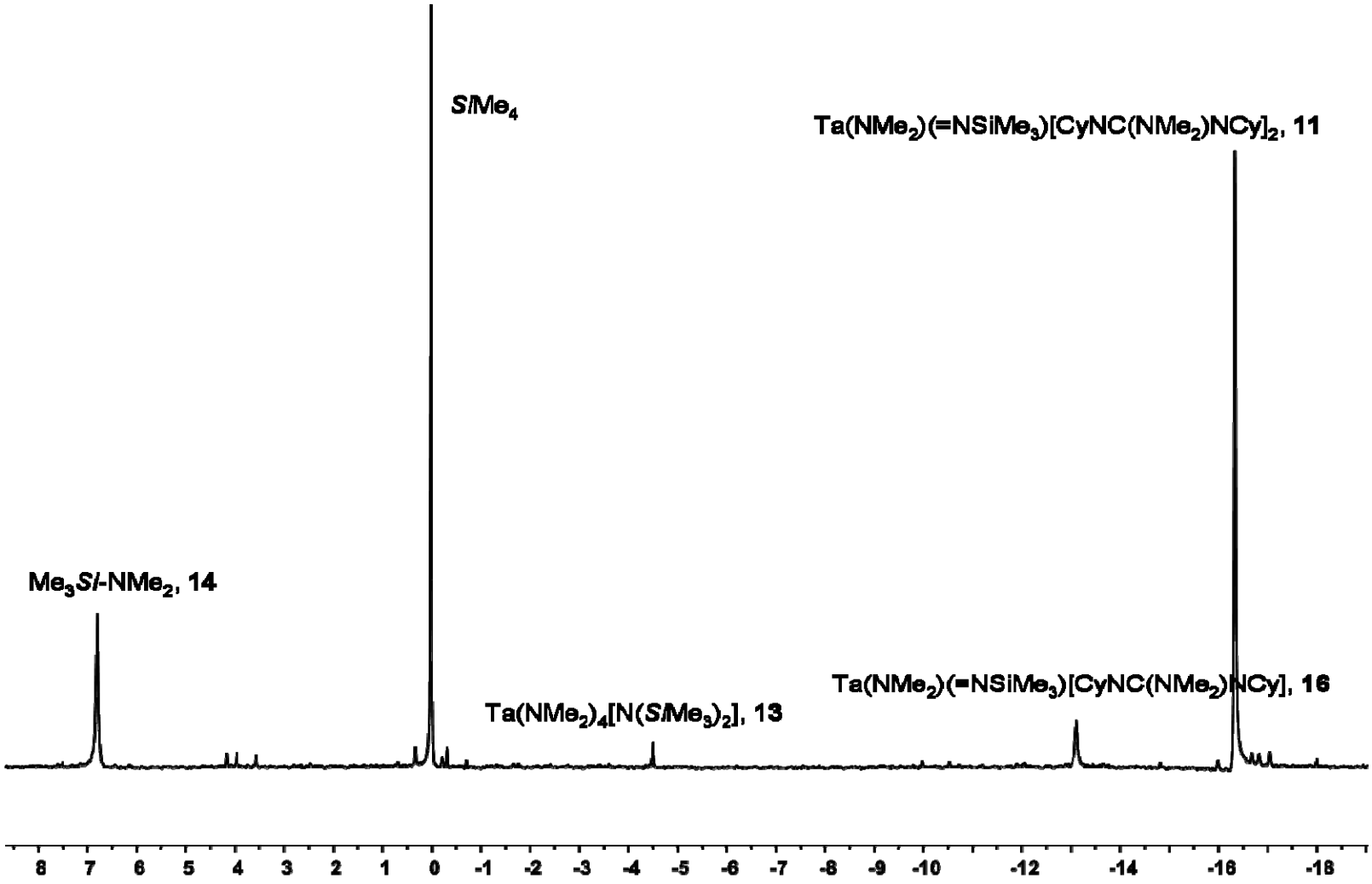

Figure 4.21. ^{29}Si NMR spectrum of the reaction between **13** and 1 equivalent of CyN=C=NCy.

4.3. Concluding Remarks

This chapter reports the synthesis, characterization and structures of new imido complexes. Under heating, $Ta(NMe_2)[N(SiMe_3)]_2$ (**13**) undergoes an α-$SiMe_3$ abstraction by an amide ligand, yielding **14** and $Ta(NMe_2)_3(=NSiMe_3)$ (**15**). To our knowledge, such formation of an imide has not been reported. In the presence of RN=C=NR, the carbodiimide reacts with imide **15**, first form mono-guanidinate $Ta(NMe_2)_2(=NSiMe_3)[CyNC(NMe_2)NCy]$ (**16**) and later di-guanidinate $Ta(NMe_2)(=NSiMe_3)[CyNC(NMe_2)NCy]_2$ (**11**). Variable-temperature NMR has been used to study the interconversion between the two inequivalent methyl groups on the $–NMe_2$ ligand in **11**.

4.4. Experimental Section

All manipulations were preformed under a dry nitrogen atmosphere with the use of either a drybox or standard Schlenk techniques. Toluene was dried over potassium/benzophenone, distilled, and stored under N_2. Benzene-d_6 and toluene-d_8 were dried over activated molecular sieves and stored under N_2. Benzene-d_6 was used in the identification of complexes after their synthesis. For the mechanistic studies, benzene-d_6 containing $SiMe_4$ was used. Toluene-d_8 was used in all variable-temperature and 2D NMR studies. $TaCl_5$ (Strem) was sublimed before use. $LiNMe_2$ (Aldrich), $LiN(SiMe_3)_2$ (Aldrich), and RN=C=NR (R = Cy, Pr^i) (Acros) were used as received. $TaCl(NMe_2)_4$ and $Ta(NMe_2)_4[N(SiMe_3)_2]$ (**13**) were prepared according to literature procedures.[153] NMR spectra were recorded on a Bruker AMX-400 Fourier transform spectrometer unless otherwise noted, and were referenced to solvents.

Elemental analyses were conducted via Complete Analysis Laboratories, Inc., Parsippany, NJ.

4.4.1. Preparation of $Ta(NMe_2)(=NSiMe_3)[CyNC(NMe_2)NCy]_2$ (11)

$Ta(NMe_2)_4[N(SiMe_3)_2]$ (**13**, 300.0 mg, 0.580 mmol) and CyN=C=NCy (299.1 mg, 1.45 mmol) were added to a flask. Excess ligand was used to ensure a complete reaction. After the reaction, the excess was removed with the solvent. To the flask, toluene was added at room temperature, and the yellow solution was heated to 60 °C in an oil bath and stirred for 6 days. No color change was observed. If higher temperatures were used, the solution turned black but still showed the same NMR spectra (crystals were not obtained from these samples). The solvent was removed under vacuum, resulting in a yellow liquid. Slight agitation of the liquid was needed to promote crystal growth. Colorless crystals were formed at room temperature (226.4 mg, 0.28 mmol, 48% yield). **11**: ^{1}H NMR (benzene-d_6, 399.87 MHz, 23 °C) δ 4.21 (s, 3H, TaN*Me*$_a$Me$_b$), 3.53 (s, 3H, TaNMe$_a$*Me*$_b$), 3.67, 3.45, 3.45, 3.28 (m, each 1H, ipso-C*H*), 2.60 [s, 6H, C(N*Me*$_2$) for one guanidinate ligand], 2.56 [s, 6H, C(N*Me*$_2$) for another guanidinate ligand], 1.131-2.201 (40H, C*H*$_2$ in Cy), 0.37 (s, 9H, Si*Me*$_3$); ^{13}C NMR (benzene-d_6, 100.55 MHz, 23 °C) δ 168.96, 166.46 [*C*(NMe$_2$)], 59.75 (Ta-N*Me*$_a$Me$_b$), 57.59, 57.04, 55.87, 54.79 (ipso C), 48.39 (Ta-NMe$_a$*Me*$_b$), 40.23 [C(N*Me*$_2$) for both guanidinate ligands], 25-37.62 (*C*H$_2$ in Cy), 4.51 (Si*Me*$_3$); ^{29}Si{^{1}H} NMR (DEPT, benzene-d_6, 127.1 MHz, 23 °C) δ -16.32 (*Si*Me$_3$). Anal. Calcd for $C_{35}H_{71}N_8SiTa$: C, 51.70; H, 8.80; N 13.79. Found C, 51.56; H, 9.02; N, 14.10.

The following experiments were conducted to test the stability of **11** to O_2 and water. A solution of $Ta(NMe_2)(=NSiMe_3)[CyNC(NMe_2)NCy]_2$ (**11**, 0.077 g, 0.095 mmol) in toluene-d_8 was frozen in liquid nitrogen, and the J. Young's tube was pumped for 5 min. The frozen solid was warmed gradually until it melted, and one equivalent of O_2 (0.095 mmol) was then added. The yellow solution was placed at room temperature for several days and heated at 60 °C for several weeks. No change in color or NMR was observed.

When a sample was left open to the air for several weeks, no change was observed in the NMR, but a very small amount of insoluble solid formed.

In another test, deionized water was degassed by nitrogen for 10 min. The water (10 μg, 0.5 μmol) was transferred by a microsyringe to dry THF (5 mL). The "wet" THF (0.5 mL) was then slowly added to **1** (25.0 mg, 0.031 mmol) in benzene-d_6. The tube was agitated. In a few minutes, the color of the sample changed from clear yellow to colorless, and a white solid formed. The solid was found to be insoluble, and was not studied further.

4.4.2. Preparation of $Ta(NMe_2)(=NSiMe_3)[Pr^iNC(NMe_2)NPr^i]_2$ (12)

$Ta(NMe_2)_4[N(SiMe_3)_2]$ (**13**, 300.0 mg, 0.580 mmol) and $Pr^iN=C=NPr^i$ (182.9 mg, 1.45 mmol) were added to a flask. Excess ligand was used to ensure complete reaction. After the reaction, the excess was removed with the solvent. To the flask, toluene was added at room temperature, and the yellow solution was heated to 60 °C in an oil bath and stirred for 6 days. No color change was observed. If higher temperatures were used, the solution turned black but still showed the same NMR

spectra (crystals were not obtained from these samples). The solvent was removed under vacuum, resulting in a yellow liquid. Only non-crystalline solid formed (208.3 mg, 0.32 mmol, 55% yield). **12**: ^{1}H NMR (benzene-d_6, 399.87 MHz, 23 °C) δ 4.21 (s, 3H, TaN*Me*$_a$Me$_b$), 4.05, 3.90, 3.83, 3.65 (septet, each 1H, -C*H*Me$_2$), 3.51 (s, 3H, TaNMe$_a$*Me*$_b$), 2.53, 2.49 [s, each 6H, C(N*Me*$_2$)], 0.90-1.65 (24H, -CH*Me*$_2$), 0.36 (s, 9H, Si*Me*$_3$); ^{13}C NMR (benzene-d_6, 100.55 MHz, 23 °C) δ 169.03, 166.68 [*C*(NMe$_2$)], 59.57 (TaN*Me*$_a$Me$_b$), 48.35 (TaNMe$_a$*Me*$_b$), 48.35, 47.28, 47.15, 46.04 (-*C*HMe$_2$), 40.12 [C(N*Me*$_2$)], 23.96-26.96 (-CH*Me*$_2$), 4.39 (Si*Me*$_3$). Anal. Calcd for $C_{23}H_{53}N_8SiTa$: C, 42.45; H, 8.21; N 13.79. Found C, 42.69; H, 8.10; N, 13.52.

4.4.3. NMR Analysis

Variable-temperature and 2D NMR studies of **11** (ca 20.0 mg) were collected in toluene-d_8 (0.5 mL) using a J. Young tube. The spectra were taken between 193 and 403 K in 5 K increments. This procedure was repeated, but only from 298 to 403 K. Significant peak overlaps were observed, precluding the accurate calculation of exchange rate constants before the colescence temperature. HMBC, HSQC, and NOESY spectra of **11** at room temperature were also obtained using the sample described above on a Varian INOVA 600 narrow-bore broadband NMR system.

4.4.4. X-ray Crystallography

The data for the X-ray crystal structure of **11** was collected on a Bruker-AXS Smart APEX II diffractometer fitted with a Nicolet LT-2 low temperature device. The data was obtained by a graphite-monochromated Mo source (K_α radiation, 0.71073

Å). A suitable crystal was selected and coated with paratone oil (Exxon) and mounted on a loop under a stream of nitrogen. The data was collected at –100 ºC. The structures were solved by direct methods. Non-hydrogen atoms were anisotropically refined. All hydrogen atoms were treated as idealized contributions. Empirical absorption correction was performed with SADABS.[186] In addition the global refinements for the unit cells and data reductions of the structure were performed using the Saint program (version 6.02). All calculations were performed using SHELXTL (version 5.1) proprietary software package.[187]

4.4.5. Mechanistic Studies in the Formation of 11

$Ta(NMe_2)_4[N(SiMe_3)_2]$ (**13**, 21.5 mg, 0.042 mmol) was added to a J. Young's tube. The tube was heated at 86 °C for a total of 50 h. ^{1}H NMR spectra were taken at 40 min, 2 h, 24 h, and 50 h. In another test, $Ta(NMe_2)_4[N(SiMe_3)_2]$ (**13**, 20 mg, 0.039 mmol) was added to a J. Young's tube. The tube was heated at 85 °C for a total of 2 h. A ^{1}H NMR spectrum was taken at 30 min. ^{1}H, ^{13}C, and ^{29}Si NMR spectra were then taken at 2 h. **15**: ^{1}H NMR (toluene-d_8, 399.87 MHz, 23 °C) δ 3.29 (s, 18H, -NMe_2), 0.16 (s, 9H, =NSiMe_3); ^{13}C NMR (toluene-d_8, 100.55 MHz, 23 °C) δ 45.91 (-NMe_2), 6.01 (=NSiMe_3); ^{29}Si{^{1}H} NMR (DEPT, toluene-d_8, 127.1 MHz, 23 °C) δ -0.23 (=NSiMe$_3$).

$Ta(NMe_2)_4[N(SiMe_3)_2]$ (**13**, 200.0 mg, 0.390 mmol) and CyN=C=NCy (40.23 mg, 0.195 mmol) were added to a J. Young's tube. Benzene-d_6 was added and the solution was heated at 60 °C for 6 days. The sample was cooled to room temperature every 24 h to take ^{1}H and ^{13}C NMR spectra. After the reaction was

completed, $SiMe_4$ was added to the sample and a ^{29}Si NMR was collected. ^{29}Si NMR spectra were also taken for compounds **13**, **11**, and **14** individually using $SiMe_4$ as an internal standard. $^{29}Si\{^1H\}$ NMR of **14** (DEPT, benzene-d_6, 127.1 MHz, 23 °C) δ 6.76 (Me_3Si-). **16**: ^1H NMR (benzene-d_6, 399.87 MHz, 23 °C) δ 3.33 (s, 12H, -NMe_2), 2.40 (s, 6H –CNMe_2) 0.34 (s, 9H, =NSiMe_3); ^{13}C NMR (benzene-d_6, 100.55 MHz, 23 °C) δ 170.60 [C(NMe_2)], 55.76 (-CHMe_2), 47.25 (-NMe_2), 39.86 [C(NMe_2)], 34.89, 26.72, 26.41 (CH_2 in Cy), 4.05 (=NSiMe_3); $^{29}Si\{^1H\}$ NMR (DEPT, benzene-d_6, 127.1 MHz, 23 °C) δ -13.16 (=N$Si$$Me_3$).

Direct Analysis in Real Time (DART) mass spectrometry was also used to identify intermediate **16**. A portion (20.0 mg) of the sample mixture in the J. Young NMR tube was placed in a vial in the glove box. Hexanes (10 mL) were added to dilute the sample, and the vial was sealed with a cap containing a rubber septum. A syringe was used to extract the liquid through the rubber septum on the vial. The air stability of the sample was tested prior to the DART analysis by leaving the J. Young tube exposed to air for approximately 1.5 h. An internal standard, bibenzyl, was added to the sample before exposure and integration of ^1H NMR showed no change of the peaks.

Chapter 5

Synthesis, Characterization, and Crystal Structures of Metal Amide Cage Complexes Containing a M_4O_4 (M = Nb, Ta) Core Unit

5.1. Introduction

Niobium and tantalum amides have been actively studied since the initial synthesis by Bradley and Thomas in the early 1960's.[188,189] These studies have focused on both the fundamental chemistry of the amide complexes and their applications.[10,11,153,154,190-205] For example, metal amides have been used as precursors or catalysts for hydroaminoalkylation[190,191] and C-H activation.[192] Metal-amide bonds are usually active, and reactions of amides with silanes[193] and other organic chemicals[194,195] have been investigated. $M(NMe_2)_5$ (M = Nb, **17**; Ta, **18**) have been used as precursors to make microelectronic metal nitride and metal oxide materials through chemical vapor deposition (CVD) and atomic layer deposition (ALD) processes.[154,196-199] With continuous scaling down of the thickness of the metal oxide gate insulator layer, SiO_2, it will not be adequate for new generations of microelectronic devices because of the fairly large current leakage of SiO_2.[11,10] Metal oxides with large dielectric constants and small current leakage are good candidates to replace SiO_2 as evidenced by Intel's recently developed HfO_2-based microprocessor (Intel® Atom™ processor).[200]

Both O_2 and water have been used as oxygen sources to react with metal

complexes in order to form microelectronic metal oxide films.[196,197,199,201] We previously studied the reactions of d^0 metal complexes with O_2 and the mechanistic pathways in the formation of the resulting metal oxides.[20,155-157,202,201,206-209] The reaction of $Ta(NMe_2)_5$ (**18**) with O_2,[155,156] e.g., yields $(Me_2N)_4Ta(\eta^2\text{-}ONMe_2)$, $(Me_2N)_3Ta(\eta^2\text{-}ONMe_2)_2$, $(Me_2N)_4Ta_2[\eta^2\text{-}N(Me)CH_2NMe_2]_2(\mu\text{-}O)_2$, and $(Me_2N)_6Ta_3[\eta^2\text{-}N(Me)CH_2NMe_2]_2(\eta^2\text{-}ONMe_2)(\mu\text{-}O)_3$.

There have been few studies of the reactions between Nb and Ta amide complexes and water. We found that the reactions between $M(NMe_2)_5$ (M = Nb, **17**; Ta, **18**) and water yield "$(Me_2N)_3M{=}O$" as tetramers **19** and **20** (Scheme 5.1). Initial NMR studies showed that there are temperature-dependant inequivalencies in the methyl groups of the amide ligands. Further NMR studies of these compounds were preformed, and the results are reported here.

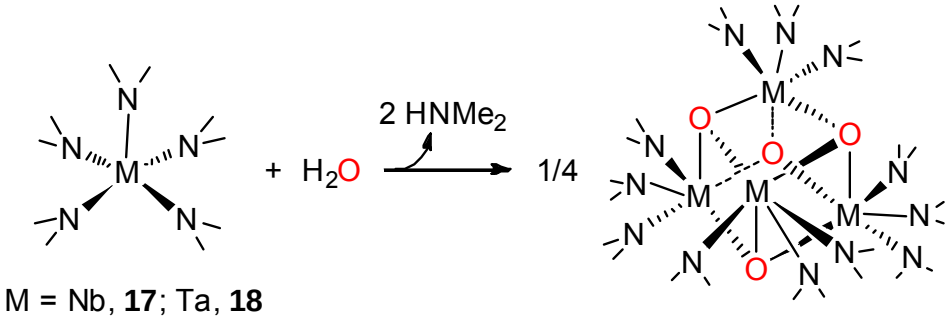

Scheme 5.1. Formation of $[(Me_2N)_3MO]_4$ (M = Nb, **19**; Ta, **20**) from the reactions of $M(NMe_2)_5$ (M = Nb, **17**; Ta, **18**) with water.

5.2. Results and Discussion

5.2.1. Synthesis and X-ray Crystal Structures of $[(Me_2N)_3MO]_4$ (M = Nb, 19; Ta, 20)

$[(Me_2N)_3MO]_4$ (M = Nb, **19**; Ta, **20**) were prepared via the reactions of **17** and **18**, respectively, with 1 equivalent of water (Scheme 5.1). Two equivalents of $HNMe_2$ were released as a byproduct. In the reactions, water was the H^+ source for the formation of $HNMe_2$.

As we reported earlier,[210] in the synthesis of $M(NMe_2)_5$ (**17**, **18**) from MCl_5 and $LiNMe_2$, $M(NMe_2)_4[N(Me)CH_2NMe_2]$ (M = Nb, **21**; Ta, **22**) are obtained as byproducts (Scheme 5.2). Purification of $M(NMe_2)_5$ (**17**, **18**) leaves ca. 5-8 mol% of **21** and **22** in the sublimed solids.[210]

In the current work, 1 equivalent of water was added to a solution containing 1 equivalent of **19** (and additional 5 mol% of **22**), and only **20** and **22** were isolated. Cooling the product solution initially gave crystals of **22**. These observations indicate that $Ta(NMe_2)_4[N(Me)CH_2NMe_2]$ (**22**) is less reactive with water than **18**. It should be pointed out that our earlier studies showed that **22** is reactive with excess water.[210] It is reasonable to assume that the Nb analog **21** is also less reactive with water than **17**. When 1 equivalent of water was added to a solution containing one equivalent of **18** (and additional 5 mol% of **21**), **19** and **21** were isolated after the reaction.

The formation of the oxo complexes **19** and **20** is similar to the formation of oxo- and chloride-bridged dimer $[(Me_2N)_3TaCl]_2O$ (**24**) from the reaction of $TaCl(NMe_2)_4$ (**23**) with water (Scheme 5.3).[153] If the acidity scale of HCl, H_2O, and

$HNMe_2$ (HCl > H_2O > $HNMe_2$) is used, it may explain why $HNMe_2$ forms in the reaction of chloro amide complex **23** with water. Interestingly, Chisholm and coworkers reported a linear, oxygen-bridged tantalum dimer $[TaCl_2(NMe_2)_2HNMe_2]_2O$ probably derived from the hydrolysis of $TaCl_2(NMe_2)_3(HNMe_2)$ with trace water during the reaction and crystallization process.[211]

The molecular structures, crystallographic data, and selected bond lengths and angles of **19** and **20** are shown in Figure 5.1, Table 5.1, and Table 5.2. The complexes are isostructural, and display a cubane-like structure. Each oxygen atom bridges three Nb or Ta atoms leading to the formation of a M_4O_4 (M = Nb, Ta) core unit. Each O atom bonds to three Nb or Ta atoms and has two negative charges. Therefore dative bonding by a lone pair on oxygen must also be contributing to create the three M-O bonds. This is evidenced by the similarities in all M-O bond distances (Table 5.2). Nb and Ta atoms are in their highest oxidation state of +5, and each $–NMe_2$ ligand has one negative charge. Thus the molecules of **19** and **20** are neutral.

M-O bond lengths are close in **19** [2.104(5)-2.114(6) Å] and **20** [2.098(8)-2.119(7) Å] with the average of 2.108 Å. Usually, bond lengths of M-O are shorter than those of M-N.[211] In **19** and **20**, however, the opposite is true. This is most likely due to the donation of the lone pair of electrons on the oxygen atoms to a third metal atom. This results in longer than normal M-O bond lengths such as those in $Nb(OC_6H_3\text{-}2,6\text{-}Ph_2)_3(NMe)(HNMe_2)$ [1.940(4)-1.965(5) Å][212] and in $[TaCl_2(NMe_2)_2HNMe_2]_2O$ [1.917(6), 1.928(6) Å].[211] In the reported structure of $Ta_6(=NPh)_{14}O$,[213] the oxygen atom binds to six tantalum atoms. The M-O bond

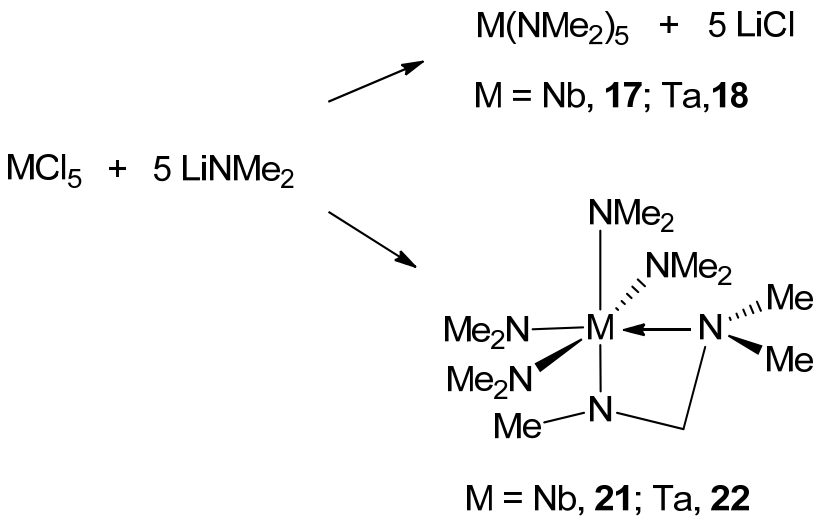

Scheme 5.2. Formation of **21** and **22** as byproducts in the formation of **17** and **18**, respectively.[210]

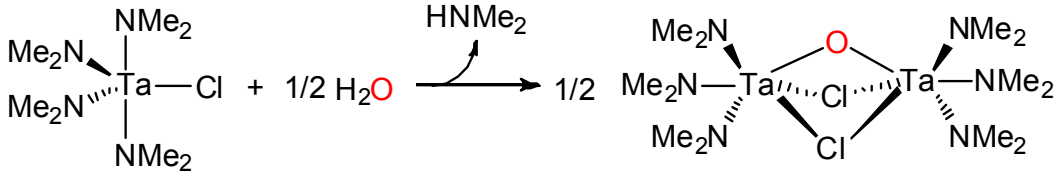

23 **24**

Scheme 5.3. Formation of $[(Me_2N)_3TaCl]_2O$ (**24**) from the reaction of $TaCl(NMe_2)_4$ (**23**) with water.[153]

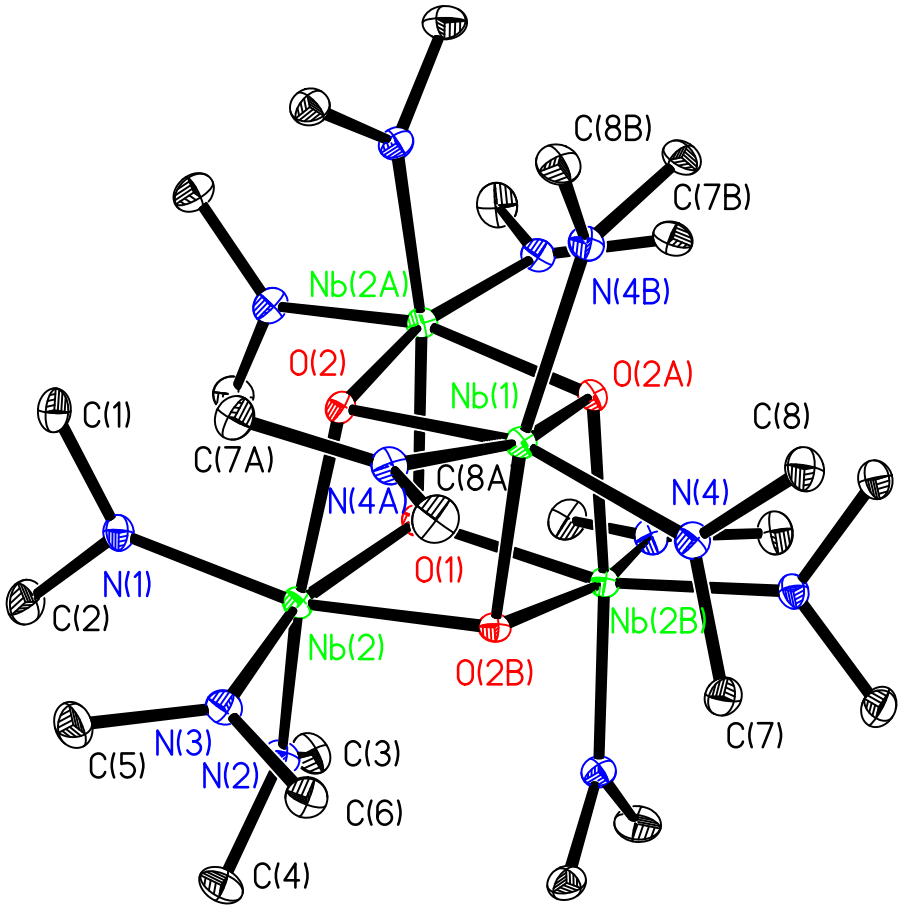

Figure 5.1. ORTEP view of $[(Me_2N)_3NbO]_4$ (**19**).

Table 5.1. X-ray crystallographic data of complexes **19** and **20**.

	19	**20**
Formula	$C_{24}H_{72}N_{12}O_4Nb_4$	$C_{24}H_{72}N_{12}O_4Ta_4$
Formula weight	964.58	1316.70
Temp (K)	173(2)	173(2)
Crystal system, Space group	Hexagonal, *P*-3	Hexagonal, *P*-3
a, b (Å)	16.21(2)	16.308(6)
c (Å)	11.169(16)	11.236(4)
V (Å^3)	2542(6)	2588.1(16)
Z	2	2
D_{calc} (g/cm^3)	1.890	1.916
Crystal size (mm^3)	0.15 × 0.20 × 0.30	0.20 × 0.20 × 0.30
θ range (°)	1.45 to 27.91	1.44 to 27.33
Reflections collected	13215	29242
Independent reflections	3837 [*R*(int) = 0.0761]	3909 [*R*(int) = 0.0486]
Completeness to *θ* (°)	94.4%, 27.91	99.8%, 27.33
GOF on F^2	1.082	1.082
Final *R* indices [$I > 2\text{sigma}(I)$] [a]	*R*1 = 0.0722,	*R*1 = 0.0659,
	w*R*2 = 0.2329	w*R*2 = 0.2019
R indices (all data)	*R*1 = 0.1008,	*R*1 = 0.0693,
	w*R*2 = 0.2596	w*R*2 = 0.2043

[a] $R = \Sigma\ ||F_o| - |F_c|| / \Sigma|F_o|$; $R_w = (\Sigma[w(F_o^2 - F_c^2)^2] / \Sigma[w(F_o^2)^2])^{1/2}$

Table 5.2. Selected bond lengths (Å) and bond angles (°) of **19** and **20**.

19		**20**	
Nb(1)-O(2)	2.104(5)	Ta(1)-O(2)	2.098(8)
Nb(1)-O(2A)	2.104(5)	Ta(1)-O(2A)	2.098(8)
Nb(1)-O(2B)	2.104(5)	Ta(1)-O(2B)	2.098(8)
Nb(2)-O(1)	2.110(4)	Ta(2)-O(1)	2.119(7)
Nb(2)-O(2)	2.114(6)	Ta(2)-O(2)	2.117(9)
Nb(2)-O(2B)	2.111(6)	Ta(2)-O(2B)	2.115(9)
Nb(1)-N(4)	2.025(7)	Ta(1)-N(4)	2.013(11)
Nb(2)-N(1)	2.012(7)	Ta(2)-N(1)	2.010(12)
Nb(2)-N(2)	2.006(7)	Ta(2)-N(2)	2.001(12)
Nb(2)-N(3)	2.009(7)	Ta(2)-N(3)	1.990(12)
O(2)-Nb(1)-O(2A)	77.5(2)	O(2)-Ta(1)-O(2A)	76.6(4)
O(1)-Nb(2)-O(2)	76.8(2)	O(1)-Ta(2)-O(2)	76.8(4)
O(2)-Nb(2)-O(2B)	77.1(3)	O(2)-Ta(2)-O(2B)	75.8(5)
Nb(1)-O(2)-Nb(2)	101.3(2)	Ta(1)-O(2)-Ta(2)	102.3(4)
Nb(1)-O(2)-Nb(2A)	101.4(2)	Ta(1)-O(2)-Ta(2A)	102.4(4)
Nb(2)-O(2)-Nb(2A)	101.8(2)	Ta(2)-O(2)-Ta(2A)	101.8(3)

length range in this system is 2.2035(5)-2.2119(4) Å, much longer than that in **20**. In **19** and **20**, the M-N bond lengths of 2.006(7)-2.025(7) Å for Nb-N bonds in **19** and 1.990(12)-2.013(11) Å for Ta-N bonds in **20** are close to those reported for $Nb(NMe_2)_3(=N\text{-}C_6H_3\text{-}2,6\text{-}^iPr)$ [1.979(2)-2.023(2) Å][212] and $[TaCl_2(NMe_2)_2HNMe_2]_2O$ [1.970(7)-1.981(7) Å].[211]

It is interesting to note that, in each $–NMe_2$ ligand, one Me group is *cis* and the other is *trans* to an O atom, as shown in the partial ORTEP view of **19** in Figure 5.2. C(1), C(3), and C(6) are *cis* to O(2), O(1), and O(2B), respectively. C(2), C(4), and C(5), are *trans* to these O atoms, respectively, and *cis* to N(2), N(3), and N(1). The tetramers **19** and **20** are electron deficient. Thus some partial M-N double bond character is expected to exist. This restricts the rotation of the $M\text{-}NMe_AMe_B$ bonds. The restricted rotation has been observed in both ^1H and ^{13}C NMR spectra of **19** and **20**, and is discussed below.

5.2.2. 2D and Variable-Temperature NMR Studies of $[(Me_2N)_3MO]_4$ (M = Nb, 19; and Ta, 20)

The ^1H NMR spectrum of $[(Me_2N)_3NbO]_4$, **19**, at 25 °C shows two slightly overlapping peaks. Its ^{13}C NMR spectrum at 25 °C shows two separate peaks. These spectra can be seen in Figure 5.3. Heteronuclear Single Quantum Coherence (HSQC) experiments at -5 °C were performed to correlate the chemical shifts of the two ^1H NMR peaks to those of the two ^{13}C NMR peaks. The HSQC spectrum at -5 °C, in Figure 5.4, reveals that the ^1H NMR peaks at 3.40 and 3.39 ppm correlate with the ^{13}C NMR peaks at 47.4 and 50.4 ppm, respectively. In other words, the Me_A

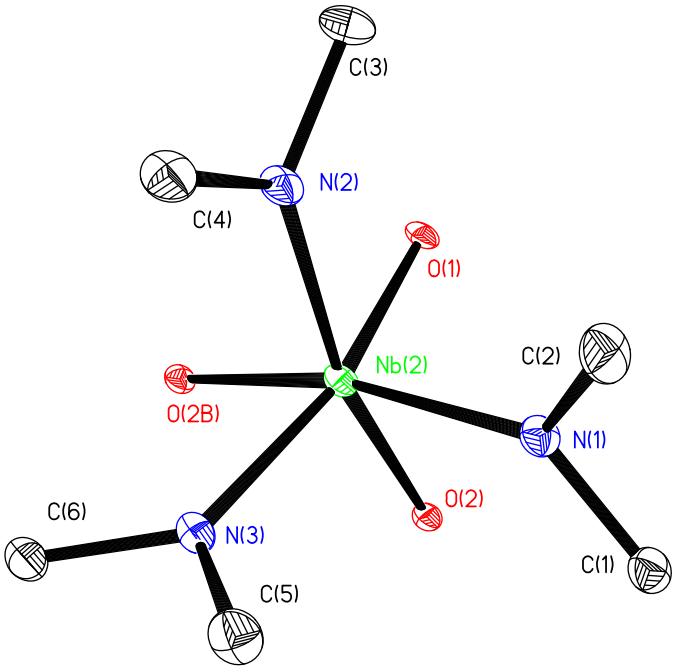

Figure 5.2. Partial structure of **19** showing the ligands bound to Nb(2).

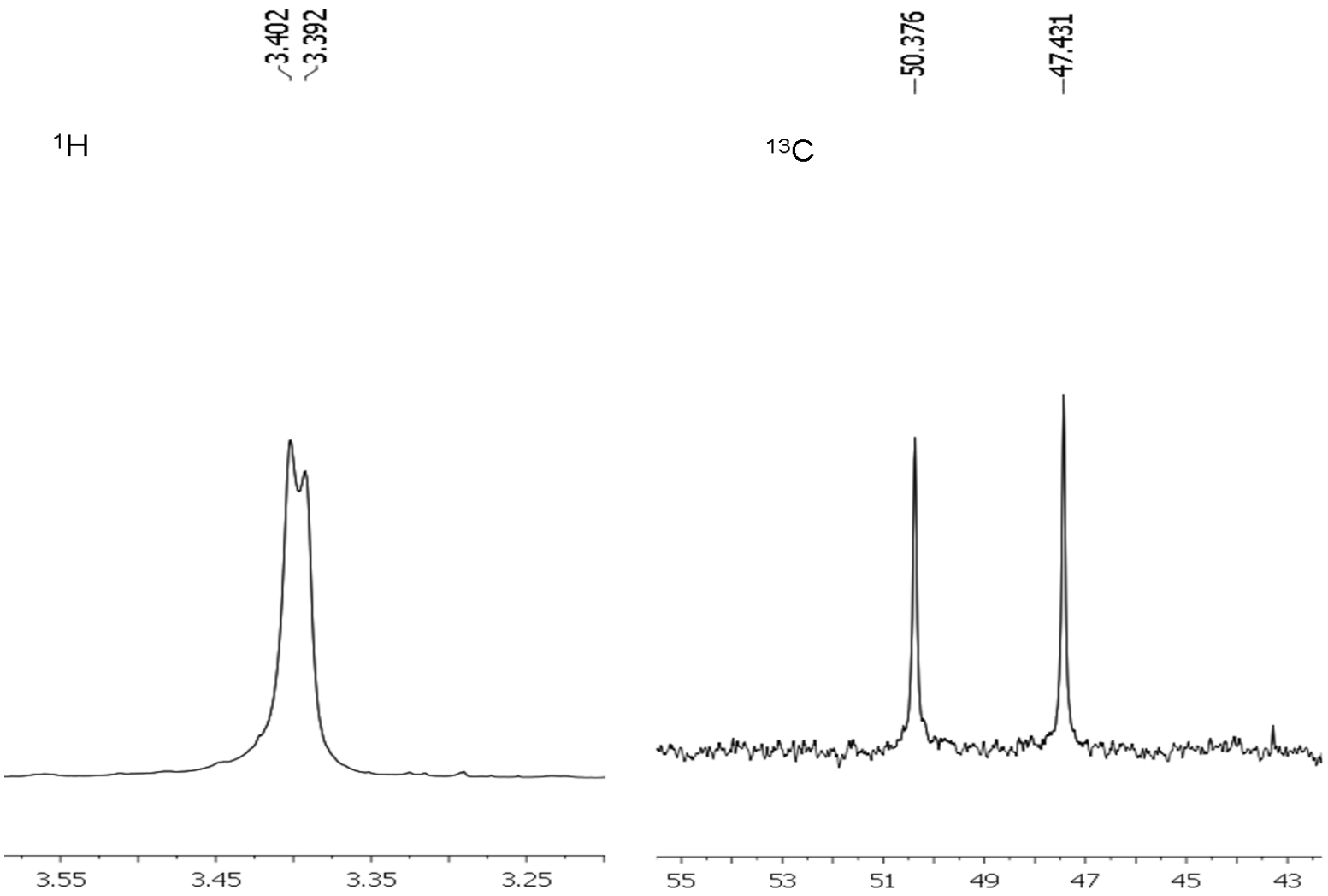

Figure 5.3. ^{1}H and ^{13}C NMR spectra of **19** at 25 °C

groups with the higher ^{1}H NMR chemical shift correlates to the ^{13}C NMR peak with a lower chemical shift, and vice versa for the Me_B groups. It is reasonable to assume that $[(Me_2N)_3TaO]_4$ (**20**) shares this NMR feature.

The X-ray crystal structure of **19** shows two types of methyl groups on the $-NMe_AMe_B$ ligands: *cis* and *trans* to the bridging O atoms (Figure 5.2). In order to confirm that these two types of methyl groups give the two ^{1}H and ^{13}C NMR peaks, a HMBC (Heteronuclear Multiple Bond Correlation) experiment was performed. HMBC experiments provide correlations between protons and carbons over two and three bonds. In other words, protons of one Me group correlate with the C atom of the other Me group in the same $-NMe_2$ ligand, which is three bonds away. At room temperature, the HMBC experiment was inconclusive because of the close proximity of the two ^{1}H peaks in the spectrum. The HMBC experiments were repeated at -5 °C when the two peaks had sufficiently decoalesed. The HMBC spectrum (Figure 5.4) reveals two cross peaks correlating the ^{1}H of Me_A group at 3.43 ppm to the ^{13}C of Me_B group at 50.1 ppm, and the ^{1}H of Me_B group at 3.40 ppm to the ^{13}C of Me_A group at 47.0 ppm, respectively. These findings support the assignment that Me_A and Me_B are both from the same $-NMe_2$ ligand.

The two methyl groups were found to undergo an exchange as the temperature increases. At 308 K, the two overlapping peaks in the ^{1}H spectrum of **19** coalesce. As the temperature decreases, the peaks begin to decoalesce and resolve as two distinct peaks. The peaks slowly move farther apart but fail to reach a static spectrum before the low temperature limit is reached at 183 K, near the melting point of toluene-d_8. The spectra taken at temperatures between 258 and 308 K are shown

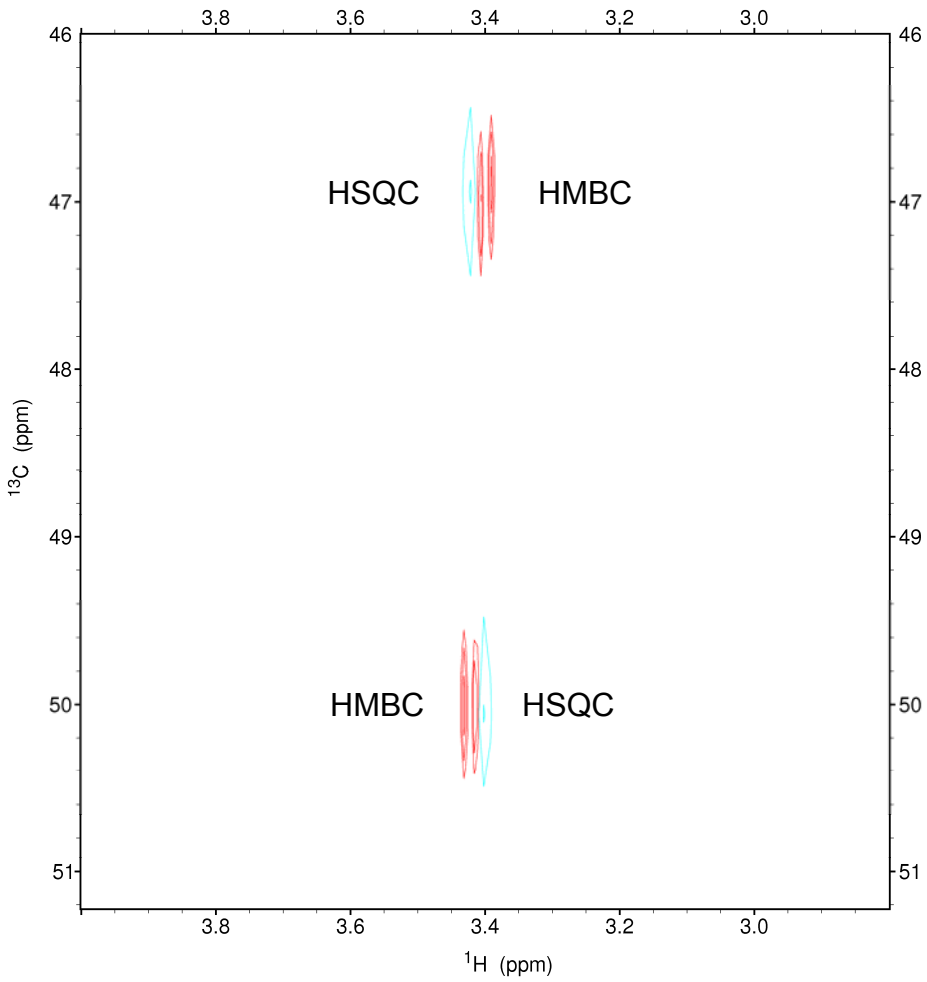

Figure 5.4. HSQC (blue) and HMBC (red) spectra of **19** at -5 °C.

in Figure 5.5. Even though a static complex (on the 400 MHz ^{1}H NMR time scale) is not reached, the interconversion in **19** was studied to obtain rate constants, using 183 K as the slow exchange limit.[182,183,185] The rate constants were calculated using Eq. 5.1:

$$k = \pi\sqrt{2(\Delta\nu_0{}^2 - \Delta\nu^2)} \qquad \text{Eq. 5.1}$$

(where $\Delta\nu$ and $\Delta\nu_0$ are the frequency differences (Hz) between the exchange-broadened site at temperature *T* and the site of the slow exchange limit, respectively.[182,183,185])

Calculated rate constants for **19** are shown in Table 5.3.[214] An Eyring plot (Figure 5.6) gives $\Delta H^{\neq}$ = -0.3(0.3) kcal/mol, $\Delta S^{\neq}$ = -49(2) eu, and $\Delta G^{\neq}_{308K}$ = 15.4(0.6) kcal/mol. The small value found for $\Delta H^{\neq}$ and the large negative value for $\Delta S^{\neq}$ indicates that the fluxional process is dominated by the entropy. Although the M-NMe_2 rotation likely breaks the M-N d-p π-bond, this bond is weak as reflected in the small observed $\Delta H^{\neq}$ value. These observations suggest that the ligands in the molecules exchange more quickly than the NMR time scale, even at very low temperatures.

A similar dynamic process was observed in the Ta complex **20**. Unlike **19**, the static complex **20** (on the 400 MHz ^{1}H NMR time scale) was reached at 198 K. Between 183 and 198 K, no further separation of the two peaks was observed. The

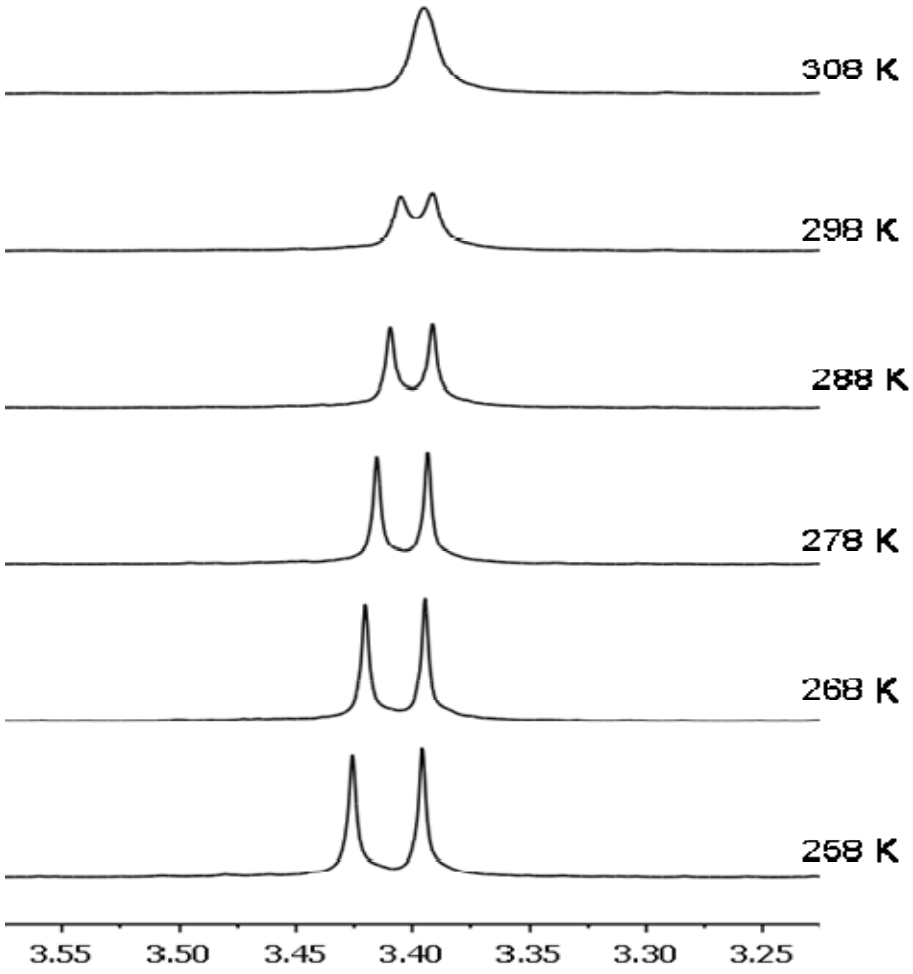

Figure 5.5. Variable-Temperature ^{1}H NMR spectra of $[(Me_2N)_3NbO]_4$ (**19**) in toluene-d_8.

Table 5.3. Rate constants for the fluxional processes in **19** and **20**.

T (K)	k (s^{-1}) for **19**[a]	k (s^{-1}) for **20**
263(1)	134.17(9)	
268(1)	135.51(7)	104.68(2)
273(1)	136.63(2)	106.34(1)
278(1)	137.59(2)	107.71(1)
283(1)	138.45(3)	108.94(1)
288(1)	139.23(1)	110.18(1)
293(1)	139.99(4)	111.34(2)
298(1)	141.5(6)	112.45(17)
303(1)	142.14(6)	113.48(14)
308(1)	142.94(0)[b]	114.65(12)[b]

[a] The rate constants shown here are the averages of two separate runs. The Δv_0 value at 183 K from the 2nd run of **19** was used to calculate rate constants k for both runs.

[b] Random uncertainties are given here. The total uncertainties $\delta k/k$ of 0.050 and 0.050 for **19** and **20**, respectively, were calculated from the largest random errors of $\delta k_{ran}/k$ = 0.004 and 0.002 for **19** and **20**, respectively, and $\delta k_{sys}/k$ = 0.05.[79,80]

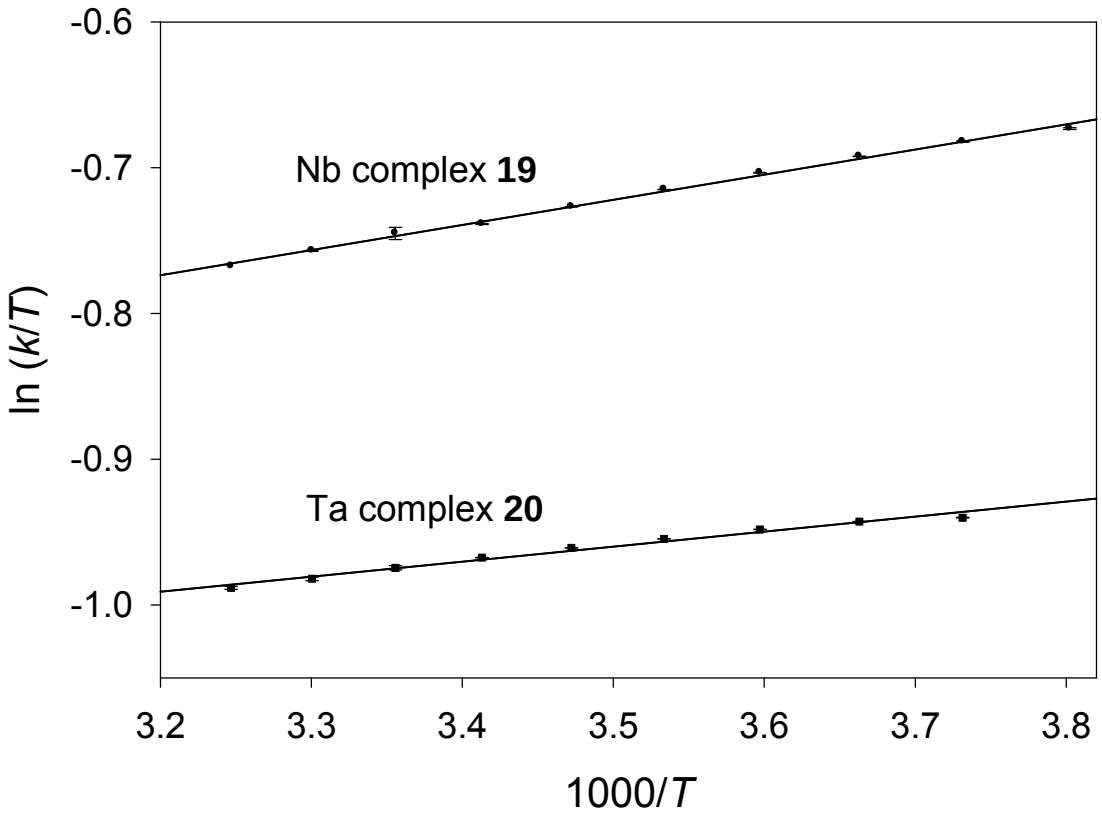

Figure 5.6. Eyring plots of the interconversions of the –NMe_AMe_B peaks in **19** and **20.**

VT ^{1}H NMR data and Eq. 5.1 give rate constants for the $-NMe_AMe_B$ exchange in **20** that are listed in Table 5.1. An Eyring plot, in Figure 5.6, gives $\Delta H^{\neq}$ = -0.2(0.3) kcal/mol, $\Delta S^{\neq}$ = -50(5) eu, and $\Delta G^{\neq}_{308K}$ = 15.4(1.5) kcal/mol for the exchange in the Ta complex **20**. These activation parameters are similar to those of the Nb analog **19**, and the fluxional process is also dominated by the entropy.

5.3. Concluding Remarks

The metal complexes $[(Me_2N)_3MO]_4$ (M = Nb, **19**; Ta, **20**) offer a view of the reactions between monomers $M(NMe_2)_5$ (M = Nb, **17**; Ta, **18**) and water that may eventually be utilized to form metal oxides used in microelectronic materials. In the reactions, amide ligands are replaced by much smaller oxo ligands. The products **19** and **20** adopt cubane-like cage structures with M-O bridges to reflect the reduced steric crowdedness and electron deficiency. Lone pair electrons on both the oxo and amido ligands are likely involved in d-p π-bonding, providing electron density to the electron deficient metal atoms. Variable temperature NMR studies of the $-NMe_AMe_B$ rotations in **19** and **20** were performed and activation parameters were obtained.

5.4. Experimental Section

All operations were performed under a dry nitrogen atmosphere with the use of a drybox or standard Schlenk techniques. Solvents were dried by distillation from potassium/benzophenone. Toluene-d_8 was dried and stored over activated molecular sieves under nitrogen. $NbCl_5$ (Strem) was purified by sublimation prior to use. $TaCl_5$ (Strem) and $LiNMe_2$ (Aldrich) were used as received. $M(NMe_2)_5$ (M = Nb,

17; Ta, **18**) were prepared by the literature procedures.[188,189] NMR spectra were obtained on a Bruker Avance 400 MHz Fourier Transform spectrometer.

The rate constants were the average of at least two separate experiments at each temperature. The *maximum* random uncertainty in the rate constants for each reaction was combined with the estimated systematic uncertainties, ca 5%.[80] The total uncertainties in the rate constants were used in the Eyring plots and in the following error propagation calculations. The estimated uncertainty in the temperature measurements for an NMR probe (used in the *k* determinations) was 1 K. The activation enthalpies ($\Delta H^{\neq}$) and entropies ($\Delta S^{\neq}$) were calculated from an unweighted nonlinear least-squares procedure contained in the SigmaPlot Scientific Graph System. The uncertainties in $\Delta H^{\neq}$ and $\Delta S^{\neq}$ were computed from the error propagation formulas derived from the Eyring equation by Girolami and coworkers.[82]

5.4.1. Synthesis of $[(Me_2N)_3NbO]_4$ (19)

Deionized water was degassed by Ar for 10 min. Water (21.2 mg, 1.18 mmol) was transferred by a microsyringe to THF (10 mL). The wet THF was then added within 2 min with vigorous stirring to the solid of $Nb(NMe_2)_5$ (0.391 g of a sample containing 0.370 g, 1.18 mmol, of **17** and 0.021 g, 0.059 mmol, of $Nb(NMe_2)_4[N(Me)CH_2NMe_2]$ (**21**) based on ^1H NMR) in a Schlenk flask cooled by a dry ice/ethanol bath to -40 ºC. The mixture was stirred at-40 ºC for 1 h and then at 23 ºC for 1 h. Volatiles were removed in vacuo. Hexanes were added to the residue to extract the product. Filtration, followed by concentration of the solution and crystallization at -32 ºC, gave crystals of unreacted **21**. The supernatant was

concentrated, and crystallization gave yellow cubic crystals of $[(Me_2N)_3NbO]_4$ (**19**, 0.062 g, 0.0643 mmol, 21.8% yield based on 1.18 mmol of **17**). **19**: ^{1}H NMR of (toluene-d_8, 400.25 MHz, 23 °C) δ 3.40 (s, 36H, –NMe_AMe$_B$), 3.39 (s, 36H, –NMe$_A$$Me_B$); ^{13}C NMR (toluene-$d_8$, 100.64 MHz, 23 °C) δ 50.4 (s, –NMe$_A$$Me_B$), 47.5 (s, –N$Me_AMe_B$). Anal. Calcd for $C_{24}H_{72}N_{12}O_4Nb_4$: C, 29.89; H, 7.52; N, 17.43. Found: C, 30.01; H, 7.43; N, 17.27.

5.4.2. Synthesis of $[(Me_2N)_3TaO]_4$ (20)

The procedure to synthesize **20** is similar to the synthesis of **19**. Deionized water was degassed by Ar for 10 min. Water (21.2 mg, 1.18 mmol) was transferred by a microsyringe to THF (10 mL). The wet THF was then added within 2 min to the solid of $Ta(NMe_2)_5$ (0.499 g of a sample containing 0.473 g, 1.18 mmol, of **18** and 0.026 g, 0.059 mmol, of $Ta(NMe_2)_4[N(Me)CH_2NMe_2]$ (**22**) based on ^{1}H NMR) with vigorous stirring in a Schlenk flask cooled by a dry ice/ethanol solution at -40 ºC. The mixture was stirred at -40 ºC for 1 h, then at 23 ºC for 1 h. Volatiles were removed in vacuo. Hexanes were used to extract the product from the residue. After filtration and concentration, crystallization at -32 ºC gave crystals of **22** first. The supernatant was concentrated, and crystallization gave pale yellow cubic crystals of $[(Me_2N)_3TaO]_4$ (**20**, 0.045 g, 0.0342 mmol, 11.6% yield based on 1.18 mmol of **18**). **20**: ^{1}H NMR of (toluene-d_8, 400.25 MHz, 23 °C) δ 3.58 (s, 36H, –NMe_AMe$_B$), 3.55 (s, 36H, –NMe$_A$$Me_B$); ^{13}C NMR (toluene-$d_8$, 100.64 MHz, 23 °C) δ 51.02 (s, –Me$_A$$Me_B$), 48.83 (s, –N$Me_AMe_B$). Anal. Calcd for $C_{24}H_{72}N_{12}O_4Ta_4$: C, 21.89; H, 5.51; N, 12.77. Found: C, 21.71; H, 5.32; N, 12.68.

5.4.3. X-ray Crystallography of $[(Me_2N)_3MO]_4$ (M = Nb, 19; Ta, 20)

The data for the X-ray crystal structures of **19** and **20** were collected on a Bruker-AXS Smart APEX II diffractometer fitted with a Nicolet LT-2 low temperature device. The data were obtained by a graphite-monochromated Mo source (K_α radiation, 0.71073 Å). A suitable crystal was selected and coated with paratone oil (Exxon) and mounted on a loop under a stream of nitrogen. The data was collected at –100 ºC. The structures were solved by direct methods.

Non-hydrogen atoms were anisotropically refined. All hydrogen atoms were treated as idealized contributions. Empirical absorption correction was performed with SADABS.[186] In addition the global refinements for the unit cells and data reductions of the structure were performed using the Saint program (version 6.02). All calculations were performed using SHELXTL (version 5.1) proprietary software package.[187]

5.4.4. Variable-Temperature and 2D NMR Studies of $[(Me_2N)_3MO]_4$ (M = Nb, 19; Ta, 20)

^{1}H NMR spectra of a solution of **19** or **20** (ca. 20.0 mg) in toluene-d_8 (0.5 mL) in a J. Young tube were taken between 183-333 K (-90 to 60 ºC) for **19** and 183-328 K (-90 to 55 ºC) for **20** in 5 K increments. This procedure was repeated once for each sample. The average of the two runs was used to study the interconversions in the $–NMe_AMe_B$ ligands. HMBC and HSQC spectra of **19** at -5 ºC were also obtained using the same sample described above.

Chapter 6

Conclusion and Future Studies

This dissertation has focused on two types of organometallic compounds: metal carbenes and imides. It is interesting to compare the archetypal Schrock carbene $(Bu^tCH_2)_3Ta{=}CHBu^t$ (**2**) and the novel imide $Ta(NMe_2)_3(=NSiMe_3)$ (**15**), their precursors penta-alkyl $Ta(CH_2CMe_3)_5$ (**1**) and penta-amide $Ta(NMe_2)_4[N(SiMe_3)_2]$ (**13**), respectively, as well as the mechanisms of the formation of the carbene and imide complexes.

Penta-alkyl complexes $Ta(CH_2R)_5$ (R = CMe_3, **1**; $SiMe_3$, **6**) contain five M-C single bonds. α-Hydrogen abstraction by an alkyl ligand is a well established process to make Schrock carbene complexes containing M=C double bonds.[21,50,51] Steric crowdedness in **1** and **6** leads to the abstraction of a hydrogen atom between two alkyl ligands, giving a M=C bond (Scheme 6.1) in the archetypical Schrock carbene complex $(Bu^tCH_2)_3Ta{=}CHBu^t$ (**2**) and in $(Me_3SiCH_2)_3Ta{=}CHSiMe_3$ (**7**).[55,109]

Penta-amide complex $Ta(NMe_2)_4[N(SiMe_3)_2]$ (**13**) contains five M-N single bonds. The "$SiMe_3^+$" group is known to behave like a proton that can be readily cleaved.[215] Steric crowdedness in **13** perhaps leads to the unprecedented α-$SiMe_3$ abstraction, giving the M=N bond in the imide complex $Ta(NMe_2)_3(=NSiMe_3)$ (**15**) (Scheme 6.1). The formation of carbenes is spontaneous at or below room

temperature, whereas the imide formation requires heating, showing that **13** is thermally more stable than **1** or **6**.

15 is coordinatively unsaturated and electron deficient. In the presence of RN=C=NR (R = Cy, Pr^i), the carbodiimide first coordinates to the metal center in **15** (Scheme 4.4), followed by migratory insertion into a Ta-NMe_2 bond to give the guanidinate derivative $Ta(NMe_2)_2(=NSiMe_3)[CyNC(NMe_2)NCy]$ (**16**). This process is repeated with a second carbodiimide coordination and then insertion to give $Ta(NMe_2)(=NSiMe_3)[CyNC(NMe_2)NCy]_2$ (**11**). A similar process may also occur to give $Ta(NMe_2)(=NSiMe_3)[Pr^iNC(NMe_2)NPr^i]_2$ (**12**).

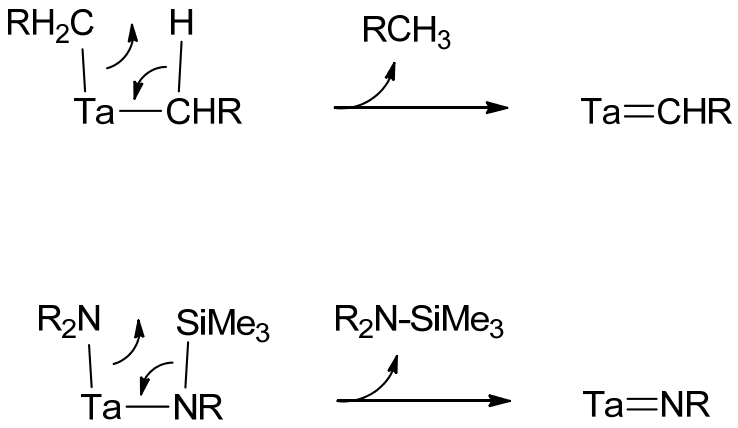

Scheme 6.1. Formation of an M=C bond from α-hydrogen abstraction between two alkyl ligands and an M=N bond from α-$SiMe_3$ abstraction between two amide ligands.

Several studies may be conducted in the future. Firstly, the imide complex $Ta(NMe_2)_3(=NSiMe_3)$ (**15**) may be isolated and further characterized. Although at 85

°C, it decomposes within 24 h, it is reasonably to assume that a shorter heating of $Ta(NMe_2)_4[N(SiMe_3)_2]$ (**13**) at a different temperature may increase the yield of **15**. Kinetics of the **13** → **15** conversion at several temperatures may also be investigated to understand the barrier of the conversion.

Secondly, if bulkier carbodiimides are used in the formation of the guanidinate complexes that are analogs of $Ta(NMe_2)(=NSiMe_3)[CyNC(NMe_2)NCy]_2$ (**11**), it may be possible to eliminate a second equivalent of $Me_3Si\text{-}NMe_2$ (**14**), and form a M≡N bond. In the current study, when more than 2 equivalents of carbodiimide were added to **11**, no further reaction was observed.

Thirdly, the formation of both carbene and imide complexes could be studied with niobium analogs. As another Group 5 metal, niobium complexes might react similarly as tantalum. It should be noted, however, that $(Bu^tCH_2)_3Nb=CHBu^t$ has been reported.[50]

Fourthly, less bulky carbodiimides than $Pr^iN=C=NPr^i$ may be used in the reactions with $Ta(NMe_2)_4[N(SiMe_3)_2]$ (**13**). Guanidinate ligands may form without heating of the mixture. Such a procedure may prevent the formation of the imide $Ta(NMe_2)_3(=NSiMe_3)$ (**15**). If indeed a guanidinate complex $Ta(NMe_2)_3[N(SiMe_3)_2][RNC(NMe_2)NR]$ is yielded from the reaction, it is sterically more crowded than **13**. α-$SiMe_3$ abstraction may follow, leading to the formation of imide $Ta(NMe_2)_2(=NSiMe_3)[RNC(NMe_2)NR]$. In such a reaction, the formation of imide ligand occurs *after* the formation of the guanidinate ligand. In comparison, the reactions we have studied thus far in Chapter 4 involves the formation of imide ligand *prior* the formation of the guanidinate ligand(s).

REFERENCES

(1) Fischer, E. O.; Maasböl, A. *Angew. Chem. Int. Ed.* **1964**, *3*, 580.

(2) Fischer, E. O.; Kreis, G.; Kreiter, C. G.; Mülle, J.; Huttner, G.; Lorenz, H. *Angew. Chem.* **1973**, *85*, 618.

(3) Schrock, R. R. *J. Am. Chem. Soc.* **1974**, *96*, 6796.

(4) Clark, D. N.; Schrock, R. R. *J. Am. Chem. Soc.* **1978**, *100*, 6774.

(5) Crabtree, R. H. *The Organometallic Chemistry of the Transition Metals*; 5th ed.; John Wiley & Sons, Inc.: Hoboken, New Jersey, 2009.

(6) Hérisson, J. L.; Chauvin, Y. *Makromol. Chem.* **1971**, *141*, 161.

(7) Grubbs, R. H. *Tetrahedron* **2004**, *60*, 7117.

(8) Grubbs, R. H. *Handbook of Metathesis*; Wiley-VCH: Weinheim, Germany, 2003; Vol. 1.

(9) Hoveyda, A. H.; Schrock, R. R. *Chem. Eur. J.* **2001**, *7*, 945-950.

(10) Smith, R. C.; Ma, T.; Hoilien, N.; Tsung, L. Y.; Bevan, M. J.; Colombo, L.; Roberts, J.; Campbell, S. A.; Gladfelter, W. L. *Adv. Mater. Opt. Electron.* **2000**, *10*, 105.

(11) Wallace, R.; Wilk, G. D. *Crit. Rev. Solid State Mater. Sci.* **2003**, *28*, 231.

(12) Son, K.; Mao, A. Y.; Sun, Y.; Kim, B. Y.; Liu, F.; Kamath, A.; White, J. M.; Kwong, D. L.; Roberts, D. A.; Vrtis, R. N. *Appl. Phys. Lett.* **1998**, *72*, 1187.

(13) Fischer, E. O. *NATO ASI Ser., Ser. C* **1989**, *269*, 1.

(14) Doetz, K. H.; Minatti, A. In *Transition Metals for Organic Synthesis*; Beller, M.; Bolm, C., Eds.; Wiley-VCH: New York, 2004; Vol. 1, pp. 397-425.

(15) Gomez-Gallego, M.; Mancheno, M. J.; Sierra, M. A. *Acc. Chem. Res.* **2005**, *38*, 44.

(16) Bernasconi, C. F. *Adv. Phys. Org. Chem.* **2002**, *37*, 137.

(17) Schrock, R. R. *Dalton Trans.* **2001**, 2541.

(18) Schrock, R. R. *Chem. Comm.* **2005**, 2773.

(19) Giesbrecht, G. R.; Gordon, J. C. *Dalton Trans.* **2004**, *16*, 2387.

(20) Chen, T.; Zhang, X.; Wang, C.; Chen, S.; Wu, Z.; Li, L.; Sorasaenee, K. R.; Diminnie, J. B.; Pan, H.; Guzei, I. A.; Rheingold, A. L.; Wu, Y.; Xue, Z. *Organometallics* **2005**, *24*, 1214.

(21) Schrock, R. R. *Chem. Rev.* **2002**, *102*, 145.

(22) Mindiola, D. J. *Acc. Chem. Res.* **2006**, *39*, 813.

(23) Doyle, M. P. *Topics Organom. Chem.* **2004**, *13*, 203.

(24) Yong, B. S.; Nolan, S. P. *Chemtracts* **2003**, *16*, 205.

(25) Kaesz, H. D.; Jensen, C. M. *Polyhedron* **1988**, *7*, 1035.

(26) Casey, C. P. In *Reactive Intermediates*; Wiley, 1985; Vol. 3, pp. 109-150.

(27) Pamplin, C. B.; Legzdins, P. *Acc. Chem. Res.* **2003**, *36*, 223.

(28) Hoveyda, A. H.; Gillingham, D. G.; Van Veldhuizen, J. J. V.; Kataoka, O.; Garber, S. B.; Kingsbury, J. S.; Harrity, J. P. A. *Org. Biomole. Chem.* **2004**, *2*, 8.

(29) Caulton, K. G. *J. Organomet. Chem.* **2001**, *617-618*, 56.

(30) Thieuleux, C.; Copéret, C.; Dufaud, V.; Marangelli, C.; Kuntz, E.; Basset, J. M. *J. Mol. Catal. A* **2004**, *213*, 47.

(31) Schrock, R. R.; Hoveyda, A. H. *Angew. Chem. Int. Ed.* **2003**, *42*, 4592.

(32) Yu, X. H.; Morton, L. A.; Xue, Z. *Organometallics* **2004**, *23*, 2210.

(33) Blanton, J. R.; Chen, T.; Diminnie, J. B.; Cai, H.; Wu, Z.; Li, L.; Sorasaenee, K.

R.; Quisenberry, K. T.; Pan, H.; Wang, C.; Choi, S.; Wu, Y.; Lin, Z.; Guzei, I. A.; Rheingold, A. L.; Xue, Z. *J. Mol. Catal. A* **2002**, *190*, 101.

(34) Xue, Z. *Comments Inorg. Chem.* **1996**, *18*, 223.

(35) Diminnie, J. B.; Liu, X.; Cai, H.; Wu, Z.; Blanton, J. R.; Chen, T.; Tuinman, A. A.; Quisenberry, K. T.; Vallet, C. E.; Zuhr, R. A.; Beach, D. B.; Peng, Z.; Wu, Y.; Concolino, T. E.; Rheingold, A. L.; Xue, Z. *Pure Appl. Chem.* **2001**, *73*, 331.

(36) Morton, L. A.; Chen, S.; Qiu, H.; Xue, Z. *J. Am. Chem. Soc.* **2007**, *129*, 7277.

(37) Morton, L. A.; Wang, R.; Yu, X.; Campana, C. F.; Guzei, I. A.; Yap, G. P. A.; Xue, Z. *Organometallics* **2006**, *25*, 427.

(38) Morton, L. A.; Zhang, X.; Wang, R.; Lin, Z.; Wu, Y.; Xue, Z. *J. Am. Chem. Soc.* **2004**, *126*, 10208.

(39) Diminnie, J. B.; Blanton, J. R.; Cai, H.; Quisenberry, K. T.; Xue, Z. *Organometallics* **2001**, *20*, 1504.

(40) Choi, S.; Lin, Z.; Xue, Z. *Organometallics* **1999**, *18*, 5488.

(41) Liu, X.; Li, L.; Diminnie, J. B.; Yap, G. P. A.; Rheingold, A. L.; Xue, Z. *Organometallics* **1998**, *17*, 4597.

(42) Diminnie, J. B.; Xue, Z. *J. Am. Chem. Soc.* **1997**, *119*, 12657.

(43) Diminnie, J. B.; Hall, H. D.; Xue, Z. *Chem. Comm.* **1996**, 2383.

(44) Li, L.; Diminnie, J. B.; Liu, X.; Pollitte, J. L.; Xue, Z. *Organometallics* **1996**, *15*, 3520.

(45) Li, L.; Xue, Z.; Yap, G. P. A.; Rheingold, A. L. *Organometallics* **1995**, *14*, 4992.

(46) Xue, Z.; Li, L.; Hoyt, L. K.; Diminnie, J. B.; Pollitte, J. L. *J. Am. Chem. Soc.*

1994, *116*, 2169.

(47) Chauvin, Y. *Angew. Chem. Int. Ed.* **2006**, *45*, 3741.

(48) Schrock, R. R. *Angew. Chem. Int. Ed.* **2006**, *45*, 3748.

(49) Grubbs, R. H. *Angew. Chem. Int. Ed.* **2006**, *45*, 3760.

(50) Schrock, R. R.; Fellmann, J. D. *J. Am. Chem. Soc.* **1978**, *100*, 3359.

(51) Schrock, R. R. *Acc. Chem. Res.* **1979**, *12*, 98.

(52) Schrock, R. R. In *Reactions of Coordinated Ligands*; Braterman, P., Ed.; Plenum: New York, 1986.

(53) Schrock, R. R. *J. Organomet. Chem.* **1986**, *300*, 249.

(54) Feldman, J.; Schrock, R. R. *Prog. Inorg. Chem.* **1991**, *39*, 1.

(55) Li, L.; Hung, M.; Xue, Z. *J. Am. Chem. Soc.* **1995**, *117*, 12746.

(56) Li, L. Ph.D. Dissertation, The University of Tennessee, Knoxville, TN, 1996.

(57) Some of the spectra in the studies reported in Ref. 55 were used to obtain kinetic data in the current work.

(58) Malatesta, V.; Ingold, K. U.; Schrock, R. R. *J. Organomet. Chem.* **1978**, *152*, C53.

(59) Wood, C. D.; McLain, S. J.; Schrock, R. R. *J. Am. Chem. Soc.* **1979**, *101*, 3210.

(60) Smith, G. M.; Carpenter, J. D.; Marks, T. J. *J. Am. Chem. Soc.* **1986**, *108*, 6805.

(61) McDade, C.; Green, J. C.; Bercaw, J. E. *Organometallics* **1982**, *1*, 1629.

(62) Bulls, A. R.; Schaefer, W. P.; Serfas, M.; Bercaw, J. E. *Organometallics* **1987**, *6*, 1219.

(63) Rothwell, I. P. *Acc. Chem. Res.* **1988**, *21*, 153.

(64) Buchwald, S. L.; Nielsen, R. B. *J. Am. Chem. Soc.* **1988**, *110*, 3171.

(65) Caulton, K. G.; Chisholm, M. H.; Streib, W. E.; Xue, Z. *J. Am. Chem. Soc.* **1991**, *113*, 6082.

(66) Jones, W. D. *Acc. Chem. Res.* **2003**, *36*, 140.

(67) Anslyn, E. V.; Dougherty, D. A. *Modern Physical Organic Chemistry*; University Science Books: Sausalito, California, 2006; pp. 421-430.

(68) Schock, L. E.; Brock, C. P.; Marks, T. J. *Organometallics* **1987**, *6*, 232.

(69) Slaughter, L. M.; Wolczanski, P. T.; Klinckman, T. R.; Cundari, T. R. *J. Am. Chem. Soc.* **2000**, *122*, 7953.

(70) Ryabov, A. D. *Chem. Rev.* **1990**, *90*, 403.

(71) Bercaw, J. E.; Chen, G. S.; Labinger, J. A.; Lin, B. *J. Am. Chem. Soc.* **2008**, *130*, 17654.

(72) Melander, L.; Saunders, W. H. J. *Reaction Rates of Isotopic Molecules*; 2nd ed.; Wiley: New York, 1980.

(73) Bell, R. P. *The Proton in Chemistry*; 2nd ed.; Cornell University Press: Ithica, NY, 1973.

(74) *Isotope Effects In Chemistry and Biology*; Kohen, A.; Limbach, H., Eds.; 1st ed.; CRC: Boca Raton, FL, 2005.

(75) Lewis, E. S.; Funderburk, L. *J. Am. Chem. Soc.* **1967**, *89*, 2322.

(76) Doering, W. V. E.; Keliher, E. J.; Zhao, X. *J. Am. Chem. Soc.* **2004**, *126*, 14206.

(77) Doering, W. V. E.; Zhao, X. *J. Am. Chem. Soc.* **2006**, *128*, 9080.

(78) Doering, W. V. E.; Keliher, E. J. *J. Am. Chem. Soc.* **2007**, *129*, 2488.

(79) The systematic uncertainties δk_{sys} were estimated based on the subjective judgment of the sensitivities of the NMR integration to the changes in concentrations. The total uncertainties δk were calculated from $\delta k = (\delta k_{ran}^2 + \delta k_{sys}^2)^{1/2}$ (δk_{ran}: random uncertainty).

(80) Taylor, J. *An Introduction to Error Analysis*; University Science Books: Milley Valley, CA, 1982; Chapter 4.

(81) Wiley, G. A.; Rein, B. M.; Hershkowitz, R. L. *Tetrahedron Lett.* **1964**, *5*, 2509.

(82) Morse, P. M.; Spencer, M. D.; Wilson, S. R.; Girolami, G. S. *Organometallics* **1994**, *13*, 1646.

(83) Some excess of Bu^tCD_2Li was used to ensure complete conversion of $(Bu^tCD_2)_3TaCl_2$ (**3-*d*$_6$**) to $Ta(CD_2Bu^t)_5$ (**1-*d*$_{10}$**). When exactly 2 equivalents of Bu^tCD_2Li were used in the reaction, the same intermediates, including **1-*d*$_{10}$**, and products were observed. A slight excess of **3-*d*$_6$**, however, was left after the reaction, probably as a result of a trace amount of moisture and error of the analytical balance.

(84) Batiz-Hernandez, H.; Bernheim, R. *Progr. Nucl. Magn. Reson. Spectrosc.* **1967**, *3*, 63.

(85) Wesener, J. R.; Moskau, D.; Guenther, H. *J. Am. Chem. Soc.* **1985**, *107*, 7307.

(86) Servis, K. L.; Domenick, R. L. *J. Am. Chem. Soc.* **1986**, *108*, 2211.

(87) Schaefer, T.; Peeling, J.; Sebastian, R. *Can. J. Chem.* **1987**, *65*, 534.

(88) Saunders, M.; Kates, M. R.; Wiberg, K. B.; Pratt, W. *J. Am. Chem. Soc.* **1977**,

99, 8072.

(89) Saunders, M.; Kates, M. R. *J. Am. Chem. Soc.* **1977**, *99*, 8071.

(90) Nguyen, T. T.; Le, T. N.; Duus, F.; Hansen, B. K. V.; Hansen, P. E. *Magn. Reson. Chem.* **2007**, *45*, 245.

(91) Hansen, P. E. *Magn. Reson. Chem.* **2008**, *46*, 726.

(92) Dziembowska, T.; Hansen, P. E.; Rozwadowski, Z. *Progr. N.M.R. Spectroscopy* **2004**, *45*, 1.

(93) Bernheim, R. A. *J. Chem. Phys.* **1966**, *45*, 2261.

(94) Berger, S.; Künzer, H. *Tetrahedron* **1983**, *39*, 1327.

(95) Nakashima, Y.; Kanada, H.; Fukunaga, M.; Suzuki, K.; Takahashi, K. *Bull. Chem. Soc. Jpn.* **1992**, *65*, 2894.

(96) Clauss, K.; Beermann, C. *Angew. Chem.* **1959**, *71*, 627.

(97) Berthold, H. J.; Groh, G. *Angew. Chem.* **1966**, *78*, 495.

(98) Schrock, R. R.; Meakin, P. *J. Am. Chem. Soc.* **1974**, *96*, 5288.

(99) Shortland, A. J.; Wilkinson, G. *J. Chem. Soc., Dalton Trans.* **1973**, 872.

(100) Latjaeva, V. N.; Razuvaev, G. A.; Malisheva, A. V.; Kiljakova, G. A. *J. Organomet. Chem.* **1964**, *2*, 388.

(101) Razuvaev, G. A.; Latyaeva, V. N.; Vishinskaya, L. I.; Rabinovitch, A. M. *J. Organomet. Chem.* **1973**, *49*, 441.

(102) Schrock, R. R.; Parshall, G. W. *Chem. Rev.* **1976**, *76*, 243.

(103) Piersol, C. J.; Profilet, R. D.; Fanwick, P. E.; Rothwell, I. P. *Polyhedron* **1993**, *12*, 1779.

(104) Haaland, A.; Hammel, A.; Rypdal, K.; Verne, H. P.; Volden, H. V.; Pulham, C.

Angew. Chem. Int. Ed. **1992**, *31*, 1464.

(105) Groysman, S.; Goldberg, I.; Kol, M.; Goldschmidt, Z. *Organometallics* **2003**, *22*, 3793.

(106) Wu, Y.; Chan, K. W. K.; Xue, Z. *J. Am. Chem. Soc.* **1995**, *117*, 9259.

(107) Albright, T. A.; Tang, H. *Angew. Chem. Int. Ed.* **1992**, *31*, 1462.

(108) Hughes, A. K.; Kingsley, A. J. *J. Organomet. Chem.* **1997**, *539*, 109.

(109) Abbott, J. K. C.; Li, L.; Xue, Z. *J. Am. Chem. Soc.* **2009**, *131*, 8246.

(110) Kost, D.; Kalikhman, I.; Raban, M. *J. Am. Chem. Soc.* **1995**, *117*, 11512.

(111) The DFT calculations were performed by Peng Yuan and Dr. Zhenyang Lin of the Hong Kong University of Science and Technology.

(112) Becke, A. D. *Phys. Rev. A* **1988**, *38*, 3098.

(113) Becke, A. D. *J. Chem. Phys.* **1993**, *98*, 5648.

(114) Miehlich, B.; Savin, A.; Stoll, H.; Preuss, H. *Chem. Phys. Lett.* **1989**, *157*, 200.

(115) Lee, C.; Yang, W.; Parr, R. G. *Phys. Rev. B* **1988**, *37*, 785.

(116) Hay, P. J.; Wadt, W. R. *J. Chem. Phys.* **1985**, *82*, 270.

(117) Hay, P. J.; Wadt, W. R. *J. Chem. Phys.* **1985**, *82*, 299.

(118) Wadt, W. R.; Hay, P. J. *J. Chem. Phys.* **1985**, *82*, 284.

(119) Gordon, M. S. *Chem. Phys. Lett.* **1980**, *76*, 163.

(120) Hariharan, P.; Pople, J. *Theor. Chim. Acta.* **1973**, *28*, 213.

(121) Binning, R.; Curtiss, L. A. *J. Comput. Chem.* **1990**, *11*, 1206.

(122) Fukui, K. *J. Phys. Chem.* **1970**, *74*, 4161.

(123) Fukui, K. *Acc. Chem. Res.* **1981**, *14*, 363.

(124) Frisch, M. J. *Gaussian 03, Revision B.05*; Gaussian, Inc.: Wallingford CT,

2004.

(125) Zarubin, D.; Ustynyuk, N. *Russ. Chem. Rev.* **2006**, *75*, 671.

(126) Berry, J. *Comments Inorg. Chem.* **2009**, *30*, 28.

(127) Schrock, R. *Chem. Rev.* **2009**, *109*, 3211.

(128) Chirik, P. *Dalton Trans.* **2007**, *1*, 16.

(129) Li, Y.; Wong, W. *Coord. Chem. Rev.* **2003**, *243*, 191.

(130) Eikey, R.; Abu-Omar, M. *Coord. Chem. Rev.* **2003**, *243*, 83.

(131) Gade, L.; Mountford, P. *Coord. Chem. Rev.* **2001**, *216-217*, 65.

(132) Wigley, D. E. *Prog. Inorg. Chem.* **1994**, *42*, 239.

(133) Bolton, P.; Mountford, P. *Adv. Synth. Catal.* **2005**, *347*, 355.

(134) Poater, A.; Solans-Monfort, X.; Clot, E.; Copéret, C.; Eisenstein, O. *J. Am. Chem. Soc.* **2007**, *129*, 8207.

(135) Jiang, A. J.; Simpson, J. H.; Müller, P.; Schrock, R. R. *J. Am. Chem. Soc.* **2009**, *131*, 7770.

(136) Blanc, F.; Thivolle-Cazat, J.; Basset, J.; Copéret, C.; Hock, A. S.; Tonzetich, Z. J.; Schrock, R. R. *J. Am. Chem. Soc.* **2007**, *129*, 1044.

(137) Baunemann, A.; Kim, Y.; Winter, M.; Fischer, R. A. *Dalton Trans.* **2006**, 121.

(138) Tsai, M. H.; Sun, S. C.; Chiu, H. T.; Tsai, C. E.; Chuang, S. H. *Appl. Phys. Lett.* **1995**, *67*, 1128.

(139) Chiu, H.; Wang, C.; Chuang, S. *Chem. Vap. Deposition* **2000**, *6*, 223.

(140) Jayaratne, K. C.; Yap, G. P. A.; Haggerty, B. S.; Rheingold, A. L.; Winter, C. H. *Inorg. Chem.* **1996**, *35*, 4910.

(141) Chong, A. O.; Oshima, K.; Sharpless, K. B. *J. Am. Chem. Soc.* **1977**, *99*,

3420.

(142) Maatta, E. A.; Haymore, B. L.; Wentworth, R. A. D. *Inorg. Chem.* **1980**, *19*, 1055.

(143) Rossi, R.; Marchi, A.; Duatti, A.; Magon, L.; Bernado, P. *Transition Met. Chem.* **1985**, *10*, 151.

(144) Burger, U.; Wannagat, U. *Monatsh. Chem.* **1963**, *94*, 761.

(145) Burger, H.; Smrekar, O. *Monatsh. Chem.* **1964**, *95*, 292.

(146) Baunemann, A.; Rische, D.; Milanov, A.; Kim, Y.; Winter, M.; Gemel, C.; Fischer, R. A. *Dalton Trans.* **2005**, 3051.

(147) Baunemann, A.; Winter, M.; Csapek, K.; Gemel, C.; Fischer, R. A. *Eur. J. Inorg. Chem.* **2006**, *2006*, 4665.

(148) Baunemann, A.; Bekermann, D.; Thiede, T. B.; Parala, H.; Winter, M.; Gemel, C.; Fischer, R. A. *Dalton Trans.* **2008**, 3715.

(149) Milanov, A.; Bhakta, R.; Baunemann, A.; Becker, H.; Thomas, R.; Ehrhart, P.; Winter, M.; Devi, A. *Inorg. Chem.* **2006**, *45*, 11008.

(150) Sun, J.; Chen, X.; Xue, Z. *Inorg. Chim. Acta* **2009**, *362*, 4251.

(151) Carmalt, C. J.; Newport, A. C.; O'Neill, S. A.; Parkin, I. P.; White, A. J. P.; Williams, D. J. *Inorg. Chem.* **2005**, *44*, 615.

(152) Devi, A.; Bhakta, R.; Milanov, A.; Hellwig, M.; Barreca, D.; Tondello, E.; Thomas, R.; Ehrhart, P.; Winter, M.; Fischer, R. *Dalton Trans.* **2007**, 1671.

(153) Chen, S.; Cai, H.; Xue, Z. *Organometallics* **2009**, *28*, 167.

(154) Chen, T.; Xu, C.; Baum, T. H.; Stauf, G. T.; Roeder, J. F.; DiPasquale, A. G.; Rheingold, A. L. *Chem. Mater.* **2010**, *22*, 27.

(155) Chen, S.; Zhang, X.; Yu, X.; Qiu, H.; Yap, G. P. A.; Guzei, I. A.; Lin, Z.; Wu, Y.; Xue, Z. *J. Am. Chem. Soc.* **2007**, *129*, 14408.

(156) Chen, S.; Zhang, J.; Yu, X.; Bu, X.; Chen, X.; Xue, Z. *Inorg. Chem.* **2010**, *49*, 4017.

(157) Wang, R.; Zhang, X.; Chen, S.; Yu, X.; Wang, C.; Beach, D. B.; Wu, Y.; Xue, Z. *J. Am. Chem. Soc.* **2005**, *127*, 5204.

(158) Sun, J.; Chen, S.; Duan, Y.; Li, Y.; Chen, X.; Xue, Z. *Organometallics* **2009**, *28*, 3088.

(159) Chen, S.; Xue, Z. *Organometallics* **2010**, *29*, 5579.

(160) Potts, S. E.; Carmalt, C. J.; Blackman, C. S.; Abou-Chahine, F.; Pugh, D.; Davies, H. O. *Organometallics* **2009**, *28*, 1838.

(161) Bailey, P. J.; Pace, S. *Coord. Chem. Rev.* **2001**, *214*, 91.

(162) Coyle, J. P.; Monillas, W. H.; Yap, G. P. A.; Barry, S. T. *Inorg. Chem.* **2008**, *47*, 683.

(163) Barker, J.; Kilner, M. *Coord. Chem. Rev.* **1994**, *133*, 219.

(164) Moore, D. S.; Robinson, S. D. *Adv. Inorg. Chem. Radiochem.* **1986**, *30*, 1.

(165) Mehrotra, R. In *Comprehensive Coordination Chemistry*; 1st ed.; Wilkinson, G, Ed.; Pergamon Books Ltd.: Oxford, 1987; Vol. 2, pp. 269-287.

(166) Bailey, P. J.; Mitchell, L. A.; Parsons, S. *J. Chem. Soc., Dalton Trans.* **1996**, 2839.

(167) Ratilla, E. M. A.; Scott, B. K.; Moxness, M. S.; Kostic, N. M. *Inorg. Chem.* **1990**, *29*, 918.

(168) Rische, D.; Baunemann, A.; Winter, M.; Fischer, R. A. *Inorg. Chem.* **2006**, *45*,

269.

(169) Rische, D.; Parala, H.; Gemel, E.; Winter, M.; Fischer, R. A. *Chem. Mater.* **2006**, *18*, 6075.

(170) Wilder, C. B.; Reitfort, L. L.; Abboud, K. A.; McElwee-White, L. *Inorg. Chem.* **2006**, *45*, 263.

(171) Tin, M. K. T.; Yap, G. P. A.; Richeson, D. S. *Inorg. Chem.* **1999**, *38*, 998.

(172) Morawitz, T.; Zhang, F.; Bolte, M.; Bats, J. W.; Lerner, H.; Wagner, M. *Organometallics* **2008**, *27*, 5067.

(173) Rakita, P. E.; Worsham, L. S. *Inorg. Nucl. Chem. Letters* **1977**, *13*, 547.

(174) Yamaji, T.; Saito, T.; Hayamizu, K.; Yanagisawa, M. Spectral Database for Organic Compounds. *http://riodb01.ibase.aist.go.jp/sdbs/cgi-bin/cre_index.cgi* July 2010.

(175) Friebolin, H. *Basic One- and Two-Dimensional NMR Spectroscopy*; Wiley-VCH: Weinheim, Germany, 2005; pp. 305-308.

(176) Pavia, D. L.; Lampman, G. M.; Kriz, G. S. *Introduction to Spectroscopy*; Thomson Learning, Inc., 2001; pp. 319-322.

(177) Rabinovitz, M.; Pines, A. *J. Am. Chem. Soc.* **1969**, *91*, 1585.

(178) Levy, G. C.; Nelson, G. L. *J. Am. Chem. Soc.* **1972**, *94*, 4897.

(179) Mann, B. E. *J. Magn. Reson.* **1977**, *25*, 91.

(180) Dimitrov, V. S.; Ladd, J. A. *Magn. Reson. Chem.* **1985**, *23*, 529.

(181) It should be noted that this experiment used a 400 MHz NMR spectrometer. The coalesence and static spectra temperatures are dependant on the magnetic field. Thus NMR spectra at other frequencies would show slightly

different temperatures of coalescence.

(182) Sandstrom, J. *Dynamic NMR Spectroscopy*; Academic Press: London, 1982.

(183) Macomber, R. S. *A Complete Introduction to Modern NMR Spectroscopy*; Wiley: New York, 1998; pp. 158-160.

(184) The rate constants here are the chemical rate constants, and they differ from the observed magnetization transfer rate constants by a factor of 2.

(185) Green, M. L. H.; Wong, L. L.; Sella, A. *Organometallics* **1992**, *11*, 2660.

(186) G. M. Sheldrick, SADABS, *A Program for Empirical Absorption Correction of Area Detector Data*, University of Göttingen, Göttingen, Germany, 2000.

(187) G. M. Sheldrick, SHELXL-97, *A Program for the Refinement of Crystal Structures*, University of Göttingen, Göttingen, Germany, 1997.

(188) Bradley, D.; Thomas, I. *Can. J. Chem.* **1962**, *40*, 449.

(189) Bradley, D. C.; Thomas, I. M. *Can. J. Chem.* **1962**, *40*, 1355.

(190) Eisenberger, P.; Ayinla, R.; Lauzon, J.; Schafer, L. *Angew. Chem. Int. Ed.* **2009**, *48*, 8361.

(191) Herzon, S. B.; Hartwig, J. F. *J. Am. Chem. Soc.* **2007**, *129*, 6690.

(192) Spencer, L. P.; Beddie, C.; Hall, M. B.; Fryzuk, M. D. *J. Am. Chem. Soc.* **2006**, *128*, 12531.

(193) Cai, H.; Chen, T.; Wang, X.; Schultz, A. J.; Koetzle, T. F.; Xue, Z. *Chem. Commun.* **2002**, 230.

(194) Thorn, M. G.; Parker, J. R.; Fanwick, P. E.; Rothwell, I. P. *Organometallics* **2003**, *22*, 4658.

(195) Herrmann, W. A.; Baratta, W.; Herdtweck, E. *Angew. Chem. Int. Ed.* **1996**, *35*,

1951.

(196) Son, K.; Mao, A. Y.; Sun, Y.; Kim, B. Y.; Liu, F.; Kamath, A.; White, J. M.; Kwong, D. L.; Roberts, D. A.; Vrtis, R. N. *Appl. Phys. Lett.* **1998**, *72*, 1187.

(197) Potts, S.; van den Elzen, L.; Dingemans, G.; Langereis, E.; Keuning, W.; van de Sanden, M.; Kessels, W. M. M. *ECS Trans.* **2009**, *25*, 233.

(198) Langereis, E.; Knoops, H. C. M.; Mackus, A. J. M.; Roozeboom, F.; van de Sanden, M. C. M.; Kessels, W. M. M. *J. Appl. Phys.* **2007**, *102*, 083517.

(199) Maeng, W. J.; Park, S.; Kim, H. *J. Vac. Sci. Technol. B* **2006**, *24*, 2276.

(200) Flynn, L. J. Intel Announces New Chip for Small Computers. *The New York Times*, March 3, 2008.

(201) Chen, S.; Zhang, X.; Lin, Z.; Wu, Y.; Xue, Z. *Sci. Chin. Ser. B Chem.* **2009**, *52*, 1723.

(202) Woods, J. B.; Beach, D.; Nygren, C.; Xue, Z. *Chem. Vap. Deposition* **2005**, *11*, 289.

(203) Kunkely, H.; Vogler, A. *Inorg. Chem. Commun.* **2001**, *4*, 252.

(204) Chisholm, M. H.; Cowley, A. H.; Lattman, M. *Report* **1979**, 28.

(205) Chisholm, M. H.; Cowley, A. H.; Lattman, M. *J. Am. Chem. Soc.* **1980**, *102*, 46.

(206) Chen, S. J.; Yap, G.; Xue, Z. *Sci. Chin. Ser. B Chem.* **2009**, *52*, 1583.

(207) Qiu, H.; Chen, S.; Wang, C.; Wu, Y.; Guzei, I. A.; Chen, X.; Xue, Z. *Inorg. Chem.* **2009**, *48*, 3073.

(208) Wu, Z.; Cai, H.; Yu, X.; Blanton, J. R.; Diminnie, J. B.; Pan, H.; Xue, Z.; Bryan, J. C. *Organometallics* **2002**, *21*, 3973.

(209) Chen, T.; Wu, Z.; Li, L.; Sorasaenee, K. R.; Diminnie, J. B.; Pan, H.; Guzei, I. A.; Rheingold, A. L.; Xue, Z. *J. Am. Chem. Soc.* **1998**, *120*, 13519.

(210) Zhang, X.; Chen, S.; Cai, H.; Im, H.; Chen, T.; Yu, X.; Chen, X.; Lin, Z.; Wu, Y.; Xue, Z. *Organometallics* **2008**, *27*, 1338.

(211) Chisholm, M. H.; Huffman, J. C.; Tan, L. *Inorg. Chem.* **1981**, *20*, 1859.

(212) Chesnut, R. W.; Fanwick, P. E.; Rothwell, I. P. *Inorg. Chem.* **1988**, *27*, 752.

(213) Krinsky, J.; Anderson, L.; Arnold, J.; Bergman, R. *Angew. Chem. Int. Ed.* **2007**, *46*, 369.

(214) The lack of the experimental Δv_0 value for the Nb complex **20** and the use of the separation of the two ^{1}H peaks at 183 K may lead to larger errors in the rate constants and the activation parameters. However, the fact that the static Ta complex **21** (on the 400 MHz ^{1}H NMR time scale) was reached at 183-198 K suggests that the temperature to give the static **20** may be near 183 K, the limiting temperature for toluene-d_8. In other words, the separation of the two ^{1}H peaks of **20** at 183 K is close to the Δv_0 value.

(215) Brook, M. A. *Silicon in Organic, Organometallic, and Polymer Chemistry*; John Wiley & Sons, Inc.: New York, 2000; Chapter 8.

APPENDIX

Table A1. Atomic coordinates (x 10^4) and equivalent isotropic displacement parameters (Å^2 x 10^3) for **11**. *U*(eq) is defined as one third of the trace of the orthogonalized U^{ij} tensor.

	x	y	z	*U*(eq)
Ta(1)	5366(1)	1183(1)	7467(1)	19(1)
Si(1)	4191(1)	1178(1)	9587(1)	29(1)
N(1)	4916(3)	1135(1)	8614(2)	25(1)
N(2)	5506(2)	361(1)	7237(2)	24(1)
N(3)	3729(2)	1348(1)	6675(2)	21(1)
N(4)	4716(2)	2076(1)	7243(2)	22(1)
N(5)	2822(3)	2250(1)	6459(2)	28(1)
N(6)	6498(2)	1374(1)	6168(2)	21(1)
N(7)	7190(2)	1405(1)	7596(2)	22(1)
N(8)	8534(2)	1656(1)	6480(2)	28(1)
C(1)	3093(4)	1772(2)	9526(3)	56(1)
C(2)	3334(4)	524(2)	9793(3)	44(1)
C(3)	5248(5)	1293(2)	10589(3)	51(1)
C(4)	5304(4)	-78(2)	7892(3)	36(1)
C(5)	5897(4)	102(2)	6422(3)	36(1)

Table A1. Continued

	x	y	z	*U*(eq)
C(6)	2631(3)	1025(2)	6496(2)	24(1)
C(7)	2283(3)	702(2)	7325(2)	31(1)
C(8)	1131(3)	367(2)	7121(3)	36(1)
C(9)	1228(3)	-20(2)	6310(3)	38(1)
C(10)	1604(3)	299(2)	5488(3)	33(1)
C(11)	2746(3)	634(2)	5696(2)	30(1)
C(12)	3737(3)	1905(1)	6791(2)	22(1)
C(13)	2277(3)	2184(2)	5557(2)	32(1)
C(14)	2360(3)	2702(2)	6982(3)	36(1)
C(15)	5102(3)	2662(1)	7317(2)	23(1)
C(16)	5064(4)	2866(2)	8287(2)	34(1)
C(17)	5447(4)	3478(2)	8388(3)	45(1)
C(18)	6691(4)	3570(2)	8058(3)	45(1)
C(19)	6756(4)	3358(2)	7097(3)	37(1)
C(20)	6354(3)	2746(2)	7016(3)	33(1)
C(21)	8128(3)	1252(1)	8295(2)	24(1)
C(22)	8086(3)	633(2)	8540(3)	32(1)

Table A1. Continued

	x	y	z	*U*(eq)
C(23)	9074(4)	497(2)	9270(3)	41(1)
C(24)	8973(4)	859(2)	10101(3)	45(1)
C(25)	9001(4)	1474(2)	9859(3)	40(1)
C(26)	8026(3)	1612(2)	9124(2)	29(1)
C(27)	7428(3)	1478(1)	6716(2)	21(1)
C(28)	9074(3)	1460(2)	5677(2)	36(1)
C(29)	9195(3)	2094(2)	6962(3)	33(1)
C(30)	6412(3)	1564(1)	5230(2)	21(1)
C(31)	6483(3)	1074(1)	4564(2)	28(1)
C(32)	6421(4)	1275(2)	3589(2)	32(1)
C(33)	5278(3)	1590(2)	3368(2)	31(1)
C(34)	5143(3)	2070(2)	4019(2)	31(1)
C(35)	5243(3)	1873(2)	5005(2)	27(1)

Table A2. Bond distances (Å) in **11**.

Bond	Distance	Bond	Distance
Ta(1)-N(1)	1.814(3)	N(8)-C(28)	1.452(4)
Ta(1)-N(2)	2.008(3)	C(6)-C(11)	1.527(5)
Ta(1)-N(7)	2.119(3)	C(6)-C(7)	1.528(5)
Ta(1)-N(3)	2.163(3)	C(7)-C(8)	1.539(5)
Ta(1)-N(4)	2.279(3)	C(8)-C(9)	1.531(5)
Ta(1)-N(6)	2.424(3)	C(9)-C(10)	1.525(6)
Si(1)-N(1)	1.710(3)	C(10)-C(11)	1.530(5)
Si(1)-C(3)	1.872(4)	C(15)-C(20)	1.518(5)
Si(1)-C(2)	1.875(4)	C(15)-C(16)	1.529(5)
Si(1)-C(1)	1.883(5)	C(16)-C(17)	1.532(5)
N(2)-C(5)	1.456(5)	C(17)-C(18)	1.529(6)
N(2)-C(4)	1.461(4)	C(18)-C(19)	1.524(6)
N(3)-C(12)	1.347(4)	C(19)-C(20)	1.538(5)
N(3)-C(6)	1.469(4)	C(21)-C(26)	1.517(5)
N(4)-C(12)	1.321(4)	C(21)-C(22)	1.527(5)
N(4)-C(15)	1.472(4)	C(22)-C(23)	1.542(5)
N(5)-C(12)	1.388(4)	C(23)-C(24)	1.521(6)
N(5)-C(14)	1.449(4)	C(24)-C(25)	1.518(7)

Table A2. Continued

Bond	Distance	Bond	Distance
N(5)-C(13)	1.451(4)	C(25)-C(26)	1.538(5)
N(6)-C(27)	1.312(4)	C(30)-C(35)	1.530(4)
N(6)-C(30)	1.467(4)	C(30)-C(31)	1.541(4)
N(7)-C(27)	1.366(4)	C(31)-C(32)	1.527(5)
N(7)-C(21)	1.483(4)	C(32)-C(33)	1.512(5)
N(8)-C(27)	1.381(4)	C(33)-C(34)	1.519(5)
N(8)-C(29)	1.451(4)	C(34)-C(35)	1.540(5)

Table A3. Bond angles (°) in **11**.

Bond	Angle	Bond	Angle
N(1)-Ta(1)-N(2)	97.27(12)	C(3)-Si(1)-C(2)	107.6(2)
N(1)-Ta(1)-N(7)	104.80(12)	N(1)-Si(1)-C(1)	110.52(18)
N(2)-Ta(1)-N(7)	100.17(11)	C(3)-Si(1)-C(1)	108.1(2)
N(1)-Ta(1)-N(3)	104.31(13)	C(2)-Si(1)-C(1)	107.2(2)
N(2)-Ta(1)-N(3)	99.17(10)	Si(1)-N(1)-Ta(1)	165.79(19)
N(7)-Ta(1)-N(3)	142.43(10)	C(5)-N(2)-C(4)	108.5(3)
N(1)-Ta(1)-N(4)	95.29(11)	C(5)-N(2)-Ta(1)	126.2(2)
N(2)-Ta(1)-N(4)	157.55(10)	C(4)-N(2)-Ta(1)	125.1(2)
N(7)-Ta(1)-N(4)	94.49(10)	C(12)-N(3)-C(6)	123.0(3)
N(3)-Ta(1)-N(4)	59.57(10)	C(12)-N(3)-Ta(1)	96.44(2)
N(1)-Ta(1)-N(6)	162.52(11)	C(6)-N(3)-Ta(1)	133.0(2)
N(2)-Ta(1)-N(6)	89.91(11)	C(12)-N(4)-C(15)	124.5(3)
N(7)-Ta(1)-N(6)	58.09(9)	C(12)-N(4)-Ta(1)	92.0(2)
N(3)-Ta(1)-N(6)	90.15(9)	C(15)-N(4)-Ta(1)	142.5(2)
N(4)-Ta(1)-N(6)	83.48(9)	C(12)-N(5)-C(14)	122.4(3)
N(1)-Si(1)-C(3)	111.83(19)	C(12)-N(5)-C(13)	121.9(3)
N(1)-Si(1)-C(2)	111.40(17)	C(14)-N(5)-C(13)	115.7(3)

Table A3. Continued

Bond	Angle	Bond	Angle
C(27)-N(6)-C(30)	122.5(3)	N(4)-C(12)-N(3)	111.8(3)
C(27)-N(6)-Ta(1)	88.74(18)	N(4)-C(12)-N(5)	125.2(3)
C(30)-N(6)-Ta(1)	144.2(2)	N(3)-C(12)-N(5)	123.0(3)
C(27)-N(7)-C(21)	122.1(3)	N(4)-C(15)-C(20)	112.3(3)
C(27)-N(7)-Ta(1)	101.00(19)	N(4)-C(15)-C(16)	110.5(3)
C(21)-N(7)-Ta(1)	130.3(2)	C(20)-C(15)-C(16)	108.5(3)
C(27)-N(8)-C(29)	122.8(3)	C(15)-C(16)-C(17)	112.0(3)
C(27)-N(8)-C(28)	122.6(3)	C(18)-C(17)-C(16)	111.4(3)
C(29)-N(8)-C(28)	114.4(3)	C(19)-C(18)-C(17)	110.5(3)
N(3)-C(6)-C(11)	110.8(3)	C(18)-C(19)-C(20)	111.2(3)
N(3)-C(6)-C(7)	112.0(3)	C(15)-C(20)-C(19)	112.1(3)
C(11)-C(6)-C(7)	110.9(3)	N(7)-C(21)-C(26)	110.1(3)
C(6)-C(7)-C(8)	111.1(3)	N(7)-C(21)-C(22)	112.2(3)
C(9)-C(8)-C(7)	111.8(3)	C(26)-C(21)-C(22)	110.6(3)
C(10)-C(9)-C(8)	111.5(3)	C(21)-C(22)-C(23)	110.0(3)
C(9)-C(10)-C(11)	111.8(3)	C(24)-C(23)-C(22)	111.5(3)
C(6)-C(11)-C(10)	111.6(3)	C(25)-C(24)-C(23)	110.9(3)

Table A3. Continued

Bond	Angle	Bond	Angle
C(24)-C(25)-C(26)	110.6(3)	C(35)-C(30)-C(31)	107.8(3)
C(21)-C(26)-C(25)	111.8(3)	C(32)-C(31)-C(30)	111.8(3)
N(6)-C(27)-N(7)	112.1(3)	C(33)-C(32)-C(31)	110.7(3)
N(6)-C(27)-N(8)	126.8(3)	C(32)-C(33)-C(34)	110.9(3)
N(7)-C(27)-N(8)	121.0(3)	C(33)-C(34)-C(35)	111.8(3)
N(6)-C(30)-C(35)	111.4(3)	C(30)-C(35)-C(34)	111.7(3)
N(6)-C(30)-C(31)	112.0(3)		

Table A4. Anisotropic displacement parameters ($Å^2$ x 10^3) for **11**. The anisotropic displacement factor exponent takes the form: $-2\pi[h^2a^{*2}U^{11} + \ldots + 2ha^*b^*U^{12}]$.

	U^{11}	U^{22}	U^{33}	U^{23}	U^{13}	U^{12}
Ta(1)	19(1)	20(1)	16(1)	1(1)	-2(1)	-1(1)
Si(1)	36(1)	33(1)	20(1)	2(1)	5(1)	-6(1)
N(1)	27(2)	29(2)	19(1)	4(1)	-1(1)	-2(1)
N(2)	31(2)	19(1)	23(1)	1(1)	-4(1)	2(1)
N(3)	21(1)	21(1)	21(1)	0(1)	-3(1)	-2(1)
N(4)	21(1)	23(1)	22(1)	-1(1)	-1(1)	0(1)
N(5)	31(2)	28(2)	26(2)	-3(1)	-6(1)	7(1)
N(6)	23(1)	21(1)	18(1)	3(1)	-1(1)	-1(1)
N(7)	20(1)	28(1)	18(1)	2(1)	-2(1)	-2(1)
N(8)	24(1)	38(2)	21(1)	-3(1)	1(1)	-5(1)
C(1)	63(3)	53(3)	55(3)	6(2)	24(2)	13(2)
C(2)	47(2)	52(3)	33(2)	6(2)	2(2)	-21(2)
C(3)	62(3)	67(3)	23(2)	-6(2)	1(2)	-27(2)
C(4)	51(2)	23(2)	32(2)	6(2)	-5(2)	-5(2)
C(5)	50(2)	26(2)	32(2)	-2(2)	2(2)	1(2)

Table A4. Continued

	U^{11}	U^{22}	U^{33}	U^{23}	U^{13}	U^{12}
C(6)	21(2)	28(2)	21(2)	-1(1)	-4(1)	-2(1)
C(7)	31(2)	36(2)	25(2)	2(1)	0(1)	-6(1)
C(8)	31(2)	37(2)	40(2)	3(2)	5(2)	-9(2)
C(9)	29(2)	28(2)	57(3)	-2(2)	-2(2)	-7(2)
C(10)	34(2)	30(2)	36(2)	-9(2)	-7(2)	-2(2)
C(11)	27(2)	33(2)	28(2)	-4(2)	1(1)	-6(1)
C(12)	23(2)	26(2)	18(2)	0(1)	3(1)	0(1)
C(13)	25(2)	36(2)	34(2)	7(2)	-7(1)	-2(1)
C(14)	31(2)	30(2)	47(2)	-6(2)	0(2)	6(2)
C(15)	25(2)	20(2)	24(2)	1(1)	-1(1)	-1(1)
C(16)	44(2)	31(2)	27(2)	-10(2)	7(2)	-9(2)
C(17)	54(2)	36(2)	48(2)	-17(2)	15(2)	-14(2)
C(18)	53(2)	36(2)	45(2)	-10(2)	5(2)	-19(2)
C(19)	42(2)	29(2)	42(2)	-4(2)	11(2)	-12(2)
C(20)	30(2)	30(2)	38(2)	-5(2)	6(2)	-7(1)
C(21)	21(2)	28(2)	22(2)	0(1)	-3(1)	-1(1)
C(22)	34(2)	26(2)	34(2)	-4(2)	-11(2)	7(2)

Table A4. Continued.

	U^{11}	U^{22}	U^{33}	U^{23}	U^{13}	U^{12}
C(23)	43(2)	36(2)	40(2)	5(2)	-14(2)	10(2)
C(24)	42(2)	58(3)	32(2)	5(2)	-13(2)	7(2)
C(25)	42(2)	52(3)	23(2)	-5(2)	-14(2)	4(2)
C(26)	31(2)	31(2)	25(2)	-4(1)	-4(1)	0(1)
C(27)	22(1)	20(2)	21(2)	2(1)	2(1)	1(1)
C(28)	23(2)	54(2)	30(2)	-2(2)	3(1)	9(2)
C(29)	31(2)	34(2)	34(2)	1(2)	-2(2)	-10(2)
C(30)	24(2)	22(2)	18(2)	1(1)	0(1)	-1(1)
C(31)	35(2)	28(2)	21(2)	-4(1)	-4(1)	4(1)
C(32)	38(2)	35(2)	21(2)	-4(1)	0(2)	5(2)
C(33)	33(2)	42(2)	18(2)	3(1)	-4(1)	2(2)
C(34)	37(2)	31(2)	25(2)	5(1)	1(1)	7(2)
C(35)	29(2)	32(2)	21(2)	4(1)	1(1)	5(1)

Table A5. Hydrogen coordinates (x 10^4) and isotropic displacement parameters (Å^2 x 10^3) for **11**.

	x	y	z	*U*(eq)
H(1A)	3514	2119	9503	84
H(1B)	2634	1765	10048	84
H(1C)	2572	1733	8995	84
H(2A)	2761	462	9299	66
H(2B)	2930	562	10339	66
H(2C)	3872	213	9846	66
H(3A)	5813	993	10636	76
H(3B)	4813	1306	11124	76
H(3C)	5660	1640	10523	76
H(4A)	4666	-314	7666	54
H(4B)	5099	88	8449	54
H(4C)	6015	-296	7993	54
H(5A)	6655	-74	6549	54
H(5B)	5970	382	5968	54
H(5C)	5326	-173	6211	54
H(6)	1990	1289	6335	28

Table A5. Continued.

	x	y	z	*U*(eq)
H(7A)	2168	961	7812	37
H(7B)	2921	449	7517	37
H(8A)	963	146	7644	43
H(8B)	473	623	7003	43
H(9A)	1806	-311	6461	46
H(9B)	465	-197	6169	46
H(10A)	971	552	5284	40
H(10B)	1729	38	5006	40
H(11A)	3402	378	5827	35
H(11B)	2925	851	5172	35
H(13A)	2650	1880	5263	48
H(13B)	2377	2522	5222	48
H(13C)	1444	2107	5589	48
H(14A)	2683	2676	7592	54
H(14B)	1509	2677	6970	54
H(14C)	2584	3053	6730	54
H(15)	4555	2891	6935	28

Table A5. Continued.

	x	y	z	*U*(eq)
H(16A)	5585	2636	8674	40
H(16B)	4261	2825	8481	40
H(17A)	4882	3712	8046	55
H(17B)	5441	3586	9015	55
H(18A)	6880	3965	8080	54
H(18B)	7272	3375	8450	54
H(19A)	7567	3390	6918	45
H(19B)	6252	3587	6694	45
H(20A)	6383	2627	6395	39
H(20B)	6901	2514	7380	39
H(21)	8902	1327	8052	29
H(22A)	8195	409	8009	38
H(22B)	7316	544	8760	38
H(23A)	9019	107	9438	49
H(23B)	9845	557	9029	49
H(24A)	8234	775	10376	53
H(24B)	9625	775	10535	53

Table A5. Continued.

	x	y	z	*U*(eq)
H(25A)	9774	1568	9646	48
H(25B)	8882	1697	10390	48
H(26A)	7252	1554	9361	35
H(26B)	8086	2002	8957	35
H(28A)	8671	1130	5457	53
H(28B)	9898	1377	5819	53
H(28C)	9010	1745	5223	53
H(29A)	8757	2219	7457	50
H(29B)	9310	2401	6562	50
H(29C)	9954	1953	7184	50
H(30)	7073	1819	5139	26
H(31A)	7222	873	4691	34
H(31B)	5832	818	4647	34
H(32A)	7095	1516	3495	38
H(32B)	6465	956	3190	38
H(33A)	4608	1338	3399	37
H(33B)	5277	1733	2759	37

Table A5. Continued.

	x	y	z	*U*(eq)
H(34A)	4376	2247	3893	37
H(34B)	5755	2347	3929	37
H(35A)	5195	2194	5399	33
H(35B)	4581	1628	5112	33

Table A6. Atomic coordinates (x 10^4) and equivalent isotropic displacement parameters (Å^2 x 10^3) for **19**. *U*(eq) is defined as one third of the trace of the orthogonalized U^{ij} tensor.

	x	y	z	*U*(eq)
Nb(1)	6667	3333	4716(1)	33(1)
Nb(2)	7327(1)	2646(1)	7095(1)	37(1)
N(1)	8653(5)	3323(5)	7778(6)	47(2)
N(2)	6808(6)	1682(5)	8419(6)	50(2)
N(3)	7611(5)	1815(5)	6039(6)	46(2)
N(4)	5506(5)	2460(5)	3726(5)	42(2)
O(1)	6667	3333	7931(7)	38(2)
O(2)	7749(4)	3865(4)	6018(4)	35(1)
C(1)	9479(7)	4155(8)	7270(9)	61(2)
C(2)	8982(8)	2998(9)	8821(10)	78(3)
C(3)	6463(8)	1807(8)	9568(8)	67(3)
C(4)	6822(9)	783(8)	8448(9)	69(3)
C(5)	8482(8)	1766(8)	6070(11)	71(3)
C(6)	6951(7)	1094(7)	5218(9)	58(2)
C(7)	4874(7)	1440(6)	3909(8)	52(2)
C(8)	5232(7)	2721(7)	2614(8)	57(2)

Table A7. Bond distances (Å) in **19**.

Bond	Distance	Bond	Distance
Nb(1)-N(4)#1	2.025(7)	Nb(2)-Nb(2)#2	3.278(5)
Nb(1)-N(4)#2	2.025(7)	Nb(2)-Nb(2)#1	3.278(5)
Nb(1)-N(4)	2.025(7)	N(1)-C(1)	1.458(12)
Nb(1)-O(2)	2.104(5)	N(1)-C(2)	1.483(12)
Nb(1)-O(2)#2	2.104(5)	N(2)-C(3)	1.453(12)
Nb(1)-O(2)#1	2.104(5)	N(2)-C(4)	1.470(12)
Nb(1)-Nb(2)#1	3.262(4)	N(3)-C(6)	1.450(12)
Nb(1)-Nb(2)#2	3.262(4)	N(3)-C(5)	1.455(12)
Nb(2)-N(2)	2.006(7)	N(4)-C(8)	1.451(10)
Nb(2)-N(3)	2.009(7)	N(4)-C(7)	1.460(11)
Nb(2)-N(1)	2.012(7)	O(1)-Nb(2)#2	2.110(4)
Nb(2)-O(1)	2.110(4)	O(1)-Nb(2)#1	2.110(4)
Nb(2)-O(2)#2	2.111(6)	O(2)-Nb(2)#1	2.111(6)
Nb(2)-O(2)	2.114(6)		

Table A8. Bond angles (°) in **19**.

Bond	Angle	Bond	Angle
N(4)#1-Nb(1)-N(4)#2	93.1(3)	O(2)-Nb(1)-Nb(2)#1	39.36(15)
N(4)#1-Nb(1)-N(4)	93.1(3)	O(2)#2-Nb(1)-Nb(2)#1	81.72(18)
N(4)#2-Nb(1)-N(4)	93.1(3)	O(2)#1-Nb(1)-Nb(2)#1	39.45(15)
N(4)#1-Nb(1)-O(2)	86.3(2)	N(4)#1-Nb(1)-Nb(2)#2	143.08(19)
N(4)#2-Nb(1)-O(2)	103.8(2)	N(4)#2-Nb(1)-Nb(2)#2	123.7(2)
N(4)-Nb(1)-O(2)	163.1(2)	N(4)-Nb(1)-Nb(2)#2	88.8(2)
N(4)#1-Nb(1)-O(2)#2	103.8(2)	O(2)-Nb(1)-Nb(2)#2	81.72(18)
N(4)#2-Nb(1)-O(2)#2	163.1(2)	O(2)#2-Nb(1)-Nb(2)#2	39.45(15)
N(4)-Nb(1)-O(2)#2	86.3(2)	O(2)#1-Nb(1)-Nb(2)#2	39.36(15)
O(2)-Nb(1)-O(2)#2	77.5(2)	Nb(2)#1-Nb(1)-Nb(2)#2	60.31(10)
N(4)#1-Nb(1)-O(2)#1	163.1(2)	N(2)-Nb(2)-N(3)	93.3(3)
N(4)#2-Nb(1)-O(2)#1	86.3(2)	N(2)-Nb(2)-N(1)	93.6(3)
N(4)-Nb(1)-O(2)#1	103.8(2)	N(3)-Nb(2)-N(1)	92.7(3)
O(2)-Nb(1)-O(2)#1	77.5(2)	N(2)-Nb(2)-O(1)	87.7(3)
O(2)#2-Nb(1)-O(2)#1	77.5(2)	N(3)-Nb(2)-O(1)	163.9(2)
N(4)#1-Nb(1)-Nb(2)#1	123.7(2)	N(1)-Nb(2)-O(1)	103.3(2)
N(4)#2-Nb(1)-Nb(2)#1	88.8(2)	N(2)-Nb(2)-O(2)#2	102.7(3)
N(4)-Nb(1)-Nb(2)#1	143.08(19)	N(3)-Nb(2)-O(2)#2	87.3(3)

Table A8. Continued

Bond	Angle	Bond	Angle
N(1)-Nb(2)-O(2)#2	163.7(3)	O(2)-Nb(2)-Nb(2)#1	39.09(1)
O(1)-Nb(2)-O(2)#2	76.8(2)	Nb(2)#2-Nb(2)-Nb(2)#1	60.0
N(2)-Nb(2)-O(2)	164.1(3)	C(1)-N(1)-C(2)	107.9(8)
N(3)-Nb(2)-O(2)	102.5(3)	C(1)-N(1)-Nb(2)	126.4(6)
N(1)-Nb(2)-O(2)	87.0(3)	C(2)-N(1)-Nb(2)	125.4(7)
O(1)-Nb(2)-O(2)	76.8(2)	C(3)-N(2)-C(4)	108.5(8)
O(2)#2-Nb(2)-O(2)	77.1(3)	C(3)-N(2)-Nb(2)	125.7(6)
N(2)-Nb(2)-Nb(2)#2	88.7(2)	C(4)-N(2)-Nb(2)	125.5(6)
N(3)-Nb(2)-Nb(2)#2	124.8(2)	C(6)-N(3)-C(5)	108.4(8)
N(1)-Nb(2)-Nb(2)#2	142.2(2)	C(6)-N(3)-Nb(2)	126.0(6)
O(1)-Nb(2)-Nb(2)#2	39.05(1)	C(5)-N(3)-Nb(2)	125.3(6)
O(2)#2-Nb(2)-Nb(2)#2	39.16(1)	C(8)-N(4)-C(7)	107.8(7)
O(2)-Nb(2)-Nb(2)#2	81.20(1)	C(8)-N(4)-Nb(1)	125.2(6)
N(2)-Nb(2)-Nb(2)#1	125.0(2)	C(7)-N(4)-Nb(1)	126.6(5)
N(3)-Nb(2)-Nb(2)#1	141.5(2)	Nb(2)-O(1)-Nb(2)#2	101.9(2)
N(1)-Nb(2)-Nb(2)#1	88.7(2)	Nb(2)-O(1)-Nb(2)#1	101.9(2)
O(1)-Nb(2)-Nb(2)#1	39.05(1)	Nb(2)#2-O(1)-Nb(2)#1	101.9(2)
O(2)#2-Nb(2)-Nb(2)#1	81.25(1)	Nb(1)-O(2)-Nb(2)#1	101.4(2)

Table A8. Continued

Bond	Angle	Bond	Angle
Nb(1)-O(2)-Nb(2)	101.3(2)	Nb(2)#1-O(2)-Nb(2)	101.8(2)

Symmetry transformations used to generate equivalent atoms:

#1 -y+1,x-y,z #2 -x+y+1,-x+1,z

Table A9. Anisotropic displacement parameters ($Å^2$ x 10^3) for **19**. The anisotropic displacement factor exponent takes the form: $-2\pi^2[h^2a^{*2}U^{11} + \ldots + 2hka^*b^*U^{12}]$.

	U^{11}	U^{22}	U^{33}	U^{23}	U^{13}	U^{12}
Nb(1)	40(1)	40(1)	19(1)	0	0	20(1)
Nb(2)	44(1)	44(1)	25(1)	0(1)	-4(1)	24(1)
N(1)	48(4)	58(4)	37(4)	-1(3)	-9(3)	28(3)
N(2)	68(5)	55(4)	31(3)	5(3)	-7(3)	32(4)
N(3)	55(4)	46(4)	39(4)	-5(3)	-4(3)	27(3)
N(4)	47(4)	48(4)	28(3)	-2(3)	-1(3)	23(3)
O(1)	49(3)	49(3)	17(4)	0	0	25(2)
O(2)	35(3)	42(3)	23(2)	-2(2)	-1(2)	16(2)
C(1)	52(5)	79(7)	57(6)	-12(5)	-10(4)	35(5)
C(2)	71(7)	94(8)	62(7)	1(6)	-27(6)	35(6)
C(3)	87(7)	89(7)	36(5)	15(5)	4(5)	53(6)
C(4)	100(8)	66(6)	52(6)	13(5)	-2(5)	50(6)
C(5)	71(7)	79(7)	81(7)	-11(6)	-6(6)	50(6)
C(6)	66(6)	59(6)	51(5)	-8(4)	-1(4)	32(5)
C(7)	56(5)	50(5)	45(5)	-8(4)	-15(4)	21(4)
C(8)	67(6)	67(6)	35(5)	-4(4)	-15(4)	33(5)

Table A10. Hydrogen coordinates (x 10^4) and isotropic displacement parameters ($Å^2$ x 10^3) for **19**.

	x	y	z	*U*(eq)
H(1A)	9766	4643	7870	92
H(1B)	9281	4390	6605	92
H(1C)	9933	3980	7002	92
H(2A)	9477	2874	8572	118
H(2B)	8458	2425	9139	118
H(2C)	9224	3484	9426	118
H(3A)	5832	1286	9705	100
H(3B)	6452	2394	9564	100
H(3C)	6878	1825	10193	100
H(4A)	7229	803	9086	103
H(4B)	7059	695	7699	103
H(4C)	6188	263	8578	103
H(5A)	8341	1150	6354	107
H(5B)	8933	2248	6597	107
H(5C)	8746	1865	5279	107

Table A10. Continued

	x	y	z	*U*(eq)
H(6A)	7225	1217	4431	87
H(6B)	6367	1109	5198	87
H(6C)	6824	478	5481	87
H(7A)	4232	1312	4006	79
H(7B)	5065	1241	4614	79
H(7C)	4908	1098	3228	79
H(8A)	5302	2373	1964	85
H(8B)	5633	3392	2478	85
H(8C)	4580	2570	2665	85

Table A11. Atomic coordinates (x 10^4) and equivalent isotropic displacement parameters (Å^2 x 10^3) for **20**. *U*(eq) is defined as one third of the trace of the orthogonalized U^{ij} tensor.

	x	y	z	*U*(eq)
Ta(1)	6667	3333	-290(1)	25(1)
Ta(2)	5324(1)	2673(1)	2095(1)	29(1)
N(1)	4218(9)	2406(10)	1048(11)	40(3)
N(2)	4680(9)	1363(9)	2772(10)	40(3)
N(3)	4888(9)	3180(10)	3412(10)	42(3)
N(4)	5526(8)	2459(8)	-1268(9)	33(2)
O(1)	6667	3333	2936(13)	30(3)
O(2)	6127(6)	2270(6)	1015(7)	27(2)
C(1)	4151(11)	3068(12)	229(15)	45(3)
C(2)	3317(11)	1543(13)	1078(16)	54(4)
C(3)	4652(12)	522(11)	2276(14)	47(4)
C(4)	4040(14)	1047(14)	3819(16)	58(4)
C(5)	3978(14)	3149(16)	3458(16)	58(5)
C(6)	5330(14)	3519(15)	4554(13)	55(4)
C(7)	4882(11)	1438(11)	-1056(13)	42(3)
C(8)	5239(12)	2720(12)	-2374(14)	48(4)

Table A12. Bond distances (Å) in **20**.

Bond	Length	Bond	Length
Ta(1)-N(4)#1	2.013(11)	Ta(2)-Ta(2)#2	3.2854(14)
Ta(1)-N(4)	2.013(11)	Ta(2)-Ta(2)#1	3.2854(14)
Ta(1)-N(4)#2	2.013(11)	N(1)-C(2)	1.44(2)
Ta(1)-O(2)#1	2.098(8)	N(1)-C(1)	1.463(19)
Ta(1)-O(2)	2.098(8)	N(2)-C(3)	1.46(2)
Ta(1)-O(2)#2	2.098(8)	N(2)-C(4)	1.484(19)
Ta(1)-Ta(2)#1	3.2831(11)	N(3)-C(6)	1.44(2)
Ta(1)-Ta(2)#2	3.2831(11)	N(3)-C(5)	1.46(2)
Ta(2)-N(3)	1.990(12)	N(4)-C(8)	1.464(18)
Ta(2)-N(2)	2.001(12)	N(4)-C(7)	1.477(19)
Ta(2)-N(1)	2.010(12)	O(1)-Ta(2)#1	2.119(7)
Ta(2)-O(2)#2	2.115(9)	O(1)-Ta(2)#2	2.119(7)
Ta(2)-O(2)	2.117(9)	O(2)-Ta(2)#1	2.115(9)
Ta(2)-O(1)	2.119(7)		

Table A13. Bond angles (°) for **20**.

Bond	Angles	Bond	Angles
N(4)#1-Ta(1)-N(4)	93.0(4)	O(2)#2-Ta(1)-Ta(2)#1	81.0(2)
N(4)#1-Ta(1)-N(4)#2	93.0(4)	N(4)#1-Ta(1)-Ta(2)#2	123.3(3)
N(4)-Ta(1)-N(4)#2	93.0(4)	N(4)-Ta(1)-Ta(2)#2	143.5(3)
N(4)#1-Ta(1)-O(2)#1	86.5(4)	N(4)#2-Ta(1)-Ta(2)#2	89.1(3)
N(4)-Ta(1)-O(2)#1	162.3(4)	O(2)#1-Ta(1)-Ta(2)#2	39.0(2)
N(4)#2-Ta(1)-O(2)#1	104.6(4)	O(2)-Ta(1)-Ta(2)#2	81.0(2)
N(4)#1-Ta(1)-O(2)	104.6(4)	O(2)#2-Ta(1)-Ta(2)#2	39.0(2)
N(4)-Ta(1)-O(2)	86.5(4)	Ta(2)#1-Ta(1)-Ta(2)#2	60.05(3)
N(4)#2-Ta(1)-O(2)	162.3(4)	N(3)-Ta(2)-N(2)	93.2(5)
O(2)#1-Ta(1)-O(2)	76.6(4)	N(3)-Ta(2)-N(1)	93.3(5)
N(4)#1-Ta(1)-O(2)#2	162.3(4)	N(2)-Ta(2)-N(1)	93.2(5)
N(4)-Ta(1)-O(2)#2	104.6(4)	N(3)-Ta(2)-O(2)#2	103.5(4)
N(4)#2-Ta(1)-O(2)#2	86.5(4)	N(2)-Ta(2)-O(2)#2	163.2(4)
O(2)#1-Ta(1)-O(2)#2	76.6(4)	N(1)-Ta(2)-O(2)#2	87.0(4)
O(2)-Ta(1)-O(2)#2	76.6(4)	N(3)-Ta(2)-O(2)	163.6(5)
N(4)#1-Ta(1)-Ta(2)#1	89.1(3)	N(2)-Ta(2)-O(2)	87.8(4)
N(4)-Ta(1)-Ta(2)#1	123.3(3)	N(1)-Ta(2)-O(2)	103.0(4)
N(4)#2-Ta(1)-Ta(2)#1	143.5(3)	O(2)#2-Ta(2)-O(2)	75.8(5)
O(2)#1-Ta(1)-Ta(2)#1	39.0(2)	N(3)-Ta(2)-O(1)	87.1(5)
O(2)-Ta(1)-Ta(2)#1	39.0(2)	N(2)-Ta(2)-O(1)	103.3(4)

Table A13. Continued

Bond	Angle	Bond	Angle
N(1)-Ta(2)-O(2)	103.0(4)	O(2)-Ta(2)-Ta(2)#1	39.1(2)
O(2)#2-Ta(2)-O(2)	75.8(5)	O(1)-Ta(2)-Ta(2)#1	39.2(2)
N(3)-Ta(2)-O(1)	87.1(5)	Ta(2)#2-Ta(2)-Ta(2)#1	60.0
N(2)-Ta(2)-O(1)	103.3(4)	C(2)-N(1)-C(1)	108.6(13)
N(1)-Ta(2)-O(1)	163.4(4)	C(2)-N(1)-Ta(2)	124.4(11)
O(2)#2-Ta(2)-O(1)	76.8(4)	C(1)-N(1)-Ta(2)	126.7(10)
O(2)-Ta(2)-O(1)	76.8(4)	C(3)-N(2)-C(4)	106.9(13)
N(3)-Ta(2)-Ta(2)#2	88.7(4)	C(3)-N(2)-Ta(2)	127.7(9)
N(2)-Ta(2)-Ta(2)#2	142.3(4)	C(4)-N(2)-Ta(2)	125.0(11)
N(1)-Ta(2)-Ta(2)#2	124.2(4)	C(6)-N(3)-C(5)	106.6(13)
O(2)#2-Ta(2)-Ta(2)#2	39.1(2)	C(6)-N(3)-Ta(2)	127.5(11)
O(2)-Ta(2)-Ta(2)#2	80.7(2)	C(5)-N(3)-Ta(2)	125.4(11)
O(1)-Ta(2)-Ta(2)#2	39.2(2)	C(8)-N(4)-C(7)	108.3(11)
N(3)-Ta(2)-Ta(2)#1	124.6(4)	C(8)-N(4)-Ta(1)	125.0(10)
N(2)-Ta(2)-Ta(2)#1	88.9(4)	C(7)-N(4)-Ta(1)	126.5(9)
N(1)-Ta(2)-Ta(2)#1	141.9(4)	Ta(2)#1-O(1)-Ta(2)	101.6(4)
O(2)#2-Ta(2)-Ta(2)#1	80.7(2)	Ta(2)#1-O(1)-Ta(2)#2	101.6(4)

Table A13. Continued

Bond	Angle	Bond	Angle
Ta(2)-O(1)-Ta(2)#2	101.6(4)	Ta(1)-O(2)-Ta(2)	102.3(4)
Ta(1)-O(2)-Ta(2)#1	102.4(4)	Ta(2)#1-O(2)-Ta(2)	101.8(3)

Symmetry transformations used to generate equivalent atoms:

#1 -y+1,x-y,z #2 -x+y+1,-x+1,z

Table A14. Anisotropic displacement parameters ($Å^2$ x 10^3) for **20**. The anisotropic displacement factor exponent takes the form: $-2\pi^2[h^2a^{*2}U^{11} + \ldots + 2hka^*b^*U^{12}]$.

	U^{11}	U^{22}	U^{33}	U^{23}	U^{13}	U^{12}
Ta(1)	31(1)	31(1)	14(1)	0	0	16(1)
Ta(2)	33(1)	36(1)	18(1)	4(1)	4(1)	16(1)
N(1)	35(6)	54(7)	33(6)	2(5)	0(5)	23(6)
N(2)	46(7)	44(6)	25(5)	10(5)	7(5)	20(6)
N(3)	50(7)	60(8)	23(5)	5(5)	12(5)	33(6)
N(4)	39(6)	38(6)	20(5)	-3(4)	1(4)	17(5)
O(1)	33(5)	33(5)	24(7)	0	0	17(2)
O(2)	36(4)	31(4)	14(4)	4(3)	1(3)	16(4)
C(1)	39(7)	53(9)	50(9)	10(7)	1(6)	27(7)
C(2)	35(8)	65(11)	48(9)	6(8)	-1(7)	15(7)
C(3)	54(9)	47(8)	34(7)	4(6)	0(6)	21(7)
C(4)	64(11)	58(10)	46(9)	21(8)	17(8)	27(9)
C(5)	65(11)	89(14)	44(9)	13(9)	19(8)	57(11)
C(6)	67(11)	77(12)	23(7)	-6(7)	12(7)	37(10)
C(7)	46(8)	43(8)	32(7)	-11(6)	-15(6)	20(6)
C(8)	56(9)	58(10)	32(8)	-6(6)	-12(6)	29(8)

Table A15. Hydrogen coordinates (x 10^4) and isotropic displacement parameters ($Å^2$ x 10^3) for **20**.

	x	y	z	*U*(eq)
H(1A)	4005	2799	-555	68
H(1B)	4745	3652	214	68
H(1C)	3661	3188	492	68
H(2A)	2884	1633	1565	81
H(2B)	3396	1043	1404	81
H(2C)	3069	1379	285	81
H(3A)	5257	566	2382	71
H(3B)	4507	478	1442	71
H(3C)	4174	-32	2676	71
H(4A)	3394	705	3555	87
H(4B)	4142	1589	4272	87
H(4C)	4170	642	4308	87
H(5A)	3664	2864	4192	87
H(5B)	3592	2782	2801	87
H(5C)	4080	3781	3409	87
H(6A)	5515	4175	4637	83

Table A15. Continued

	x	y	z	*U*(eq)
H(6B)	5879	3449	4614	83
H(6C)	4889	3159	5172	83
H(7A)	4254	1325	-907	62
H(7B)	5098	1239	-380	62
H(7C)	4874	1086	-1745	62
H(8A)	5136	2264	-2980	72
H(8B)	5729	3335	-2625	72
H(8C)	4664	2734	-2242	72

VITA

Julia Kathryn (Covington) Abbott was born on September 18th, 1983 in Ft. Worth, TX, to Merry Alvey Covington and Robert Dean Covington. In 2001 she graduated from Batesville High School in Batesville, AR, in the top 10 of her class. She played for the 2001 state champion Lady Pioneer's softball team, pitching a shut out in the state finals, and a no-hitter in the all-star game. In the fall of 2001 she began her undergraduate studies at Centre College in Danville, KY. During her time at Centre, she joined Alpha Delta Pi sorority and served as the Membership Education Vice President as well as playing softball for the Lady Colonels. She also conducted undergraduate research under the direction of Dr. Preston Miles. Her research involved testing soil samples from a local tree farm for their heavy metal content using atomic absorption spectroscopy. She met her future husband, Josh Abbott, who was also a chemistry major, while at Centre. They were married August 4th, 2007. Julia graduated from Centre in May 2005 with a B.S. degree in chemistry.

In August 2005 Julia began her graduate studies in the chemistry department at The University of Tennessee, Knoxville. She joined Dr. Ziling Xue's organometallic group where she studied the formation of the archetypal Schrock carbene as well as novel tantalum guanidinate complexes. She published a paper in *the Journal of the American Chemical Society* (JACS) on her work with the archetypical Schrock carbene in which she finally answered the long standing question regarding the mechanistic pathway of its formation. This work was also reported in *Chemical and Engineering News* (June 15, 2009).

Julia has presented research at several national ACS meetings including Boston in fall 2007, Salt Lake City in spring 2009, and San Francisco in spring 2010. Julia also served as president of the Association of Chemistry Graduate Students, and won several awards while at UT. In 2006 she was awarded a first year academic achievement award. In 2007 the East Tennessee Section of the ACS awarded her a graduate fellow. In 2009 the UT chemistry department awarded her the Eugene John Barber Fellowship in chemistry for her work on the Schrock carbene. In 2010 the university awarded her a Citation for Professional Promise, and the chemistry department awarded her the first annual Graduate Award for Achievement in Inorganic Chemistry.